Coordination Chemistry of *cis,trans*-1,3,5-Triaminocyclohexane – From Mononuclear Complexes to Supramolecular Architectures

by
Georg Peter Maria Seeber

A thesis submitted to
The University of Birmingham
for the degree of
DOCTOR OF PHILOSOPHY

School of Chemistry
The University of Birmingham
September 2003

3 RESULTS AND DISCUSSION

To date, four different routes to the preparation of 1,3,5-triaminocyclohexane are present in literature. The synthetic methods reported by *Stetter and Bremen*,[153] *Fleischer et al.*[154] and *Bowen et al.*[155] result in the isomerically pure *cis*-derivative **30**. The only synthetic strategy described thus far producing the geometrical *trans*-isomer **29** is the method published in 1957 by *Lions and Martin.*[156] This route involves the synthesis of 1,3,5-cyclohexanetrionetrioxime (chtt, **31**)[157] from phloroglucinol (**32**) followed by non-stereospecific reduction with sodium in liquid ammonia (Figure 25). Separation of the two *cis*- and *trans*- isomers is achieved by the method of *Urbach et al.*[158] using nickel(II) nitrate followed by concentrated hydrochloric acid to obtain the amines in their protonated forms. The major disadvantages of this preparation lie in the low yield of 11% for each isomer upon reduction and in the poor separation of the isomers upon complexation.[159] Before investigating the coordination chemistry of *trans*-tach, it was therefore important to optimise the reaction conditions and to improve the separation of the two isomers.

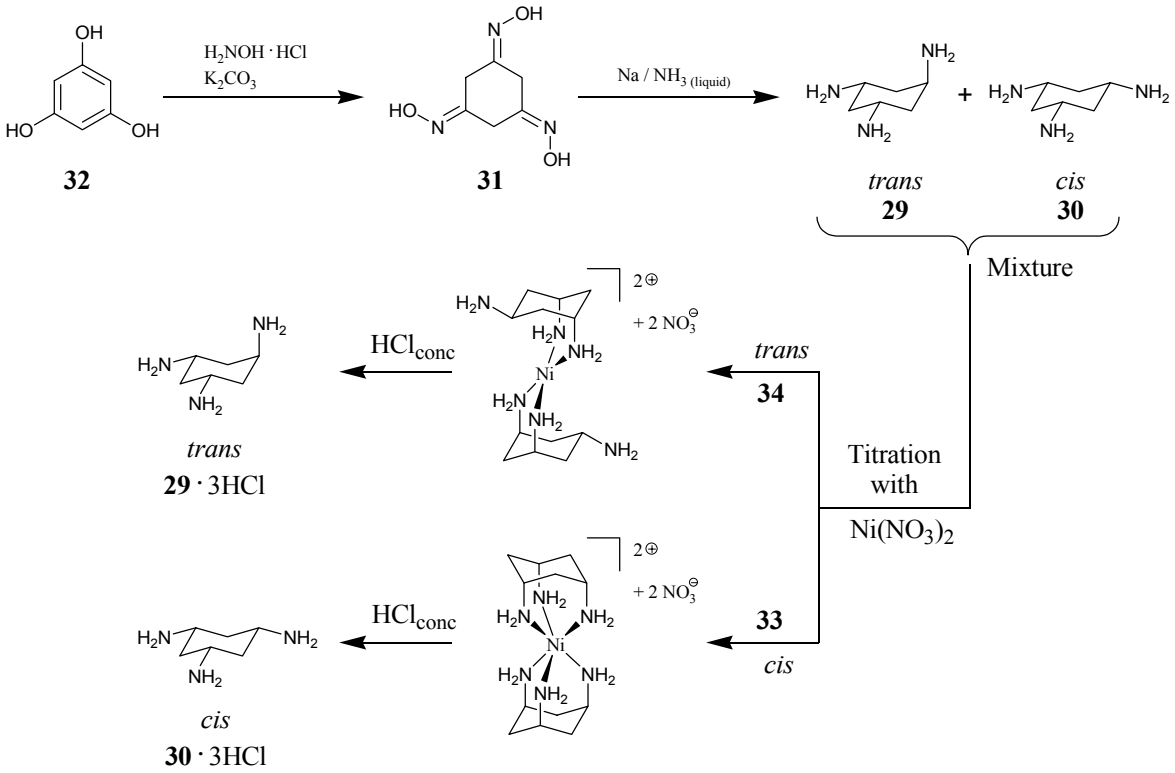

Figure 25 Synthesis of tach by the method of *Lions and Martin*,[156] separation of the isomers by the method of *Urbach et al.*[158]

3.1 Optimised synthesis of trans-tach

Optimisation of the reduction conditions to improve the overall yield of tach up to 46% was achieved by using (i) smaller scale reactions, (ii) a large excess of sodium and (iii) a large volume of liquid ammonia (Figure 26).

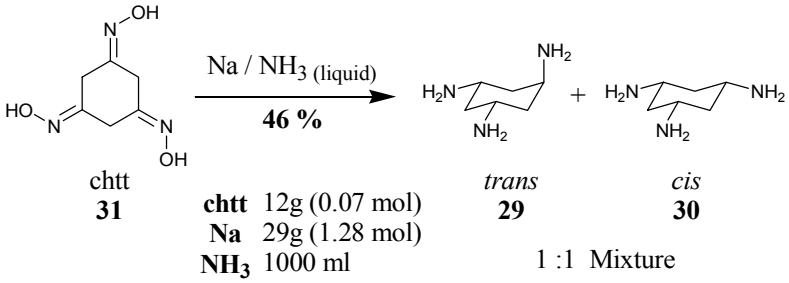

Figure 26 Improved conditions for the tach synthesis *via* reduction of chtt.

The non-stereospecific reduction of phloroglucinol with sodium yields both tach isomers in a 1:1 ratio. Separation of the isomers is achieved by titration with nickel(II) nitrate in methanol. The less soluble pink nickel(II)-*cis*-tach complex **33** precipitates first, before the orange nickel(II)-*trans*-tach complex **34**. Treatment of both nickel(II) complexes with concentrated hydrochloric acid results in the protonation of the coordinating amines and precipitation of the *tris*-hydrochloric acid salts of *trans*- (**29** • 3 HCl) and *cis*- (**30** • 3 HCl) tach (Figure 25). Two different approaches to isolating the amines in their deprotonated forms were established: (i) adsorption of aqueous solutions of the *tris*-hydrochloride salts onto a strongly alkaline ion exchange resin followed by distillation for *trans*-tach and sublimation for *cis*-tach results in moderate yields of 50-60 % of the neutral amines and (ii) neutralisation of methanolic solutions of the *tris*-hydrochloride salts with sodium hydroxide followed by distillation for *trans*-tach and sublimation for *cis*-tach yields the non-protonated amines in 92-96 % yield.

However, ^{1}H-NMR spectra of *trans*-tach were slightly contaminated with the corresponding *cis*-isomer with typical *trans* to *cis* ratios of 27:1 (based on ^{1}H-NMR integration). This contamination can be explained by the method of separation. While the titration with nickel(II) nitrate precipitates the less soluble nickel(II)-*cis*-tach complex **33** first and analytically pure, the subsequent precipitation of nickel(II)-*trans*-tach complex **34** always contains trace amounts of *cis*-impurity. To obtain the *trans*-isomer analytically pure, a different separation procedure was applied. This procedure removes the *cis*-isomer as before

via titration with nickel(II) nitrate, after which a small excess of nickel(II) nitrate is added to start precipitation of the nickel(II)-*trans*-tach complex **34**. The remaining solution is then distilled to give non-protonated *trans*-tach in moderate yield. A comparison of the different methods of isolation and separation with overall yields relative to chtt are given in Figure 27.

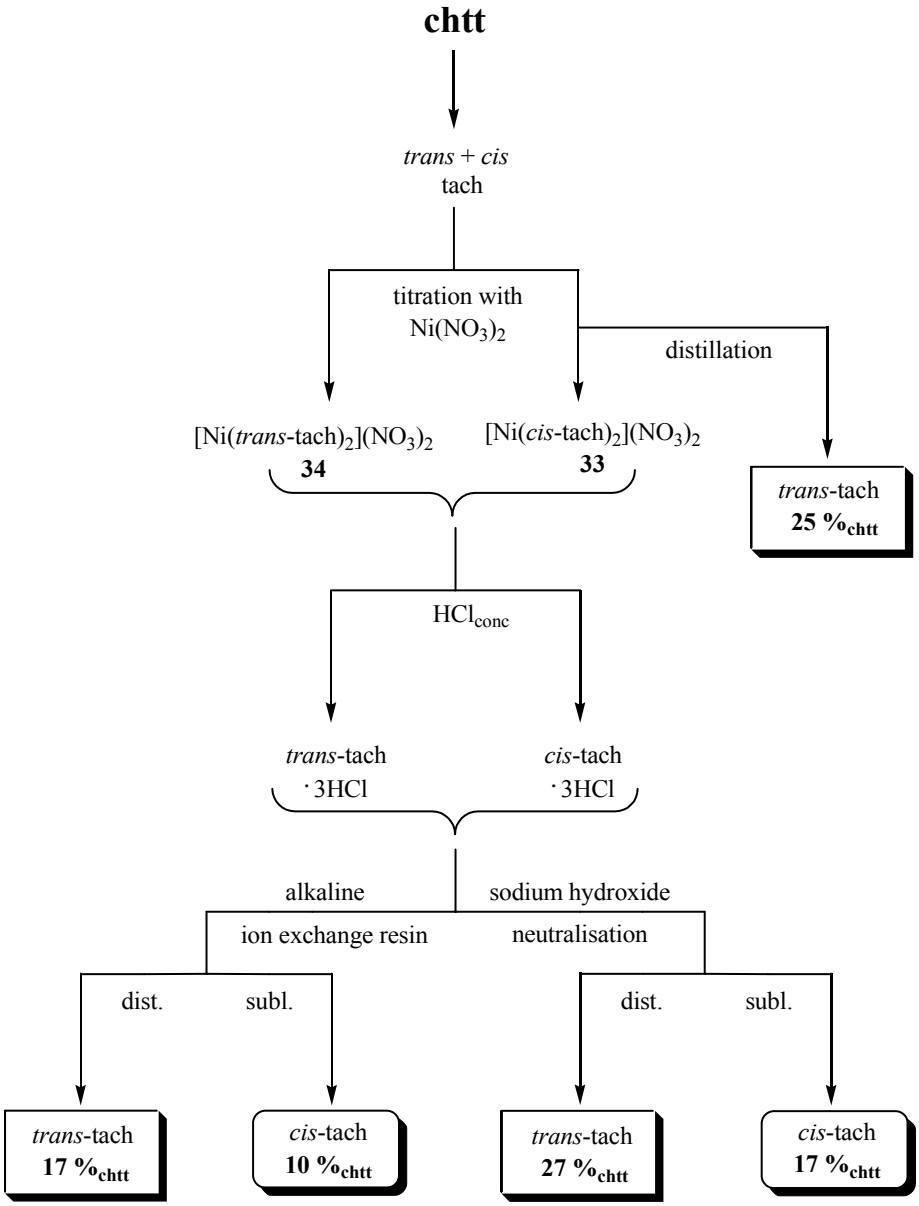

Figure 27 Overview of possible isolation and separation procedures for *trans*- and *cis*-tach. Overall yields are based on chtt.

The most convenient way of obtaining *trans*-tach in its non-protonated form is found to be *via* distillation after separation of the *cis*-isomer by complexation. This procedure yields 25% of the triamine with respect to the chtt starting material, thus significantly improving the original

yield of 11%. Furthermore, no contamination by the *cis*-isomer was found in *trans*-tach samples isolated in this way.

3.1.1 Spectroscopy of *trans*-tach

The ligand *trans*-tach (**L**) has been characterised by elemental analysis, IR, MS and NMR spectroscopy. The ^{1}H-NMR spectrum in deuterated water shows six different environments of a total of nine protons, which is consistent with the C_s symmetry of *trans*-tach (H_a : $2^{\bullet}H_d$: H_e : $2^{\bullet}H_b$: $2^{\bullet}H_c$: H_f). The amine protons are not observed presumably due to fast exchange with the solvent molecules. The signals are unambiguously assigned by correlated 2-D-spectroscopy (^{1}H-^{1}H COSY and ^{1}H-^{13}C HSQC) and NOE experiments.

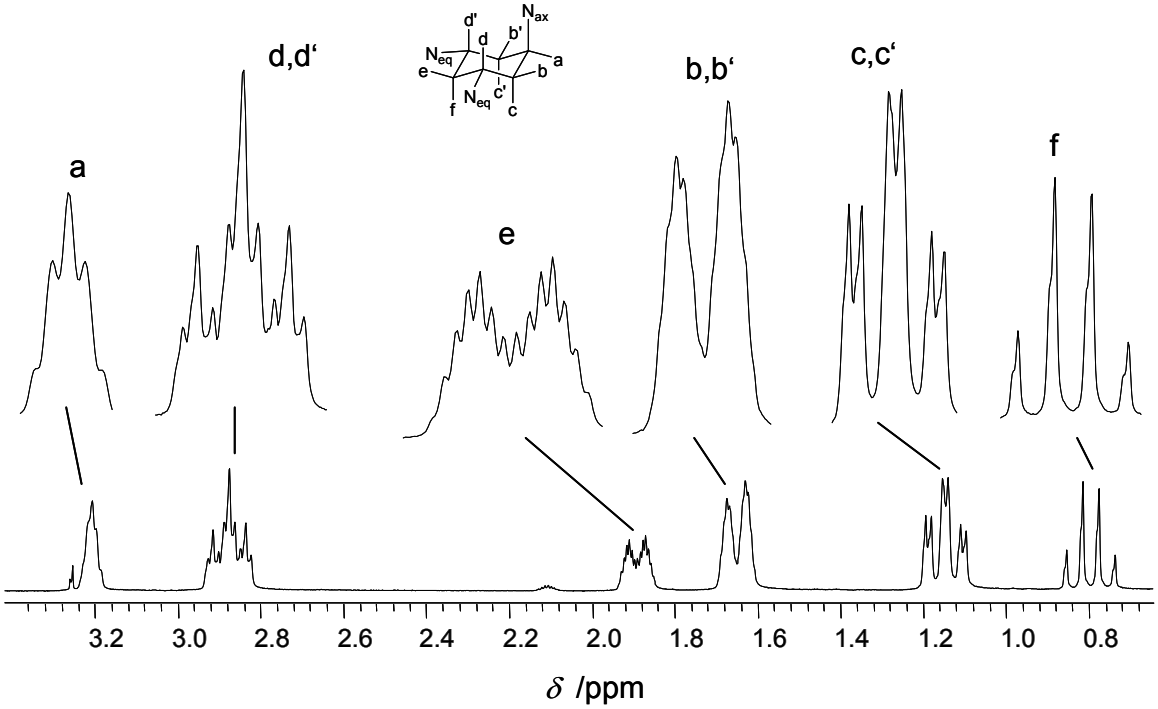

Figure 28 ^{1}H-NMR (300 MHz, D_2O) spectrum of *trans*-tach **29**.

Due to the plane of symmetry present in the molecule, *trans*-tach represents an ABB'CC'DD'EF[‡] spin system. However, the coupling constants of the higher order spin systems for the B, C and D protons are small and not resolved in the obtained spectra. Thus

[‡] This nomenclature is chosen to be consistent to the assignment of the *trans*-tach protons.

the signals are broadened and interpreted as pseudo first order spin systems (pseudo-$AB_2C_2D_2EF$)[§].

The most deshielded protons are expected to be the methine protons. H_a (δ = 3.21 ppm) resonates as a quintet with the fine splitting embedded in the shoulders of the broad signal. This spin multiplicity is due to a small splitting to four H_b and H_c protons with identical coupling constants ^3J = 3.2 Hz. The small coupling and the integration of one proton suggest an *equatorial* position on the cyclohexane ring. The second set of methine protons H_d integrate to two protons (δ = 2.88 ppm) and show a triplet of triplet splitting. The *axial-axial* coupling of ^3J = 11.8 Hz is identical to both H_c and H_f protons resulting in the larger triplet splitting, whereas the *axial-equatorial* coupling of ^3J = 3.7 Hz to both *equatorial* methylene protons H_b and H_e gives rise to the smaller triplet splitting. The large coupling indicates the methine protons H_d being in *axial* position of the cyclohexane ring, thus confirming the bis*equatorial*-mono*axial* conformation of *trans*-tach. Additionally DEPT-135 measurements show two sets of methine carbons at 48.1 and 45.8 ppm in the ^{13}C-spectrum and HSQC experiments highlight their correspondence to H_a and H_d. The pairs of methylene protons H_b / H_c and H_e / H_f, integrating in a 2:1 ratio are easily distinguished by their magnitude in coupling constants. Both sets of *axial* methylene protons H_c and H_f exhibit large *axial-axial* coupling to H_d, whereas the *equatorial* methylene protons H_b and H_e show only small *equatorial-axial* coupling to H_d (Figure 29). H_e (δ = 1.89 ppm) shows a large *geminal* coupling (^2J = 11.8 Hz) to H_f and a small *vicinal* coupling to H_d (^3J = 3.7 Hz). With an additional *w*-coupling (^4J = 2.2 Hz) to H_b, the resulting signal is an overlap of a doublet of triplets of triplets. The remaining *equatorial* methylene protons H_b (δ = 1.61 ppm) give rise to a pseudo doublet of doublet splitting with a large *geminal* coupling to H_c and a small *vicinal* coupling to H_d (^3J = 3.7 Hz). The additional couplings to H_a (^3J = 3.2 Hz) and H_e (^4J = 2.2 Hz) are not resolved and result in a broadening of the signal. Both sets of *axial* methylene protons H_c and H_f resonate at highest field (δ = 1.11 and 0.77 ppm respectively). The protons H_c are found as a triplet of doublets due to a large *geminal* coupling (^2J = 11.8 Hz) to H_b and an identical *vicinal* coupling to H_d. The doublet splitting is due to the small *axial-equatorial* coupling to H_a. The quartet splitting of H_f can be attributed to identical *geminal* and *vicinal*

[§] The interpretation of the *trans*-tach spin system as pseudo first order also applies to the spectra recorded upon metal coordination (Chapter **3.4.3** and **3.5**) and Schiff base derivatisation (Chapter **3.6**).

couplings ($^{2,3}J$ = 11.8 Hz) to H_e and H_d, respectively. An overview of the coupling pattern and the resulting spin multiplicities is given in Figure 29.

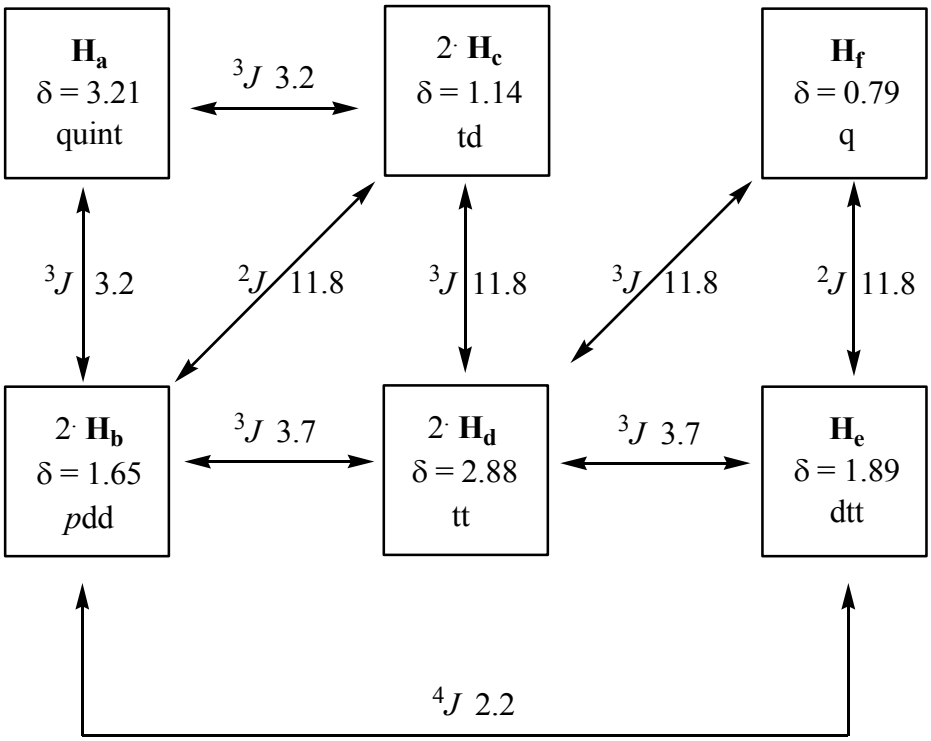

Figure 29 Coupling constants *J* /Hz as absolute values and chemical shifts *δ* /ppm for *trans*-tach (**29**).

3.2 Crystal structures of trans-tach · 3 HX (X = Cl, Br, NO_3, ClO_4)

Further to the analysis of the non-protonated ligand described in the previous chapter, four crystal structures of *trans*-tach as *tris*-protonated salts with chloride, bromide, nitrate and perchlorate counterions were obtained. These crystal structures unambiguously confirm the *cis,trans* orientation of the three primary amino groups on the cyclohexane ring. The ligand adopts the more stable non-flipped conformation with one amino group in *axial* and two in *equatorial* positions (Figure 30).

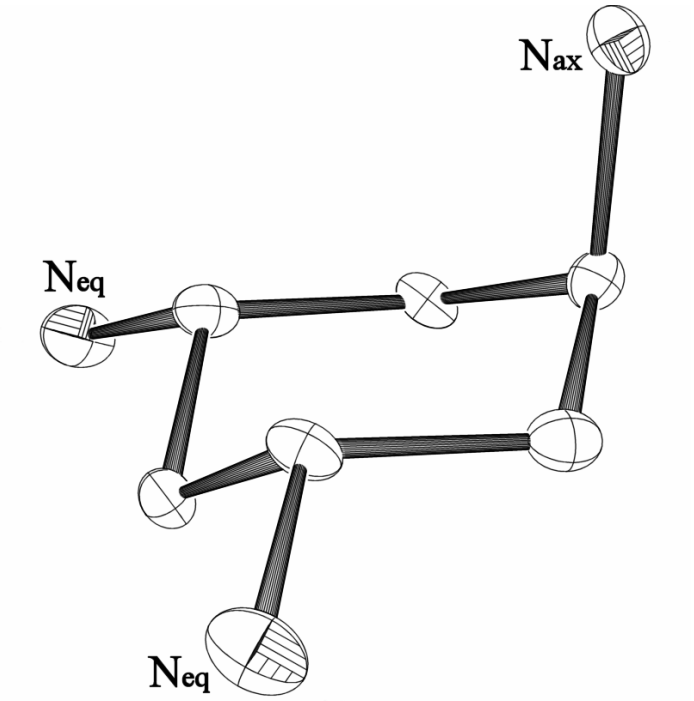

Figure 30 *Tri*-cation of *trans*-tach. The bis*equatorial*-mono*axial* conformation of the three amino residues can be seen clearly. Counterions are omitted for clarity.

A common feature in the crystal packing of the tri-cationic *trans*-tach ligand with the four counterions chloride, bromide, nitrate and perchlorate is the presence of 3-dimensional hydrogen-bonded networks. The arrangement of the cations in the lattice, however, depends strongly on the counterion. In case of chloride and perchlorate counterions, one water molecule is incorporated within the lattice for each ligand, whereas bromide and nitrate do not incorporate any solvent molecules into the crystal lattice. The cationic arrangement for the chloride, bromide and nitrate salts along the crystallographic *a* and *b* axes are shown in Figure 31. The ligands are packed hexagonally along the *a* axis and particularly noteworthy are the 'pairs' of ligands facing each other in the chloride salt. For both chloride and bromide salts, the *axial* amino groups are oriented parallel to the *a* axis, projecting *trans*-tach as regular hexagons onto the *bc* plane, whereas in the nitrate salt, the orientation of *trans*-tach is somewhat twisted. Along the crystallographic *b* axis, *trans*-tach is arranged in layers in the chloride and bromide salts projecting the *equatorial* amino groups onto each other, whereas in the nitrate salt, the ligand is twisted and arranged hexagonally. The arrangement of the ligand in the perchlorate salt is somewhat different. The cations are arranged in layers along the crystallographic *a* and *c* axes and arranged hexagonally along the *b* axis.

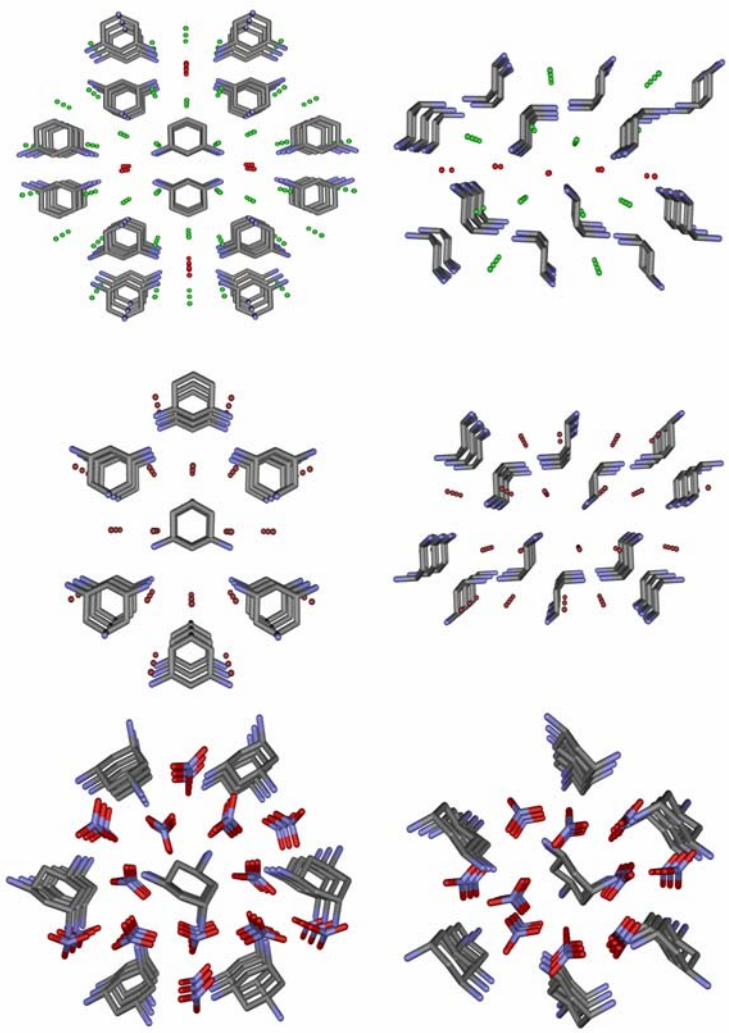

Figure 31 Crystal packing of *trans*-tach • 3 HX along the *a* (*LHS*) and *b* (*RHS*) axis. X = Cl (*Top*), Br (*Centre*) and NO_3 (*Bottom*). Nitrogen is shown in light blue, chloride in green, bromide in maroon, oxygen in red and carbon in grey.

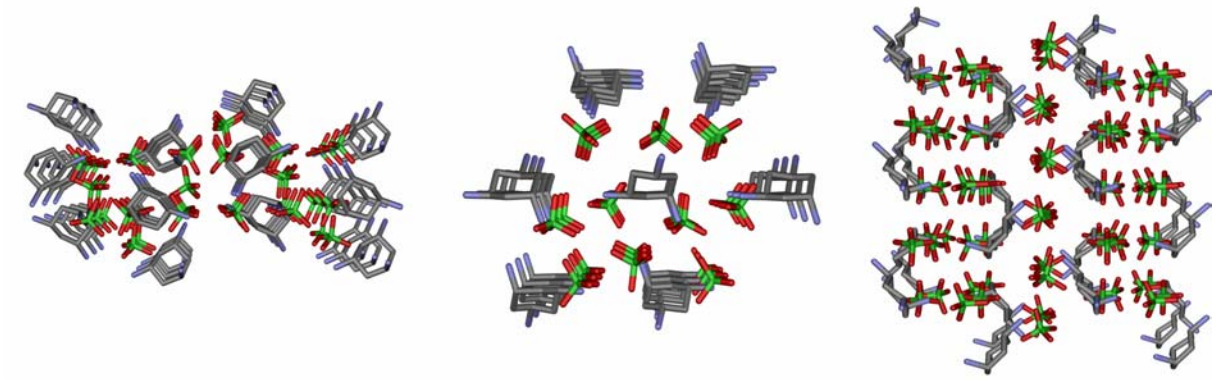

Figure 32 Crystal packing of *trans*-tach • 3 $HClO_4$. View along the crystallographic *a* (*left*), *b* (*centre*) and *c* (*right*) axes. Solvent molecules are omitted for clarity. Nitrogen is shown in light blue, chloride in green, oxygen in red and carbon in grey.

3.3 *trans*-Tach as a ligand in coordination chemistry

The cyclohexane ring structure gives *trans*-tach the rigidity needed to form supramolecular architectures. In both conformations of *trans*-tach, the more stable bis*equatorial*-mono*axial* conformation (Figure 33, *LHS*) and in the ring-flipped bis*axial*-mono*equatorial* conformation (Figure 33, *RHS*), either the *cis*- or the *trans*- donor set lies within the cyclohexane ring plane with the other arranged perpendicular to the plane, thus preventing coordinative interactions to the same metal centre. In the non-flipped form, *trans*-tach can act as a μ_3-bridging, *tris*-monodentate ligand as observed in the complexes of the closed-shell transition metals silver(I) and zinc(II) (see Chapter 3.5). Coordination to open-shell transition metals such as nickel(II), copper(II) and palladium(II) (see Chapter 3.4) occur *via* the ring-flipped conformation, whereby *trans*-tach can act as a μ_2-bridging ligand providing a bidentate chelating moiety with its two *cis*-*axial* amino groups and a monodentate coordination site *via* the *trans*-*equatorial* amino group.

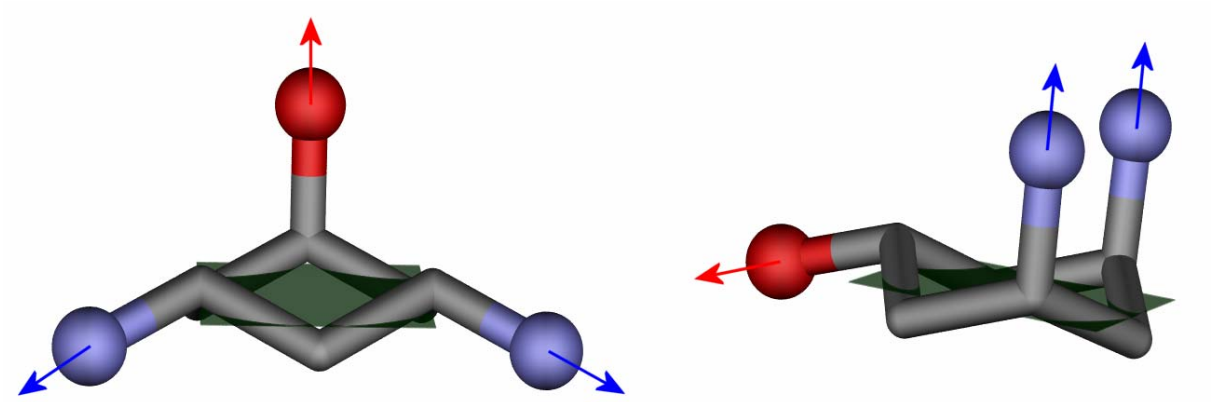

Figure 33 *trans*-tach in its two conformations. The two *cis* amino groups are shown in light blue, the *trans* amino group in red. *LHS*: non-flipped conformation with *tris*-monodentate coordination sites. *RHS*: ring-flipped conformation with *cis*-bidentated chelating and *trans*-monodentate coordination sites. The green plane represents the mean plane of the cyclohexane ring atoms, showing the orientation of *cis*- and *trans*- amino groups within or perpendicular to the plane for both conformations.

Of particular interest for constructing supramolecular architectures is the coordination of *trans*-tach in its ring-flipped conformation. Not only are the *cis*- and *trans*- coordination sites *non-interacting*, they are also *non-equivalent* due to the *cis*-bidentate ('Head') and *trans*-monodentate ('Tail') binding sites. This non equivalency results in a differentiation of both

binding sites upon complexation since coordination to the bidentate chelating moiety is entropically favored.[43]

Contrary to the rigidity of the cyclohexane ring, a certain degree of flexibility is given upon coordination to the primary amino groups. This flexibility is expressed by the ability of the ligand to accommodate strained coordination environments. One important measure is the compressibility of the six membered metallacycle formed upon 'Head' chelation. This flexibility is demonstrated by variation of the interplanar angle Θ (Figure **34**, blue) between the coordination plane of the chelated metal M^c (plane A) and the mean plane of the two *axial* nitrogens and their corresponding methine carbons (plane B). The smaller the angle Θ becomes, the more regular the metallacyclic chair conformation is and the more the metal ion is orientated towards the cyclohexane centre, resulting in an overall compressed structure. Additional flexibility is given to the molecule upon coordination of the 'Tail' amino group, which is expressed by torsion around the C-N bond of the pendant amino group (Figure **34**, red). This torsion describes the relative position of the coordinated metal ion with respect to the centre of the cyclohexane ring. Free rotation principally allows every value between ±180°. *Syn*-periplanar and *syn*-clinal values ($0 \leq |\chi| \leq 90°$) represent the metal ion pointing below the cyclohexane mean plane, whereas *anti*-clinal and *anti*-periplanar angles ($90 \leq |\chi| \leq 180°$) indicate the metal centre located above the cyclohexane ring. A comparison of the angles Θ and χ for all complexes is given in the supplementary data and discussed for each structure where appropriate.

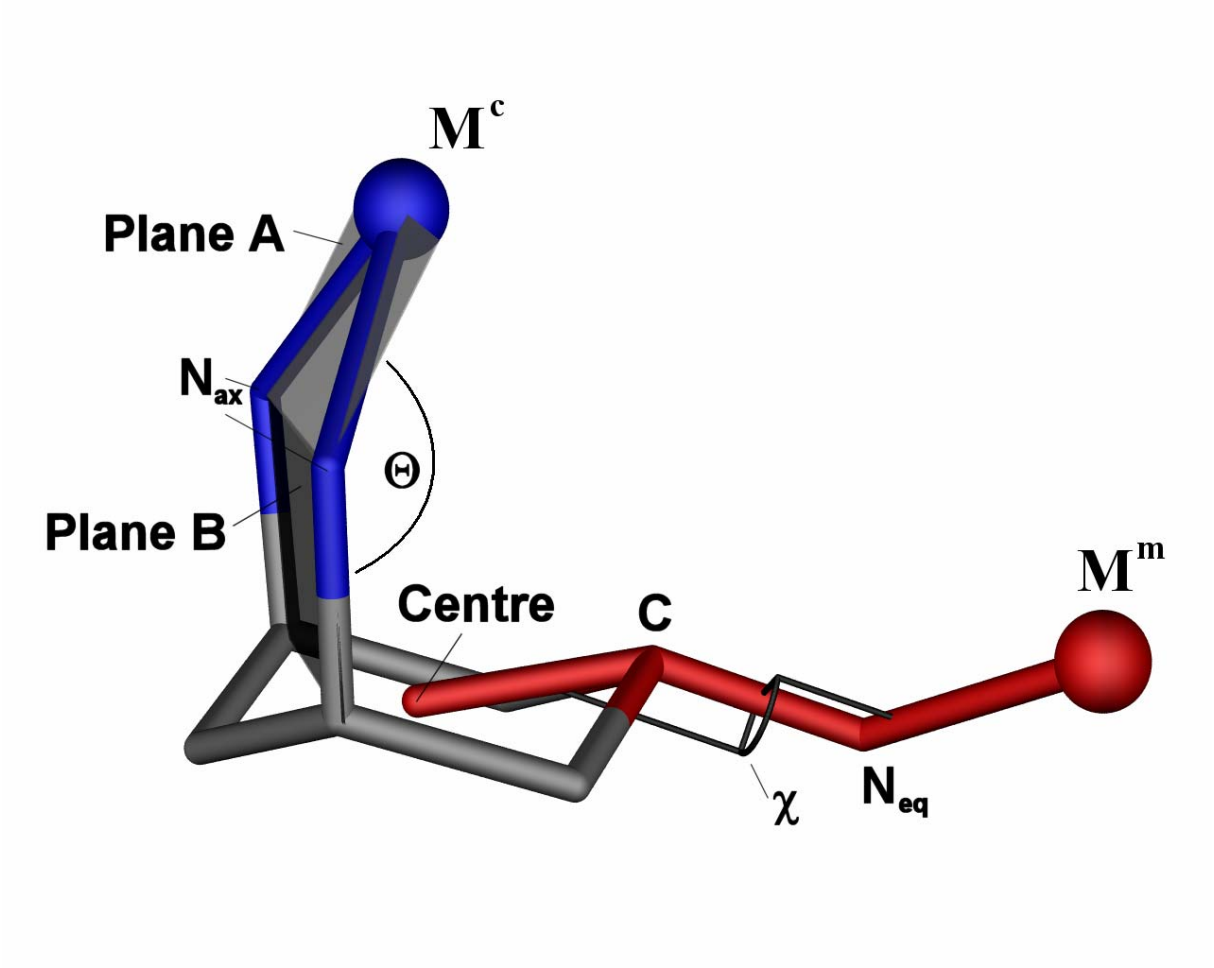

Figure 34 Interplanar angle Θ (blue) between planes A and B. Plane A is the coordination plane of the chelated metal M^c; plane B is the mean plane of the two nitrogens N_{ax} and the corresponding methine carbons. Torsion angle** χ (red) lies between the centre of the cyclohexane ring, carbon C, nitrogen N_{eq} and metal M^m.

It is shown for multi-amine donor ligands, that partial protonation of donor moieties influences the geometry of the resulting complex.[147] Further interest lies therefore in controlling the protonation state of the three amino groups of *trans*-tach. Protonation of non-coordinating amino moieties also increase the acceptor abilities for hydrogen-bonded interactions. These intermolecular interactions facilitate the formation of supramolecular architectures as observed upon copper(II) coordination (Chapter 3.4.2). In order to evaluate the pH range in which selective protonation occurs, preliminary pH titrations of *trans*-tach determined the pK_a values to pK_{a1} = 4.5, pK_{a2} = 7 and pK_{a3} = 9. These values are

** The torsion angle χ can also be applied to the non-flipped conformation of *trans*-tach, resulting in one *axial* and two *equatorial* values.

approximations, particularly with respect to pK_{a2} and pK_{a3} differing by only two pK_a units. However, the values broadly agree with other triprotic amino systems such as *cis*-3,5-diaminopiperidine (pK_a = 4.21, 7.56 9.47), *cis*-3,4-diaminopyrrolidine (pK_a = 2.96, 6.63, 9.90) and *trans*-3,4-diaminopyrrolidine (pK_a = 4.19, 6.72, 9.80).[134,148] A detailed pK_a analysis proved to be difficult due to complicated speciation equilibria in solution. The principal speciation for a triprotic ligand **A** with three equivalent hydrogen donor groups is shown in Figure 35.[160,161] This example shows the pH dependence of the fractional composition of species in solution.[††] The three pK_a equilibrium constants are separated by more than 4 magnitudes of pH. Because of this large separation, the pK_a values are identical with the pH values at intersection points of two species. Additionally, the maximum for each species lies half-way between adjacent equilibrium constants.

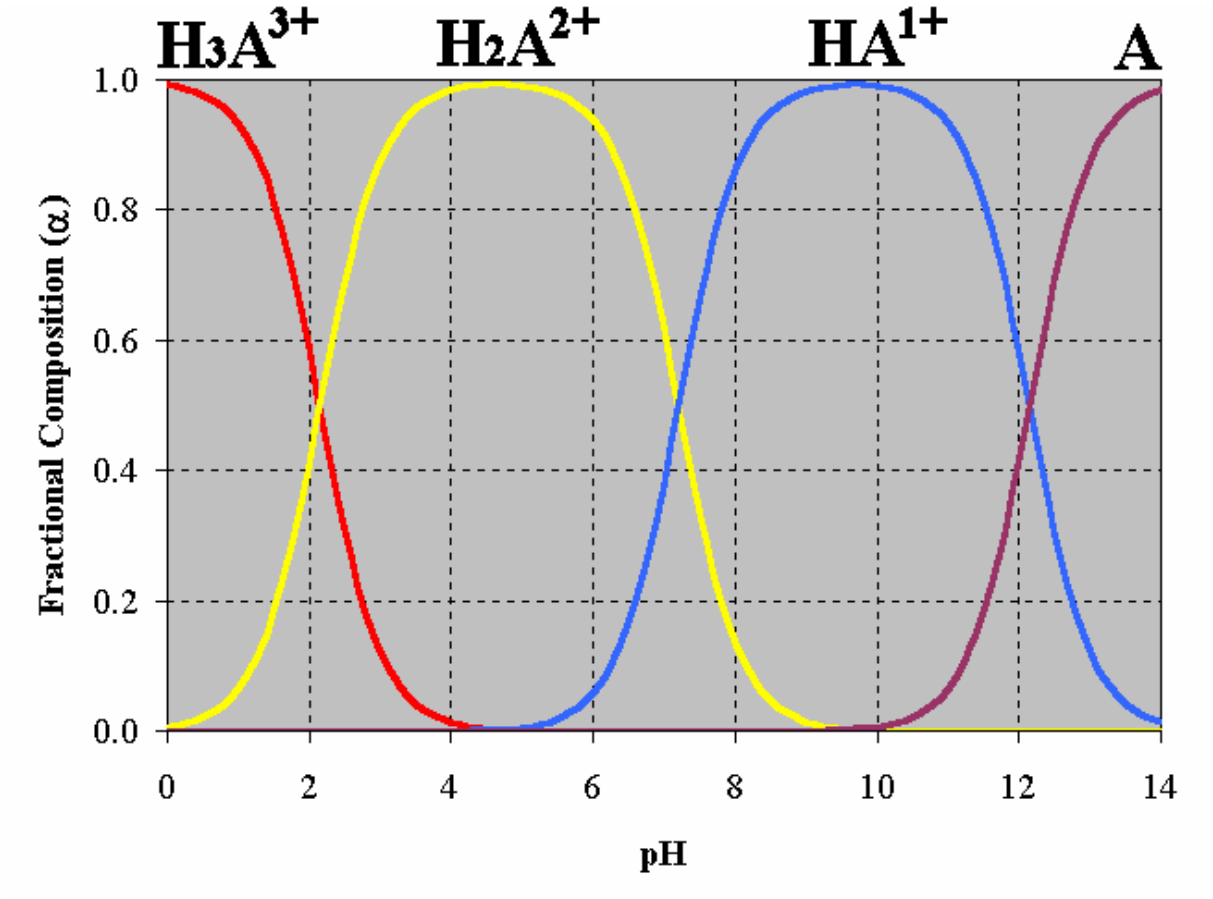

Figure 35 Speciation example of a triprotic ligand **A** with equivalent hydrogen donor groups.

[††] A detailed description of the speciation equilibria of the example ligand **A** is given in the supplementary data.

In case of *trans*-tach (**L**), the equilibria are more complicated and the pK_a values are not as well resolved as in the example ligand **A**. Assuming *trans*-tach in the non-flipped conformation as confirmed by ^{1}H-NMR spectroscopy, the inequivalent *equatorial* and *axial* amino groups result in six micro-species with statistically varying probabilities upon protonation (Figure 36). Earlier studies have shown on both cyclic[148] and linear triamines,[162,163] that the basicity of primary and secondary amino groups are of the same magnitude. It is therefore anticipated that the difference in basicity between the *equatorial* and *axial* amino groups in the *trans*-tach system are negligable and the protonated species in solution are statistically distributed.

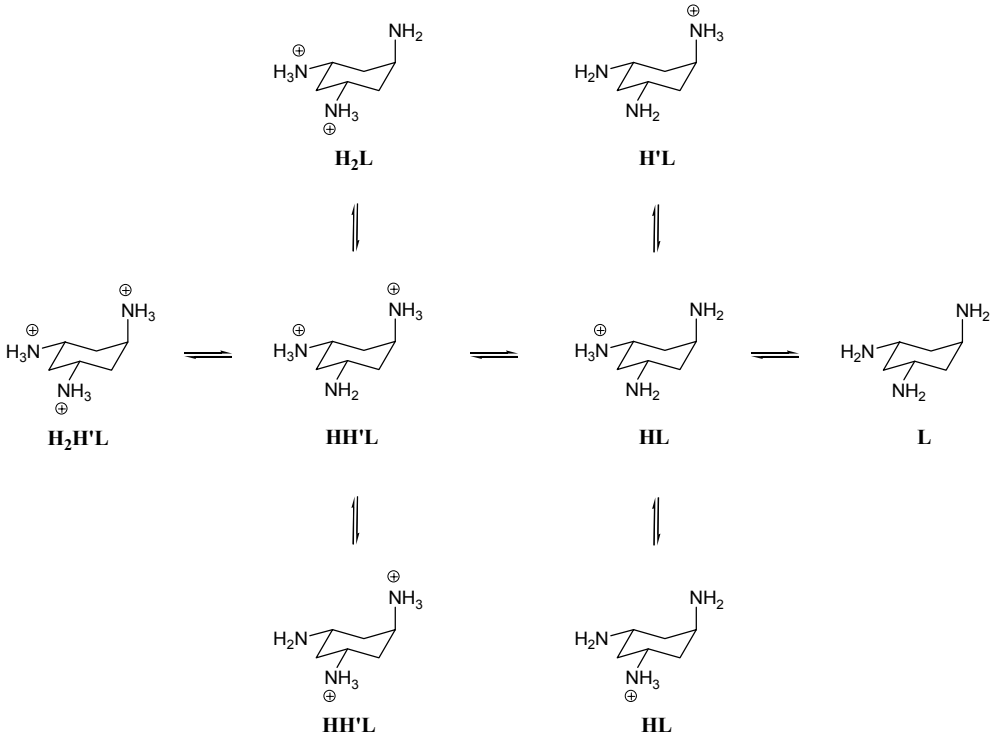

Figure 36 Speciation equilibria of *trans*-tach (**L**) upon protonation in its non-flipped conformation. H, H' indicate protonation of the *equatorial* and *axial* amino groups respectively. Six micro-species with varying probability are expected: $H_2H'\mathbf{L}^{3+}$: $H_2\mathbf{L}^{2+}$: 2•$HH'\mathbf{L}^{2+}$: 2•$H\mathbf{L}^{1+}$: $H'\mathbf{L}^{1+}$: **L**.

Furthermore, metal complexation to multi-donor ligands results in *coordinative* speciation in solution.[134,148] These coordinative interactions additionally influence the protonation equilibria, complicating the overall speciation of *trans*-tach beyond the scope of this thesis. This work therefore concentrates on solid state analysis of the labile transition metal complexes with nickel(II), copper(II), zinc(II) and silver(I) and also solution analysis in the case of the more inert palladium(II) complexes.

3.4 Open shell TM coordination chemistry

Although *trans*-tach was first synthesised in 1957, it was not until 2002 that the first crystal structure of *trans*-tach metal complexes was reported.[164] Following on this work, a variety of complexes were crystallographically characterised in order to evaluate the ligand as a potential building block in supramolecular chemistry. Of particular interest are the geometric coordination preferences of metals with varying kinetic labilities upon coordination to this bidentate chelating ligand. Coordination chemistry of *trans*-tach to copper(II) ions, as discussed in chapter 3.4.2, exemplifies the formation of labile complexes with a variety of potential coordination geometries. In contrast, palladium(II) represents kinetically inert coordination with a preferred square planar coordination as discussed in chapter 3.4.3. Confirmation of the proposed structure of the *trans*-tach - nickel(II) nitrate complex is of particular academic interest, since titration with nickel(II) nitrate has been used to separate the two tach isomers since 1968.[158]

3.4.1 Nickel(II) coordination 34 and 35

Upon separation of both tach isomers *via* complexation with nickel(II) nitrate, the octahedral coordinated *bis*(*cis*-tach)nickel(II) nitrate complex **33** precipitates first from a methanolic solution as a pink solid. After removal of the *cis*-isomer from solution, the more soluble orange *bis*(*trans*-tach)nickel(II) nitrate complex **34** starts to precipitate. The structure of complex **33** has been reported in 1979[165] as an octahedral coordinated nickel(II) ion with two *face* capping *cis*-tach ligands (Figure 37, *RHS*). However, no structure with the *trans*-isomer is in the literature. Crystals of the *bis*(*trans*-tach)nickel(II) nitrate **34** • 2 HNO_3 were obtained by slow diffusion of ether into a methanolic solution of nickel(II) nitrate and *trans*-tach. The orange crystals obtained were suitable for single crystal X-ray analysis and exhibit two *trans*-tach ligands coordinating in a bidentate fashion to a square planar nickel(II) ion. The structure confirms the originally proposed *anti* arrangement of the protonated pendant amino residues (Figure 37, *LHS*).

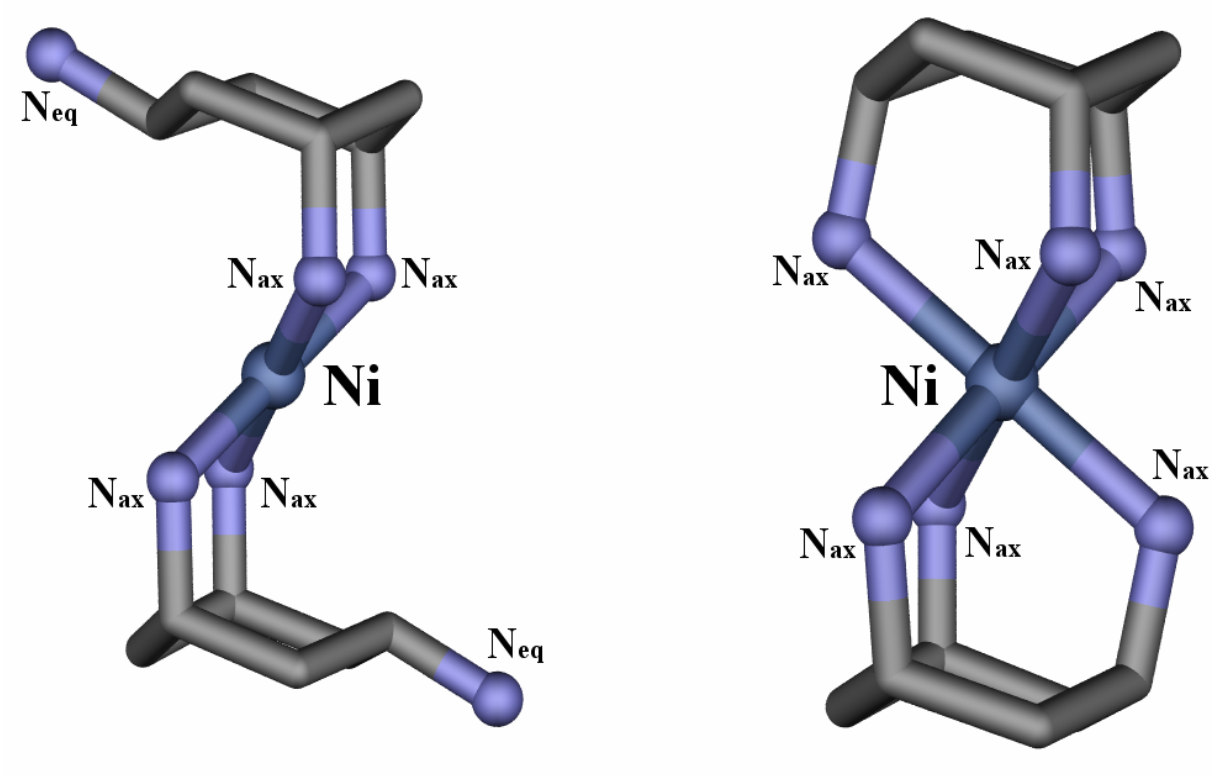

Figure 37 Comparison of nickel(II) nitrate cations of both *trans*- (*LHS*) and *cis*- (*RHS*) tach isomer. Nickel(II) is shown as dark blue, nitrogen as light blue spheres carbon is grey. *LHS*: square planar coordination with two *axial* amino groups coordinating each *trans*-tach **34** · 2 HNO_3. *RHS*: octahedral environment with three coordinating *axial* amino groups each *cis*-tach **33**.

An identical coordination motif is obtained upon complexation with nickel(II) chloride (**35**). The nickel(II) ion coordinates two *trans*-tach ligands through their bidentate chelating moiety in an *anti*-arrangement of the pendant residues. The non-coordinating amino residues are, however, not protonated as confirmed by elemental analysis on the crystalline material. Both cations adopt the most compressed conformations observed in this work for *trans*-tach, with the lowest interplanar angles Θ being 140.4° (**34** · 2 HNO_3) and 141.2° (**35**) (Figure 38). The similar compression is further illustrated by nearly identical centroid separations of the *anti*-orientated ligands by 5.71 and 5.68 Å, respectively.

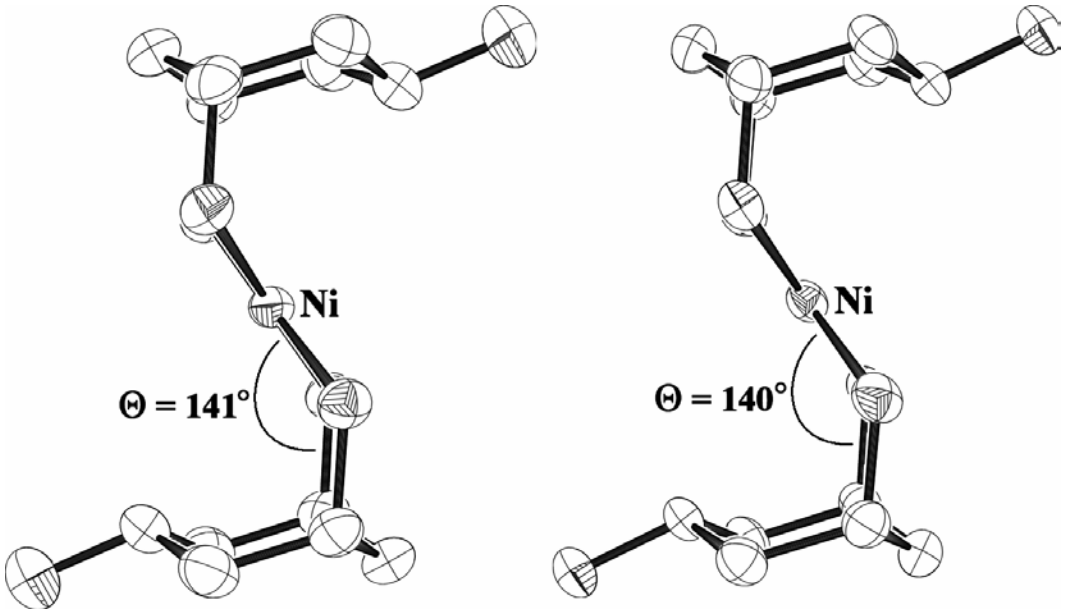

Figure 38 Ortep-3 representation of the diligand cations of $[Ni(\mathbf{L})_2]Cl_2$ (**35**, *LHS*) and $[Ni(\mathbf{L}H)_2](NO_3)_4$ (**34** • 2 HNO_3, *RHS*) at 50% thermal ellipsoids. Counterions and solvent molecules are omitted. The similar compression in both structures can be seen clearly.

The crystal structures of both complexes comprise 3-dimensional hydrogen-bonded networks. The network of **35** (Table 1) comprises less extensive hydrogen-bonded interactions than complex **34** • 2 HNO_3 (Table 2). Influencing factors on the formation of extended hydrogen–bonded networks presumably include the difference in hydrogen acceptor capabilities for the mono-atomic chloride counterions in comparison to the three oxygen atoms in the nitrate counterions. Another factor might be the influence of the protonated pendant amino residues in **34** • 2 HNO_3 compared to the non-protonated amino groups in **35**.

Table 1 3-D-hydrogen-bonded network[166] (Å /°) for $[Ni(\textit{trans}\text{-tach})_2]Cl_2$ (**35**)

D-H ··· A	D-H	H ··· A	D ··· A	D-H ··· A
N(1) – H(1A) ··· Cl(1)[a]	0.90	2.42	3.298(3)	166
N(1) – H(1B) ··· Cl(1)[b]	0.90	2.44	3.336(4)	171
N(2) – H(2A) ··· O(3)[b]	0.90	2.05	2.950(5)	175
N(2) - H(2B) ··· Cl(1)[c]	0.90	2.44	3.315(4)	163
N(3) - H(3B) ··· Cl(1)[d]	0.89	2.77	3.634(4)	164
N(3) - H(3C) ··· O(2)	0.89	1.94	2.834(6)	177

N(3) represents the pendant amino group nitrogen atom, Cl(1) the chloride counterion, O(2) and O(3) solvent water molecules.

Symmetry Code: a) 1/2-x,-1/2+y,1/2-z; b) 1/2+x,1/2-y,1/2+z; c) 3/2+x,1/2-y,1/2+z; 1+x,y,z.

Table 2 3-D-hydrogen-bonded network[166] (Å /°) for $[Ni(trans\text{-}tachH)_2](NO_3)_4$ (**34** • 2 HNO_3)

D-H ··· A	D-H	H ··· A	D ··· A	D-H ··· A
N(1) - H(1A) ··· O(1)[a]	0.90	2.45	2.979(2)	139
N(1) - H(1B) ··· O(4)[a]	0.90	2.45	3.013(3)	142
N(2) - H(2A) ··· O(5)[b]	0.90	2.20	3.038(3)	155
N(2) - H(2A) ··· O(6)[b]	0.90	2.45	3.239(3)	146
N(2) - H(2B) ··· O(2)[c]	0.90	2.06	2.924(2)	160
N(3) - H(3A) ··· O(3)[d]	0.89	2.09	2.902(2)	151
N(3) - H(3B) ··· O(5)[c]	0.89	1.96	2.846(2)	177
N(3) - H(3C) ··· O(2)	0.89	2.41	3.090(2)	132
N(3) - H(3C) ··· O(3)	0.89	2.11	2.977(2)	163

N(3) represents the pendant amino group nitrogen atom. O(1)-O(6) the oxygen atoms of the nitrate counterions.

Symmetry Code: a) 1+x,y,1+z; b) 2-x,-y,1-z; c) 1-x,-y,1-z; d) x,1/2-y,1/2+z.

The stronger hydrogen-bonded interactions in **34** • 2 HNO_3 result in a packing array with a calculated density of 1.669 g/cm^3. In comparison, the calculated density for **35** is only 1.341 g/cm^3. The looser packing of **35** with fewer counterions, due to non-protonated amino residues, is compensated for by incorporation of five water molecules in the crystal lattice per complex unit. Both complexes arrange in hexagonal layers along the crystallographic *a* axis. The more dense packing of **34** • 2 HNO_3 can be seen in Figure 39, *Top*. Complex **35** is also hexagonally packed along the *c* axis, whereas **34** • 2 HNO_3 is packed in layers held together by hydrogen-bonded interactions to the nitrate counterions (Figure 39, *Bottom*).

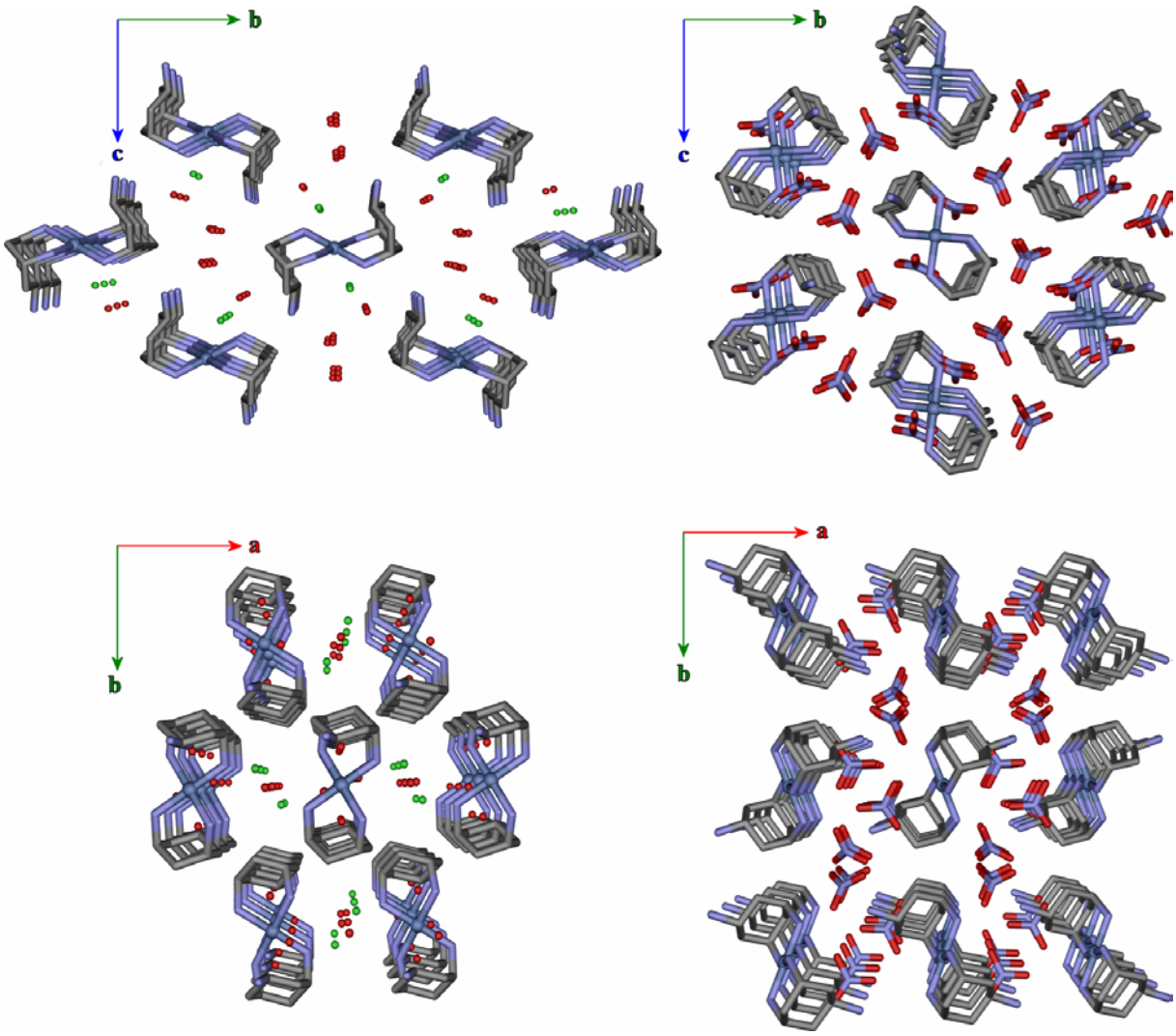

Figure 39 Packing along the crystallographic *a* (*Top*) and *c* (*Bottom*) axis of *anti*-diligand complexes **35** (*LHS*) with non-protonated amino residues and **34** · 2 HNO_3 (*RHS*) with protonated pendant amino moieties. Nickel(II) is shown as dark blue spheres, nitrogen in light blue, chloride in green, oxygen in red and carbon in grey.

3.4.2 Copper(II) coordination

The coordination chemistry of *trans*-tach (**L**) with copper(II) has proven particularly fruitful in demonstrating the ligand's application as a supramolecular building block. A variety of complexes, primarily mono- and diligand species, were obtained upon ring-flip to the bis*axial*-mono*equatorial* conformation. Complexation reactions were carried out with copper(II) -nitrate, -bromide, chloride, -fluoride and -sulphate. Each of these reactions at the unadjusted pH of *trans*-tach (pH 11.0) resulted in the formation of diligand complexes with

both *syn*- and *anti*- orientation of the pendant amino residues. Protonation[‡‡] of the pendant amino group causes these complexes to form an interesting variety of secondary structures. Both [Cu(*trans*-tach)$_2$](NO$_3$)$_2$ and [Cu(*trans*-tach)$_2$Br]Br diligand species fragment upon protonation to form monoligand, mononuclear species.

Protonation of [{Cu(*trans*-tach)$_2$}$_2$Cl]Cl$_3$ on the other hand, also results in the fragmentation of the diligand complex to a monoligand unit but effects the formation of a trinuclear array. This secondary structure makes use of a trigonal planar μ_3 bridging chloro ligand around which three mononuclear copper-protonated tach units assemble. This is the first structure reported in which such a trigonal planar μ_3 bridging chloro ligand with open shell transition metals is observed.

Protonation of [Cu(*trans*-tach)$_2$F]F leads to the self-assembly of the first known copper fluoro cubane. Each cubane is constructed from four monoligand copper fluoro units, resulting in a discrete tetranuclear structure. These units form a three-dimensional nanoporous cubic network due to hydrogen-bonded interactions between the protonated pendant amines and fluoride counterions. Interesting to note is that the fluoride counterions are partially incorporated into the network structure, which exhibits 11 Å voids in all three dimensions.

Contrary to the above complexes, protonation of the diligand [Cu(*trans*-tach)$_2$(SO$_4$)] complex maintains the *syn* diligand arrangement around the copper centre with the pendant amino groups protonated. These protonated amines form strong hydrogen-bonded interactions to sulphate counterions and methanol solvent molecules, resulting in a three-dimensional hydrogen-bonded array comprising one-dimensional channels of 15 Å in diameter. Contrary to the cubane structure, all counterions are incorporated into the network structure.

It is interesting to note that some of the pendant amino residues are also protonated in crystal structures obtained from reactions at unadjusted pH. These observations are in accordance with a drop in pH upon addition of copper(II) to the methanolic *trans*-tach solution. The reduced pH enables protic speciation and crystallisation in the protonated form.

---

‡‡ pH values were measured in mixed methanol / water solutions. Control measurements in pure aqueous solutions were in good agreement with the obtained values of the mixed solvent systems.

3.4.2.1 Copper(II) nitrate

3.4.2.1.1 $Cu(NO_3)_2$ at unadjusted pH, complex 36 • 0.5 HNO_3

Reaction of *trans*-tach with copper(II) nitrate at unadjusted pH results in the formation of the diligand complex **36**. Two ring-flipped *trans*-tach ligands coordinate to the copper(II) ion in a bidentate fashion with the pendant amino residues positioned *anti* to each other. Complex **36** crystallises as its *tris*-nitrate salt with half of the pendant amino moieties protonated. Interestingly, the asymmetric unit of the crystal structure contains two independent diligand units with notable differences. The crystallographically independent complex cations vary in their corresponding interplanar angles Θ by 20° (Figure 40). This separates the centroids of the *anti*-orientated ligands by 5.96 and 6.32 Å, resulting in a more compressed arrangement for Cu1. This remarkable difference in structural compressibility within a single crystal lattice demonstrate the geometric flexibility of *trans*-tach coordination. The Cu1 (red) and Cu2 (blue) cationic units arrange in alternating layers within the crystal lattice (Figure 41).

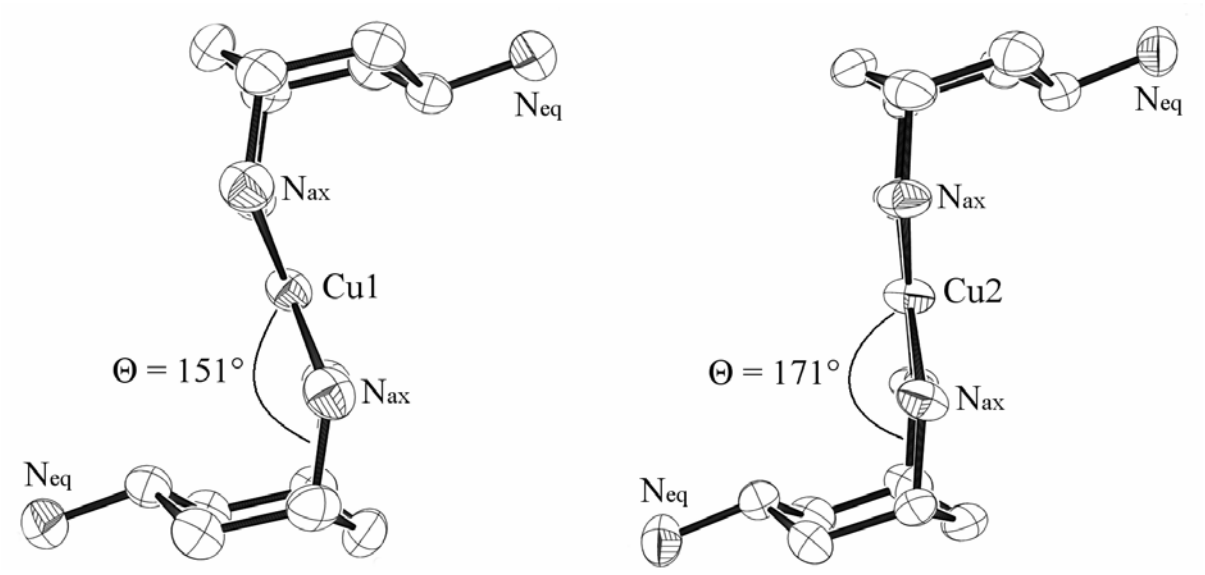

Figure 40 Ortep-3 representation of the two crystallographically independent diligand cations of $[Cu(\mathbf{L})_2](NO_3)_2$ • 0.5 HNO_3 (**36** • 0.5 HNO_3) at 50% thermal ellipsoids. Counterions and solvent molecules are omitted. The different compression in both structures can be seen clearly.

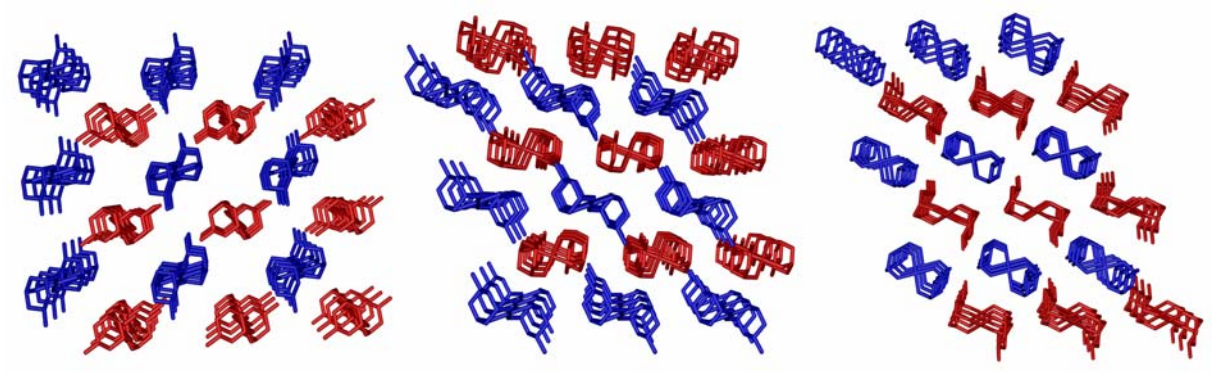

Figure 41 Crystal packing of **36** · 0.5 HNO_3 along the crystallographic *a* (*Left*), *b* (*Centre*) and *c* (*Right*) axes. The layers of the two crystallographically independent cationic complexes can be seen clearly. Solvent molecules and counterions are omitted for clarity. Cu1 unit is shown in red, Cu2 unit in blue.

3.4.2.1.2 $Cu(NO_3)_2$ adjusted to pH 6.5 with nitric acid 37

In the case of complexation to copper(II) nitrate, reducing the pH of the amine solution to 6.5 with nitric acid before complexation results in the formation of the monoligand complex **37**. In this complex, the pendant amino residue is protonated and the copper(II) ion is chelated by *trans*-tach in the ring-flipped conformation. Three nitrato ligands complete the tetragonal pyramidal coordination sphere ($\tau = 0.06$).[§§,167] The apical copper(II) oxygen bond is elongated ($Cu\ldots O_{ap} = 2.450$ Å) with respect to the basal coordinating nitrato ligands ($Cu\ldots O_{bas}$ =1.991 and 2.032 Å), indicating a distortion along this axis. Complex **37** is packed in alternating layers along the crystallographic *a* (*Left*), *b* (*Centre*) and *c* (*Right*) axes (Figure 43).

[§§] τ lies between 0 and 1 : The structural parameter τ is calculated as $(\beta-\alpha)/60$ where α and β are the basal angles with β being the larger angle. This parameter describes coordination motifs with CN = 5, being closer to a tetragonal pyramidal ($\tau = 0$) or a trigonal bipyramidal ($\tau = 1$) coordination environment.

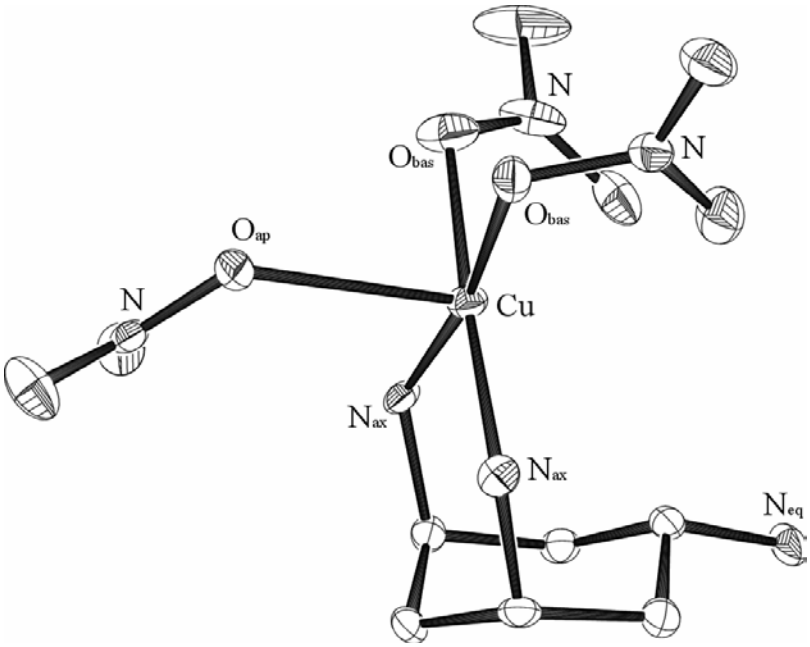

Figure 42 Ortep-3 representation of [Cu(**L**H)$(NO_3)_3$] (**37**) at 50% thermal ellipsoids. The tetragonal pyramidal coordination environment around the copper(II) ion can be seen clearly. Solvent molecules are omitted.

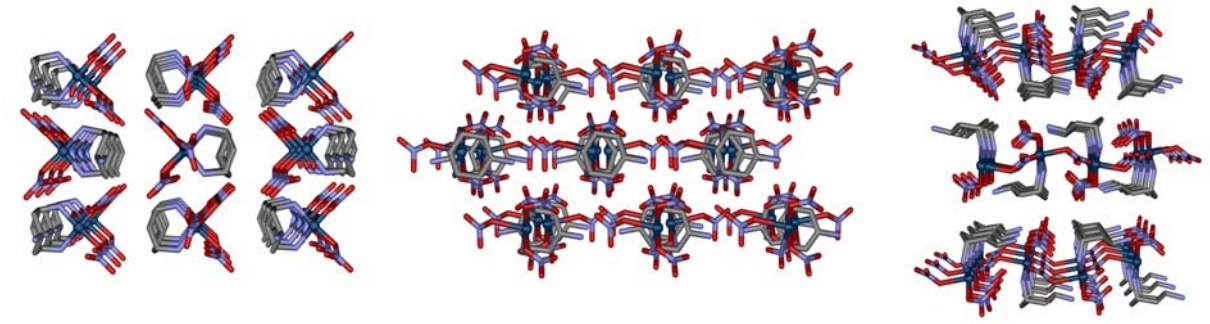

Figure 43 Crystal packing of **37** along the crystallographic *a* (*Left*), *b* (*Centre*) and *c* (*Right*) axes. The alternating orientation of **37** arranged in layers can be seen clearly. Copper(II) is shown in dark blue, nitrogen in light blue, oxygen in red and carbon in grey.

3.4.2.2 Copper(II) bromide

3.4.2.2.1 $CuBr_2$ at unadjusted pH, complexes *syn*-38, *twist*-38 and 39

Reaction of *trans*-tach with copper(II) bromide at unadjusted pH results in the formation of three different species, each isolated and characterised by single crystal X-ray crystallography. The structures represent diligand complexes with each copper(II) ion chelated by two *trans*-tach ligands. The complexes vary in the arrangement of the pendant

amino residues and by coordination to bromo ligands. Crystallisation by *diffusion* of ether into a methanolic solution of *trans*-tach and copper(II) bromide results in the formation of inseparable violet crystals of complexes *syn*-**38** and **39** in an estimated ratio of 1:1. In both structures, the pendant amino groups are orientated *syn* to each other. The cyclohexane rings are orientated in a parallel fashion, with centroid separations of 5.53 and 5.63 Å for syn-**38** and **39**, respectively (Figure 44, *Left* and *Right*). This results in a tetragonal planar copper(II) coodination for *syn*-**38**. The regular tetragonal pyramidal coordination sphere in **39** is completed by apical coordination to a bromo ligand ($\tau = 0.00$).[167] The long copper(II)-bromo distance of 2.945 Å lies beyond the van-der-Waals radii sum of copper(II) and bromide (2.61 Å),[168] but is still considered a bonding interaction, as compared to analogous copper(II) complexes.[169-173] The closest copper(II) *bromide* distance in the lattice of *syn*-**38** is 3.103 Å, yet further beyond the van-der-Waals radii sum of copper(II) and bromide. This interaction is, therefore, not considered to be a bonding contact. However, a search of the Cambridge Crystallographic Database (CSD) reveals one (!) complex, in which a tetra-nitrogen coordinated copper(II) ion with a distance of 3.106 Å is considered a bonding interaction.[174] It is therefore open to discussion whether *syn*-**38** and **39** are interpreted as unique complexes or as polymorphic crystals of the same complex.

Faster crystallisation by *layering* ether onto an identical methanolic reaction mixture as before results in the formation of the intermediate complex *twist*-**38**. This complex is formed within one hour of crystallisation and redissolves after 2-3 hours. Characterisation by single crystal X-ray crystallography of the extremely unstable crystals of *twis*t-**38** reveals the twisted geometry around the copper(II) centre (Figure 44, *Centre*). The coordination planes including the copper(II) ion and pairs of chelating nitrogen atoms are twisted by 37.3(5)° from an *anti*-arrangement of the two ligands with a cyclohexane centroid separation of 5.96 Å. Although the poor crystal quality does not allow a detailed analysis of the crystal packing or other intermolecular interactions, the coordination geometry around the heavy copper(II) ion is established crystallographically. Interestingly, the ether layered solutions from which the metastable complex *twist*-**38** crystallises, produces crystals of both *syn*-**38** and **39** overnight. Complex *twist*-**38** could be interpreted as the kinetic product which crystallises from the faster *layering* technique, which then over time rearranges to form the thermodynamically more stable *syn*-**38** and **39** structures.

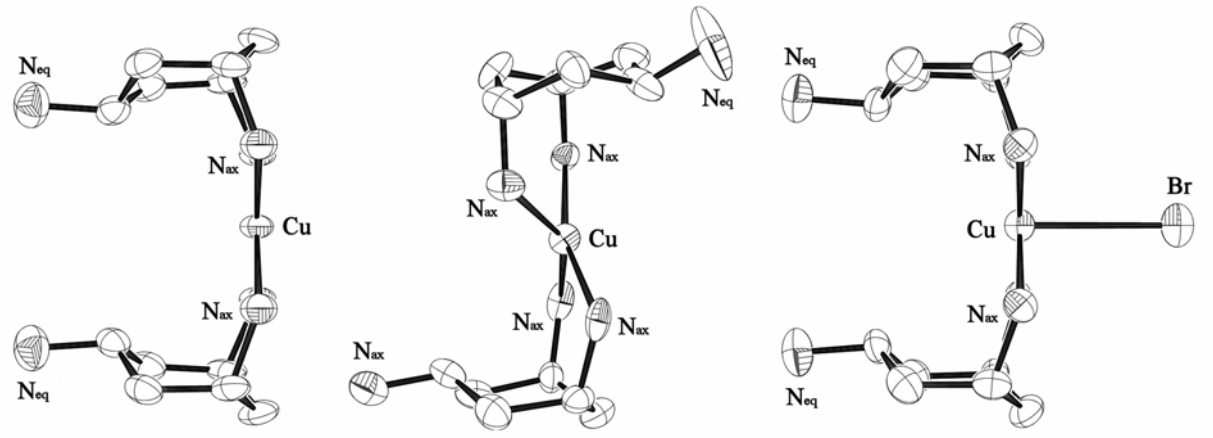

Figure 44 Ortep-3 representation of the three diligand cations of $[Cu(\mathbf{L})_2]Br_2$ (*syn*-**38**, *Left*), $[Cu(\mathbf{L})_2]Br_2$ (*twist*-**38**, *Centre*) and $[Cu(\mathbf{L})_2Br]Br$ (**39**, *Right*), at 50% thermal ellipsoids. Counterions and solvent molecules are omitted.

The crystal packing of *syn*-**38** and **39** is similar with respect to the relative arrangement of the diligand cations. **39** forms isolated 'back to back' dimeric units along the crystallographic *a* axis and arranges in alternating layers along the *b* and *c* axes (Figure 45).

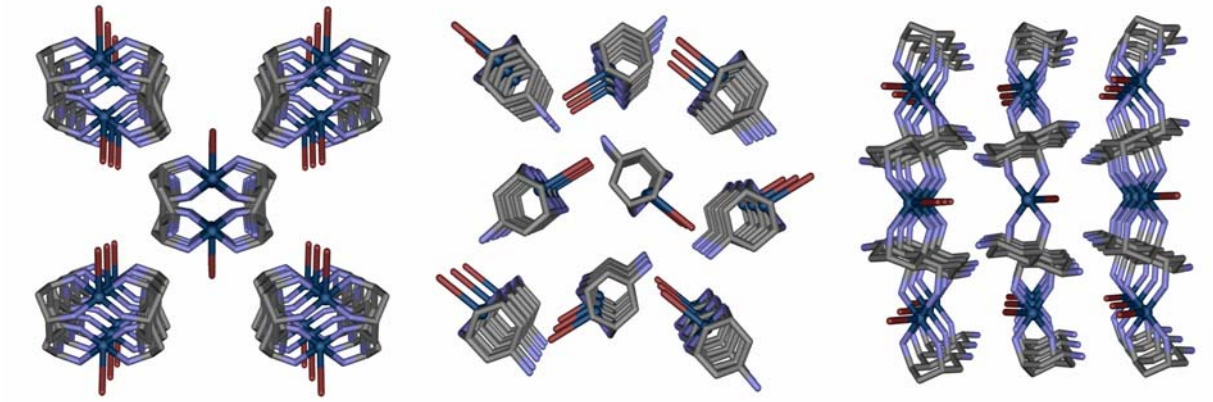

Figure 45 Crystal packing of **39** along the crystallographic *a* (*Left*), *b* (*Centre*) and *c* (*Right*) axes. Solvent molecules and counterions are omitted for clarity. Copper(II) is shown as dark blue spheres, nitrogen in light blue, bromide in maroon and carbon in grey.

3.4.2.2.2 $CuBr_2$ adjusted to pH 6.5 with hydrobromic acid 40

As observed in the case of the pH adjusted copper(II) nitrate reaction, a monoligand species is obtained upon reaction at reduced pH with copper(II) bromide.The mononuclear, monoligand complex **40** is formed when hydrobromic acid is used to reduce the pH of the amine solution

to pH 6.5. **40** comprises a tetragonal planar coordinated copper(II) ion by coordination of two terminal bromo ligands and the chelating amino groups of *trans*-tach in the ring-flipped conformation (Figure 46). The pendant amino residue is protonated and the complex crystallises as its hydrobromide salt.

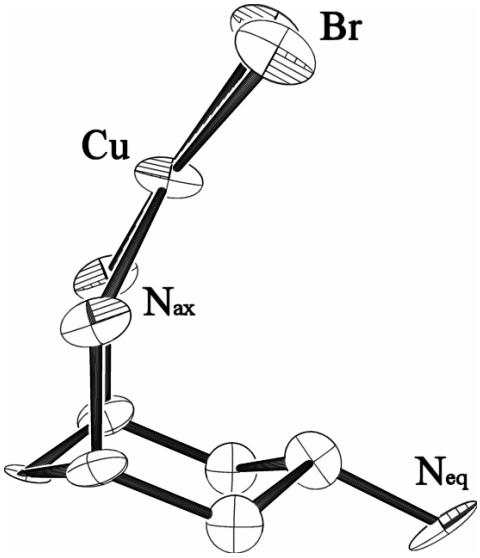

Figure 46 Ortep-3 representation of the monoligand cation of [Cu(**L**LH)Br_2]Br (**40**) at 50% thermal ellipsoids. Counterions are omitted.

The closest copper(II) bromide distance in the crystal lattice is 3.088 Å and therefore not considered as a bonding interaction. **40** shows alternating layer packing along the crystallographic *a* (*Left*), *b* (*Centre*) and *c* (*Right*) axes, as is shown in Figure 47.

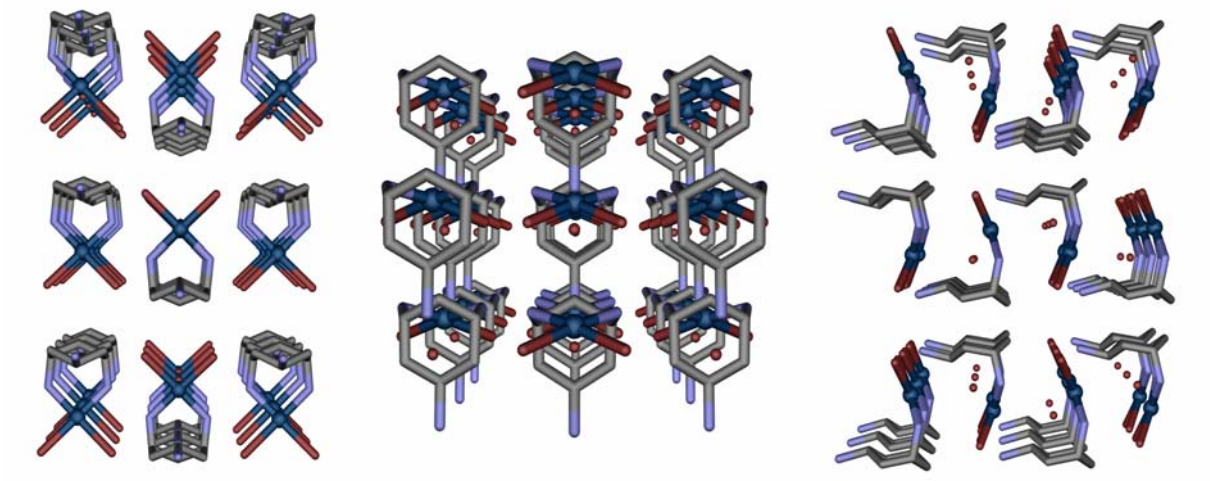

Figure 47 Crystal packing of **40** along the crystallographic *a* (*Left*), *b* (*Centre*) and *c* (*Right*) axes. The alternating orientation of **40** in layers can be seen clearly. Copper(II) is shown as dark blue spheres, nitrogen in light blue, bromide in maroon and carbon in grey.

Although reaction of copper(II) bromide acidified with hydrobromic acid leads to the mononuclear complex **40**, acidification with hydro*chloric* acid results in the formation of a trimeric copper(II) complex bridged by a trigonal planar μ_3-chloro ligand. This complex is structurally identical to the complex observed upon reaction at adjusted pH with copper(II) chloride. Both complexes are discussed in the following chapter.

3.4.2.3 Copper(II) chloride

3.4.2.3.1 $CuCl_2$ at unadjusted pH, complex 41 • 2 HCl

Reaction of *trans*-tach with copper(II) chloride at unadjusted pH results in the formation of the dinuclear copper(II) complex **41**. Two *trans*-tach ligands coordinate to each copper(II) centre in a *syn* fashion *via bis*-bidentate coordination, with the cyclohexane ring planes separated by 5.58 Å. Both copper(II) units are linked by a linear μ_2 bridging chloro ligand that completes the tetragonal pyramidal coordination around the copper(II) centres with $\tau = 0.07$[167] (Figure 48). As observed in the copper(II) nitrate complex at unadjusted pH, half of the pendant amino residues are protonated, crystallising as the dihydrochloride salt **41** • 2 HCl. The linear μ_2 chloro bridging motif between two copper(II) centres is rare and lies with a copper(II) chloro distance of 2.65 Å in the range observed for the few reported complexes.[175-179]

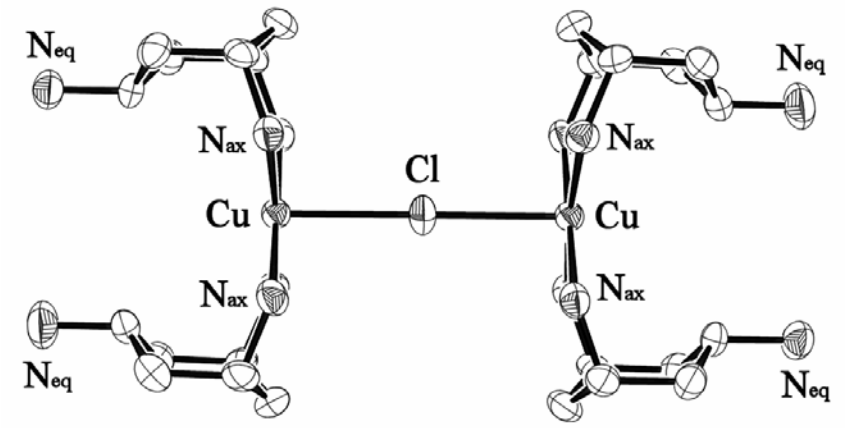

Figure 48 Ortep-3 representation of the dinuclear copper(II) cation of $[\{Cu(\mathbf{L})_2\}_2Cl]Cl_3$ (**41**) at 50% thermal ellipsoids. Counterions and solvent molecules are omitted.

The dinuclear copper(II) cations of **41** • 2 HCl arrange hexagonally along the crystallographic *a* axis. The packing of the crystal lattice is shown in Figure 49.

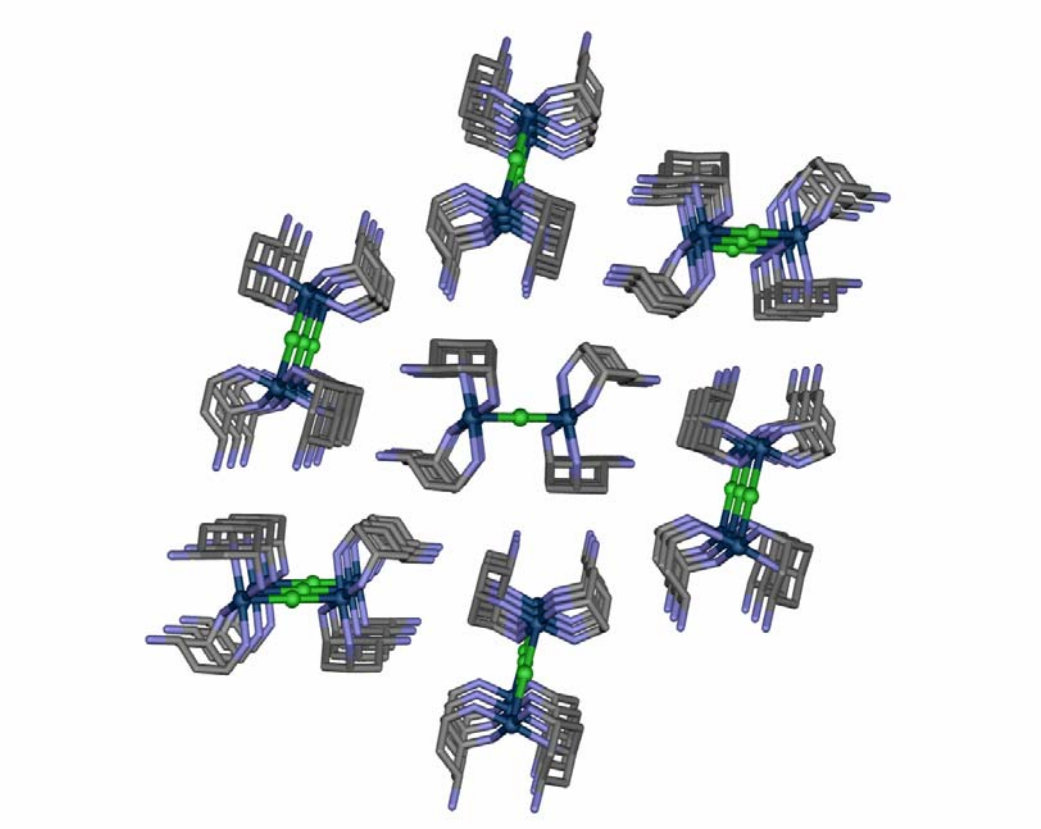

Figure 49 Crystal packing of **41** · 2 HCl along the crystallographic *a* axis. Counterions and solvent molecules are omitted. Copper(II) is shown as dark blue spheres, nitrogen in light blue, chloride in green and carbon in grey.

3.4.2.3.2 $CuCl_2$ and $CuBr_2$ adjusted to pH 6.5 with hydrochloric acid 42 and 43

Interestingly, reactions of *trans*-tach with both copper(II) chloride and bromide at a pH reduced in both instances to 6.5 with hydrochloric acid, form the trigonal planar μ_3 chloro bridged trinuclear complexes **42** and **43** (Figure 50). Compounds **42** and **43** were characterized by single crystal X-ray crystallography, elemental analysis, infra-red spectroscopy and mass-spectrometry. The identities of the microcrystalline precipitates of **42** and **43** were also confirmed by powder X-ray diffraction measurements. Single crystal X-ray crystallographic analysis of compounds **42** and **43** reveals that the structures and their corresponding supramolecular networks are identical, except for the nature of the hydrogen-bonded halide counterions (chloride for **42** and bromide for **43**).

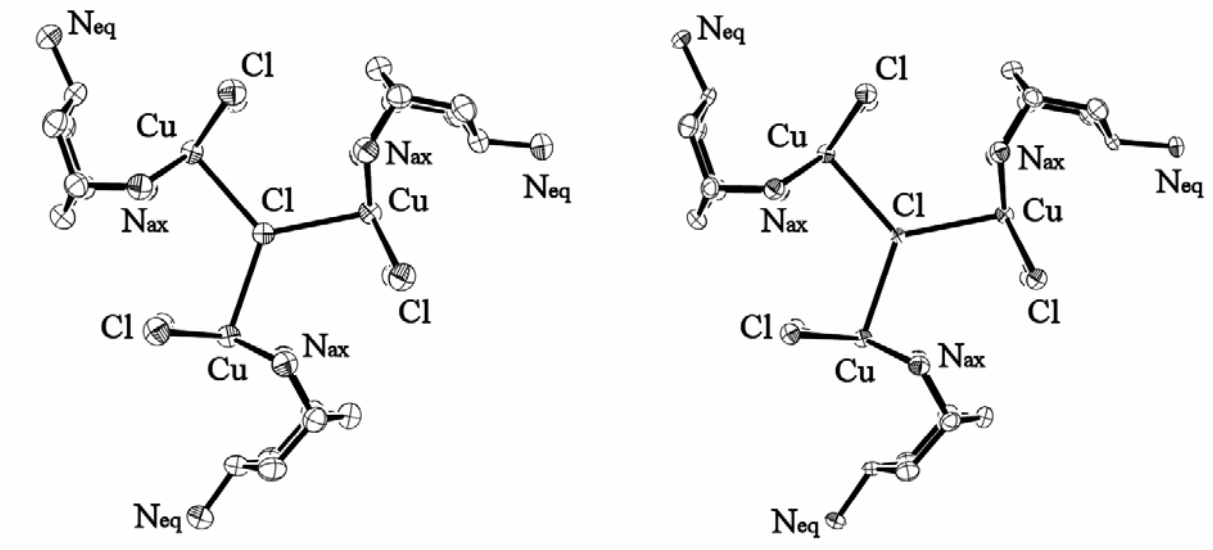

Figure 50 Ortep-3 representations of the planar μ_3 chloro bridged trinuclear copper(II) cations of $[\{Cu(\mathbf{L}H)Cl_2\}_3Cl]Cl_2$ (**42**, *LHS*) and $[\{Cu(\mathbf{L}H)Cl_2\}_3Cl]Br_2$ (**43**, *RHS*) at 50% thermal ellipsoids. Counterions are omitted.

The structural diversity of coordination compounds incorporating halide ions as ligands ranges from the common occurrence of terminal halides,[180-182] μ_2-halide ligands[183,184] and the frequently observed capping μ_3-halide coordination to less common higher coordination numbers for halide ligands in discrete molecules.[185,186] Evaluation of CSD database searches suggest that μ_3-bridging halide complexes can be classified into three categories: (i) trigonal planar (ii) *T* shaped with one angle approximately 180° (ii) *Y* shaped with one angle between 90 and 120°.

Unlike the more commonly reported planer μ_3-oxo ligands,[187-189] database searches reveal that the trigonal planar coordination mode is extremely rare for halides – with only few examples reported in the literature for trimeric copper(I),[190] iron(II)[191] and silver(I)[192] fluoro complexes. The observation of the unprecedented trigonal planar μ_3-chloro coordination motif to transition metals is therefore of extreme interest as it represents a new binding mode for chloro ligands.

As such, **42** and **43** represent a novel type of coordination cluster with unprecedented geometry, high symmetry and a three-dimensional supramolecular framework facilitated by hydrogen-bonded interactions that include both coordinated and non-coordinated halide ions.

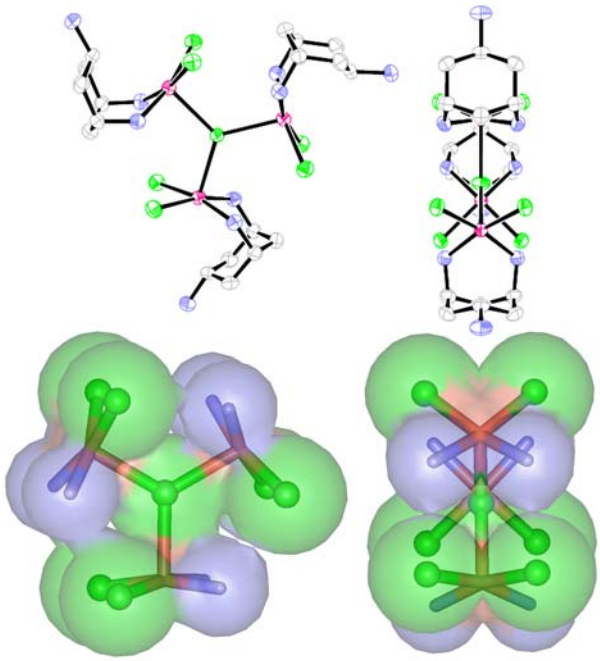

Figure 51 Two representations of the isostructural tri-copper(II) clusters **42** and **43** are shown. (*LHS:* Top view; *RHS:* Side view). The hydrogen-bonded halide counterions are omitted. Ortep-3 representations *above* and ball and stick representations of the primary coordination sphere with a CPK surface *below*. Copper(II) ions are shown in pink, chloride in green and nitrogen in blue.

Each trimeric cluster comprises three tetragonal {Cu(**L**H)Cl_2} subunits with the copper(II) ions chelated by *trans*-tach and coordinated by two terminal chloro ligands. The apical coordination to the trigonal planar μ_3 bridging chloro ligand (Cu… μ_3-Cl distance is 2.575 Å for both **42** and **43**) completes the pyramidal coordination (τ = 0.00) of each subunit. The remaining *trans* amino groups are protonated and involved in *inter*molecular hydrogen-bonded interactions to chloride (**42**) and bromide counterions (**43**). Additionally, the trimeric clusters show *intra*molecular hydrogen-bonded interactions between each subunit [Cu$(NH_2)_2$…Cl_2Cu], which presumably facilitate the trigonal planar coordination of the bridging chloro ligand (Table 3, *intra*molecular N(1)-H(1B) ··· Cl(1)).

Table 3 3-D-hydrogen-bonded network[166] (Å /°) for $[\{Cu(\mathbf{L}H)Cl_2\}_3Cl]X_2$ X = Cl for **42**, Br for **43**

	42				**43**			
D-H ··· A	**D-H**	**H ··· A**	**D ··· A**	**D-H ··· A**	**D-H**	**H ··· A**	**D ··· A**	**D-H ··· A**
N(1) – H(1A) ··· Cl(1)[a]	0.90	2.59	3.297(4)	136	0.90	2.59	3.301(5)	136
N(1) – H(1B) ··· Cl(1)[b]	0.90	2.51	3.391(4)	168	0.90	2.50	3.383(5)	167
*intra*molecular								
N(2) – H(2A) ··· X*[,c]	0.89	2.32	3.180(4)	163	0.89	2.45	3.313(5)	164
N(2) – H(2B) ··· Cl(1)[d]	0.89	2.56	3.232(5)	133	0.89	2.55	3.215(9)	132
N(2) – H(2B) ··· Cl(1)[e]	0.89	2.56	3.232(5)	133	0.89	2.55	3.215(9)	132
N(2) – H(2C) ··· X*[,f]	0.89	2.30	3.180(4)	168	0.89	2.44	3.313(5)	168

*) X = Cl(3) for **42** and Br(1) for **43**.

N(1) represents the coordinating, N(2) the protonated pendant amino group nitrogen atom. Cl(1) represents the coordinating chloro ligand and X the halide counterion.

Symmetry Code: a) x-y,x,-1/2+z; b) -y,x-y,1/2-z; c) -x+y,-x,1/2-z; d) 1-x+y,-x,z; e) 1-x+y,-x,1/2-z; f) x,-1+y,z.

It is interesting to note that both coordinating and non-coordinating halides rest on trigonal coordination sites with C_{3h} symmetry. One site is trigonal planar by coordination to three copper(II) centres (Figure 52, *Lower left*). The second site is trigonal bipyramidal, coordinating *via* hydrogen-bonded interactions to three of the trimeric clusters (Figure 52, *Lower right*). These *inter*molecular hydrogen-bonded interactions connect the trimeric clusters into hexagonally packed layers, as shown in Figure 52, *Upper* and *Centre*.

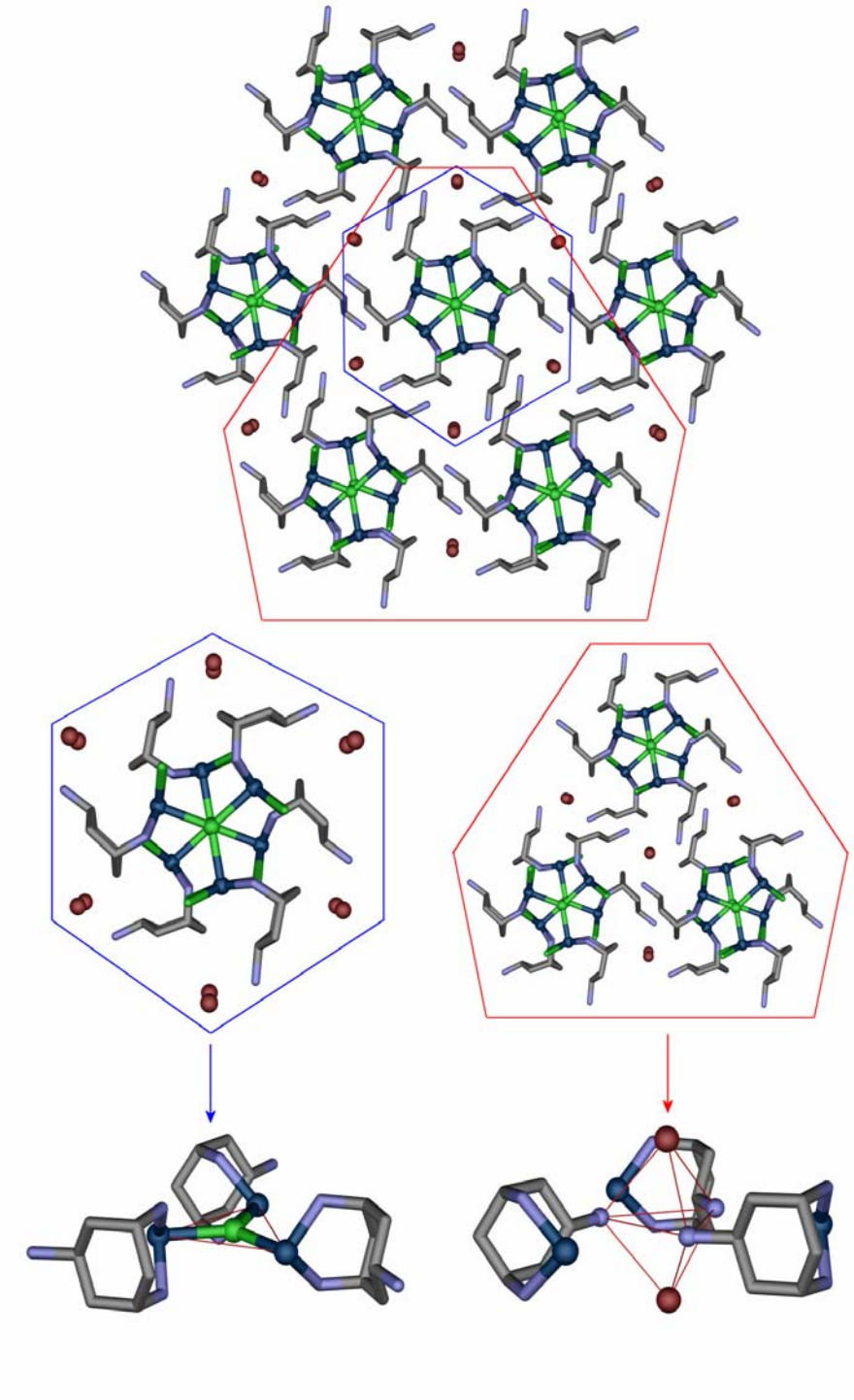

Figure 52 *Upper*: Hexagonal layers of **42** and **43** along the crystallographic *c* axis. *Centre*: 3-fold symmetric arrangement around the trigonal planar μ_3 chloro coordination (*left*) and the hydrogen-bonded halide counterions (*right*). *Lower*: C_{3h} symmetric arrangement with the terminal chloro ligands omitted for clarity; trigonal planar coordination around the μ_3 bridging chloro ligand (*left*) and trigonal bipyramidal hydrogen-bonded geometry around the halide counterions (*right*). Copper(II) is shown as dark blue spheres, nitrogen in light blue, chloro ligands in green, halide counterions in maroon and carbon in grey.

Further to hydrogen-bonded interactions within each layer, the donor atoms that facilitate the *intra*molecular hydrogen-bonded interactions, $[Cu(NH_2)_2 \ldots Cl_2Cu]$, connect the trimeric clusters of adjacent layers into one-dimensional chains. The layers are stacked hexagonally with the planar μ_3 chloro ligands located on a 6_3 screw axis (Figure 52, *Centre left*). Thus, rotation by 60° and projection along the principal symmetry axis results in a staggered conformation of trimeric clusters in adjacent layers as shown in Figure 53 (*inter*-layer separation is 6.314 Å (**42**) and 6.326 Å (**43**); *intra*-layer distance between trimeric clusters is 12.680 Å (**42**) and 12.6961 Å (**43**)).

This staggered conformation of trimeric clusters throughout the layers represents a one-dimensional chain of parallel orientated triangular copper(II) clusters, formed by six hydrogen-bonded interactions between coordinating amino groups and terminal chloro ligands of adjacent layers. (Figure 53).

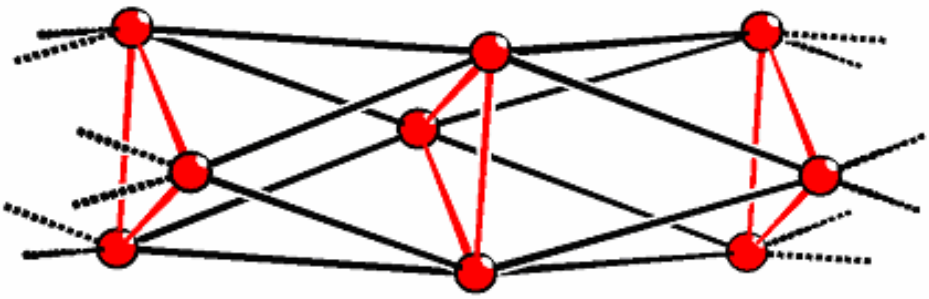

Figure 53 Framework representation of the one-dimensional Cu_3 chain present in both trimeric complexes **42** and **43**. View perpendicular to the crystallographic *c* axis. Hydogen bonded interactions are shown in red (*intra*-triangle) and black (*inter*-triangle). The *intra* / *inter*-triangle Cu···Cu distances are 4.46 and 6.82 Å, respectively. Copper(II) ions are shown as red spheres.

3.4.2.4 Copper(II) fluoride

3.4.2.4.1 CuF_2 at unadjusted pH, complex 44

Reaction of copper(II) fluoride with *trans*-tach at unadjusted pH results in the formation of the diligand complex **44**. Both *trans*-tach ligands coordinate *via* their bidentate amino groups to the copper(II) ion and are orientated *syn* to each other with a separation of 5.51 Å between the centroids of the cyclohexane rings. The tetragonal pyramidal coordination ($\tau = 0.11$)[167] around the copper(II) centre is completed by apical coordination of a fluoro ligand (Cu…F = 2.417 Å).

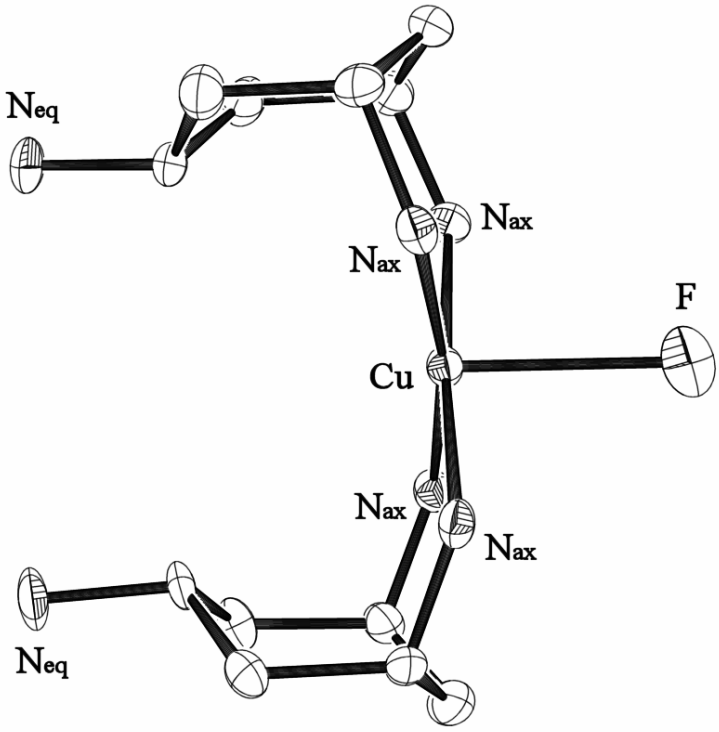

Figure 54 Ortep-3 representation of the diligand cation of $[Cu(\mathbf{L})_2F]F$ (**44**) at 50% thermal ellipsoids. Counterions and solvent molecules are omitted.

Analysis of the crystal lattice of **44** shows the complex cations to be involved in hydrogen-bonded interactions to both fluoride counterions and solvent molecules (Table 4). These interactions occur between layers in which the cations are orientated with their coordinating fluoro ligands pointing along the crystallographic *c* axis. It is noteworthy that packing of **44** does not result in a nanoporous lattice as observed in the crystal lattice of the protonated complex **45**.

Table 4 3-D-hydrogen-bonded network[166] (Å /°) for

[Cu(*trans*-tach)$_2$F]F (**44**)

D-H ··· A	D-H	H ··· A	D ··· A	D-H ··· A
N(1) – H(1B) ··· F(2)	0.90	1.90	2.798(3)	171
N(2) – H(2A) ··· F(2)[a]	0.90	1.89	2.771(3)	165
N(2) – H(2B) ··· O(4)[b]	0.90	2.16	3.015(3)	157
N(3) – H(3A) ··· F(1)[c]	0.89	2.48	3.254(3)	146
N(3) – H(3B) ··· O(4)	0.89	2.11	2.783(3)	132
N(3) – H(3C) ··· O(3)	0.89	2.57	3.193(3)	127
N(4) – H(4A) ··· F(2)	0.90	1.94	2.813(3)	163
N(4) – H(4B) ··· O(2)[d]	0.90	2.13	2.963(3)	153
N(5) – H(5A) ··· O(3)[b]	0.90	1.99	2.872(3)	165
N(5) – H(5B) ··· F(2)[a]	0.90	1.97	2.851(3)	166
N(6) – H(6A) ··· O(1)[a]	0.89	2.48	3.286(3)	151
N(6) – H(6B) ··· O(3)[e]	0.89	2.36	3.216(3)	161
N(6) – H(6C) ··· O(4)	0.89	1.98	2.842(3)	162

N(3) and N(6) represent the pendant amino group nitrogen atoms, F(1) the coordinating fluoro ligand, F(2) the fluoride counterion and O(1)-O(4) the oxygen atoms of solvent molecules (water and methanol).

Symmetry Code: a) 1+x,y,z; b) 1/2+x,1/2-y,-1/2+z; c) 1/2+x,1/2-y,1/2+z; d) -1/2+x,1/2-y,-1/2+z; e) 1/2+x,1/2+y,z.

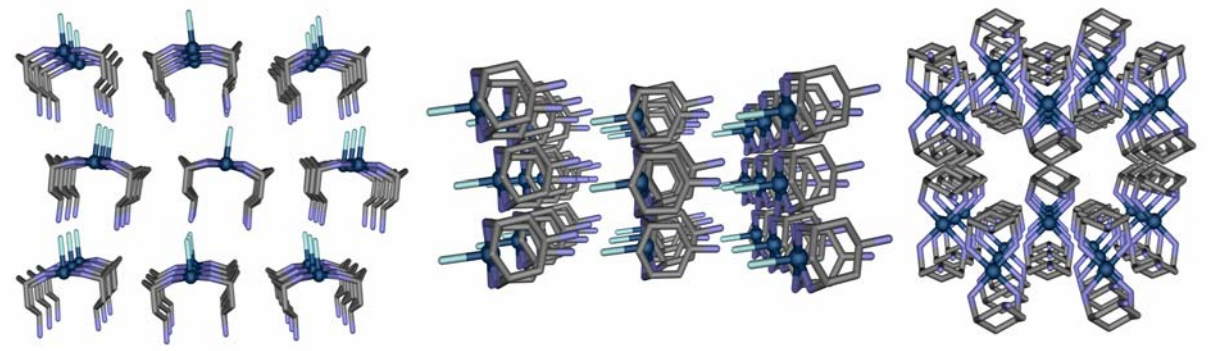

Figure 55 Crystal packing of **44** along the crystallographic *a* (*Left*), *b* (*Centre*) and *c* (*Right*) axes. The arrangement of **44** in layers with fluoro ligands pointing along the *c* axis can be seen clearly. Copper(II) is shown as dark blue spheres, nitrogen in light blue, fluoride in sky blue and carbon in grey. Counterions and solvent molecules are omitted.

3.4.2.4.2 CuF_2 adjusted to pH 7.7 with hydrofluoric acid 45

Reaction of *trans*-tach with copper(II) fluoride at pH 7.7 *via* addition of hydrofluoric acid results in the tetrameric copper(II) cluster **45**.[193] The asymmetric unit of the complex comprises one protonated *trans*-tach ligand, one copper(II) ion and one fluoro ligand. These assemble into the tetranuclear cubane-type structure **45**, in which four copper(II) ions and four μ_3-bridging fluoro ligands are alternately positioned on the vertices of the cube. Unlike the

commonly reported cubane structures assembled from copper and chloride,[194,195] bromide,[194,196] iodide[194,197] or oxygen donor ligands,[198,199] complex **45** represents the first example of a copper-fluoride cubane (Figure 56).

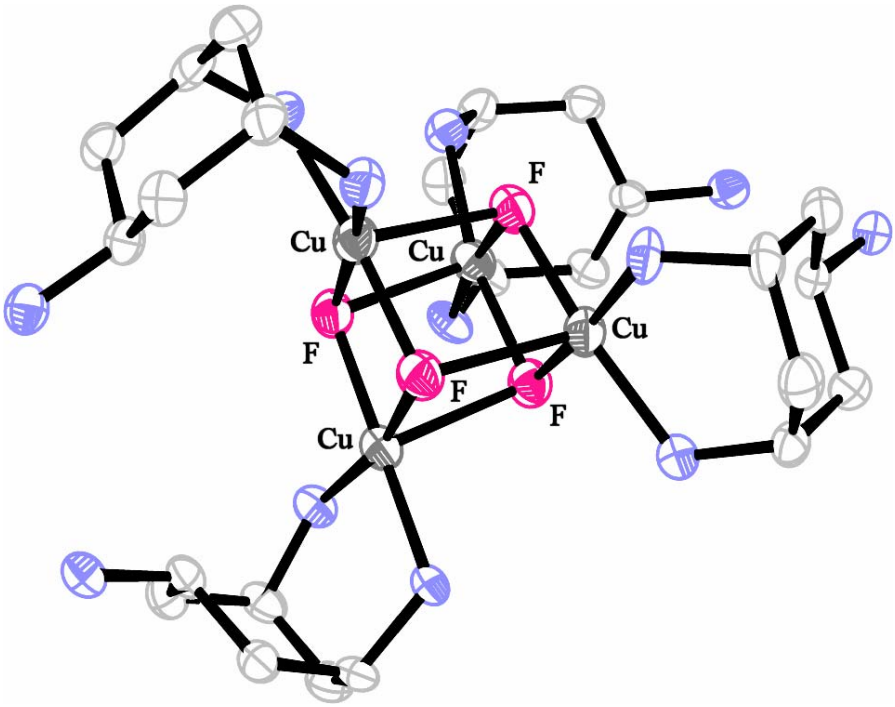

Figure 56 Ortep-3 representation of the tetranuclear cation of $[\{Cu(\mathbf{L}H)F\}_4]F_4$ (**45**) at 50% thermal ellipsoids. Copper(II) is shown in dark grey, fluoride in pink and nitrogen in blue. Counterions and solvent molecules are omitted.

The structure itself shows only a small distortion from the regular cubic arrangement. The angles around the fluoro centres are slightly widened with 95.7, 96.3 and 98.9°, whereas the angles around the copper(II) centres are compressed to 83.6, 83.2 and 80.9°. The copper(II) coordination environment is tetragonal pyramidal (τ = 0.10)[167] with a basal coordination formed by two bridging fluoro ligands ($d_{Cu\ldots F\ basal}$ = 1.962 and 1.983 Å) and chelation to one *trans*-tach ligand. The distance to the apical coordinated fluoro ligand is elongated to 2.317 Å but lies within observed ranges for μ_3-fluoro bridging copper(II) trimers.[200] The copper(II) distances within the cube are 2.997 and 3.196 Å, demonstrating the minor distortion of the overall structure. The average length of the edge of the cube is 2.087 Å, resulting in an estimated volume of 9.09 Å^3. The *trans*-tach ligands of two copper(II) ions that share basal coordination of two fluoro ligands are orientated *syn* to each other. The centroid separation of these *syn* orientated ligands is 6.97 Å, separating the protonated pendant amino residues by

only 3.563 Å. This short distance is due to strong hydrogen-bonded interactions to fluoride counterions (Table 5, Figure 57, *LHS*), which enable the formation of extensive hydrogen-bonded interactions to other cubane units. Each pendant amino residue forms hydrogen-bonded interactions to three fluoride counterions. Overall, six cubane complexes with twelve pendant amino groups hydrogen bond to twelve fluoride counterions. The 24 pendant nitrogen atoms and fluoride counterions are positioned on the vertices of a truncated octahedron, which incarcerates a crystallographically disordered methanol solvent molecule (Figure 57, *RHS*).

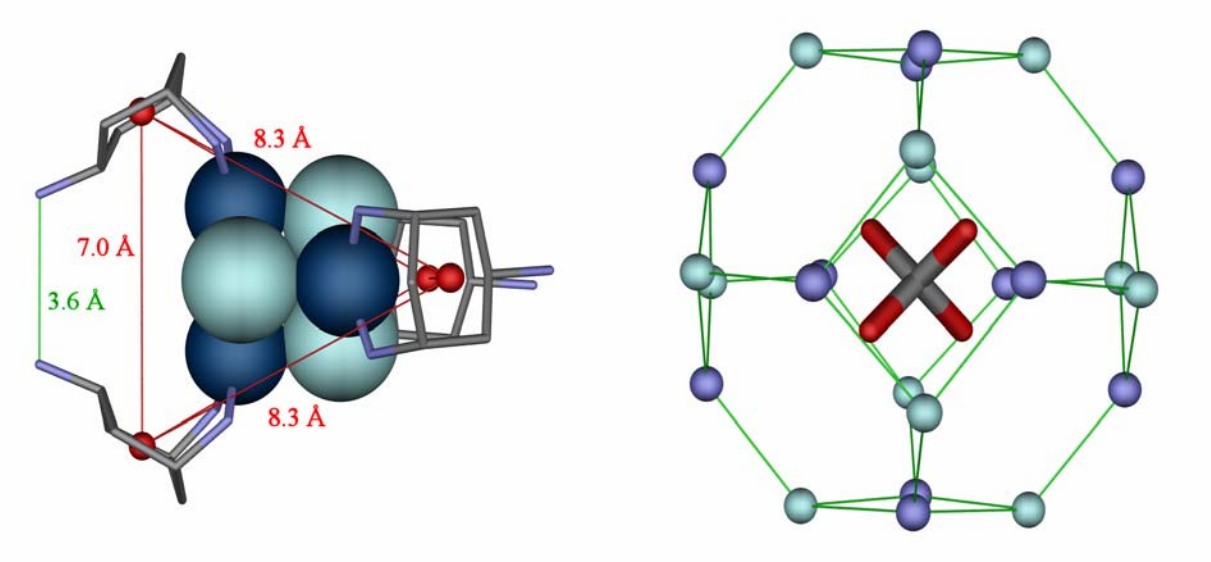

Figure 57 *LHS*: View along the apical edge of the cubane complex **45** showing the separation of the cyclohexane rings (*red*) and pendant amino group nitrogens (*green*). The coordination cube is shown as a space filling representation and the *trans*-tach as a stick representation. The red spheres represent the centroids of the cyclohexane rings. *RHS*: View along the four-fold axis of the 'octahedral junction'; the truncated octahedron is formed by hydrogen-bonded interactions between protonated pendant amino groups and fluoride counterions. The crystallographically disordered methanol solvent molecule is incorporated within the polyhedron. Copper(II) is shown in dark blue, nitrogen in light blue, fluoride in sky blue and carbon in grey.

Table 5 3-D-hydrogen-bonded network[166] (Å /°) of

[{Cu(*trans*-tachH)F}$_4$]F$_8$ (**45**)

D-H ··· A	D-H	H ··· A	D ··· A	D-H ··· A
N(1) – H(1C) ··· O(14)[a]	0.90	2.44	3.245(8)	149
N(1) – H(1D) ··· O(2)[b]	0.90	2.04	2.942(8)	177
N(2) – H(2C) ··· O(13)[c]	0.90	2.18	3.042(9)	160
N(2) – H(2D) ··· O(2)[a]	0.90	2.19	3.007(8)	151
N(3) – H(3C) ··· F(2)[d]	0.89	1.88	2.731(6)	159
N(3) – H(3D) ··· F(2)[e]	0.89	1.81	2.685(6)	166
N(3) – H(3E) ··· F(2)	0.89	1.76	2.649(6)	176

N(3) represents the pendant amino group nitrogen atom, F(2) the fluoride counterion that is involved in the formation of the hydrogen-bonded truncated octahedron and O(x) the oxygen atoms of solvent molecules (water and methanol).

Symmetry Code: a) z,x,y; b) 1/2-y,-x,z; c) 1/2-z,-1/2+y,1/2-x;
d) 1/2-y,z,1/2-x; e) y,z,x.

This hydrogen-bonded polyhedron acts as an ‘octahedral junction’, positioning six cubane clusters along the four-fold symmetry axes on the vertices of an octahedron. This perpendicular arrangement of cubane subunits forms an infinite three-dimensional network with overall cubic symmetry. Because of the 90° restrictions at each junction, the resulting framework exhibits channels along each axis (Figure 58). The accessible voids in these channels are 11 Å in diameter and occupied by solvent molecules and additional fluoride counterions not incorporated into the framework. **45** crystallises in the highly symmetric cubic space group *F*-43*c* (219) with 24 equivalent positions resulting in 96 monomeric copper(II) units assembling to 24 cubane clusters within the unit cell. The unit cell volume is over 50,000 Å^3, one of the largest observed for organometallic coordination compounds. The cubanes are separated by 18.65 Å along each crystallographic axis and by 26.37 Å across the voids. The three-dimensional hydrogen-bonded cubic framework is shown in Figure 59.

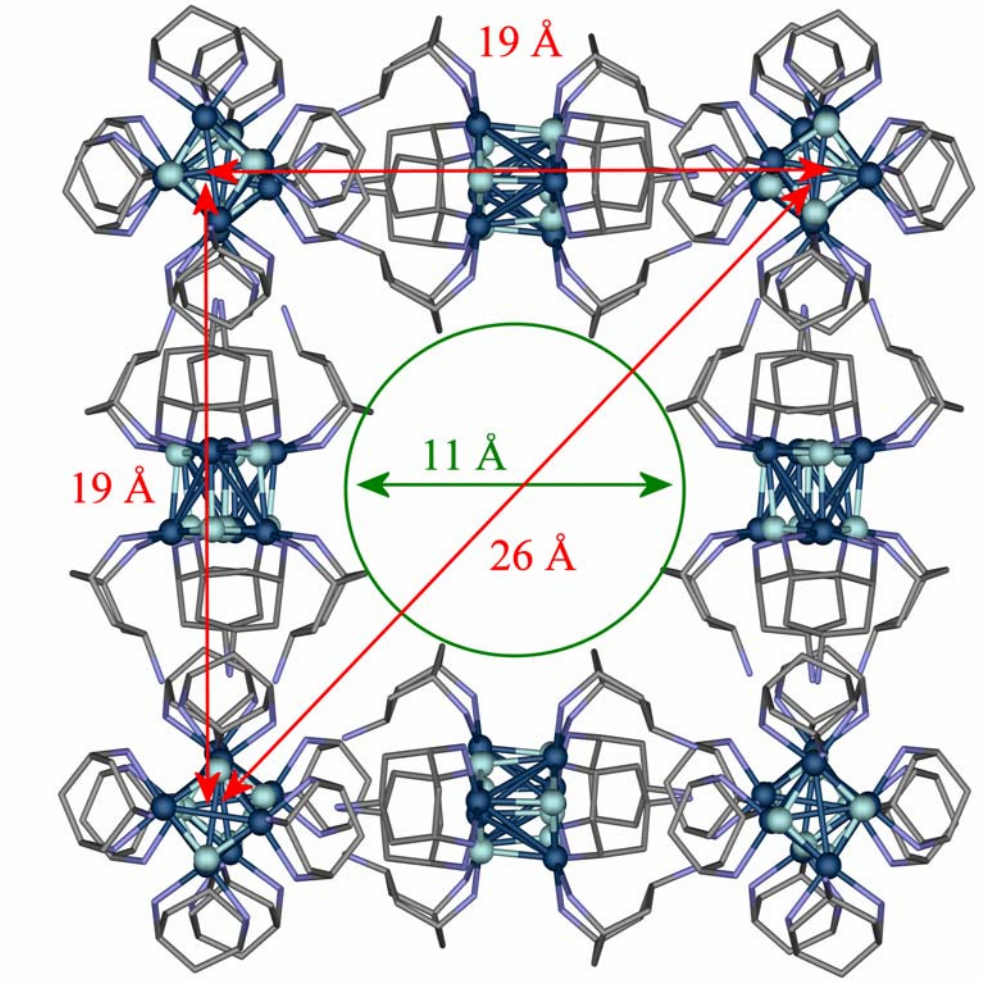

Figure 58 Unit cell representation of the cubane complex **45**. The distances of separate cubane units are shown in red (accurate values are 18.65 and 26.37 Å). The void accessible to solvent molecules is shown in green. Copper(II) is shown as dark blue spheres, fluoride as sky blue spheres, nitrogen in light blue and carbon in grey. Counterions and solvent molecules are omitted.

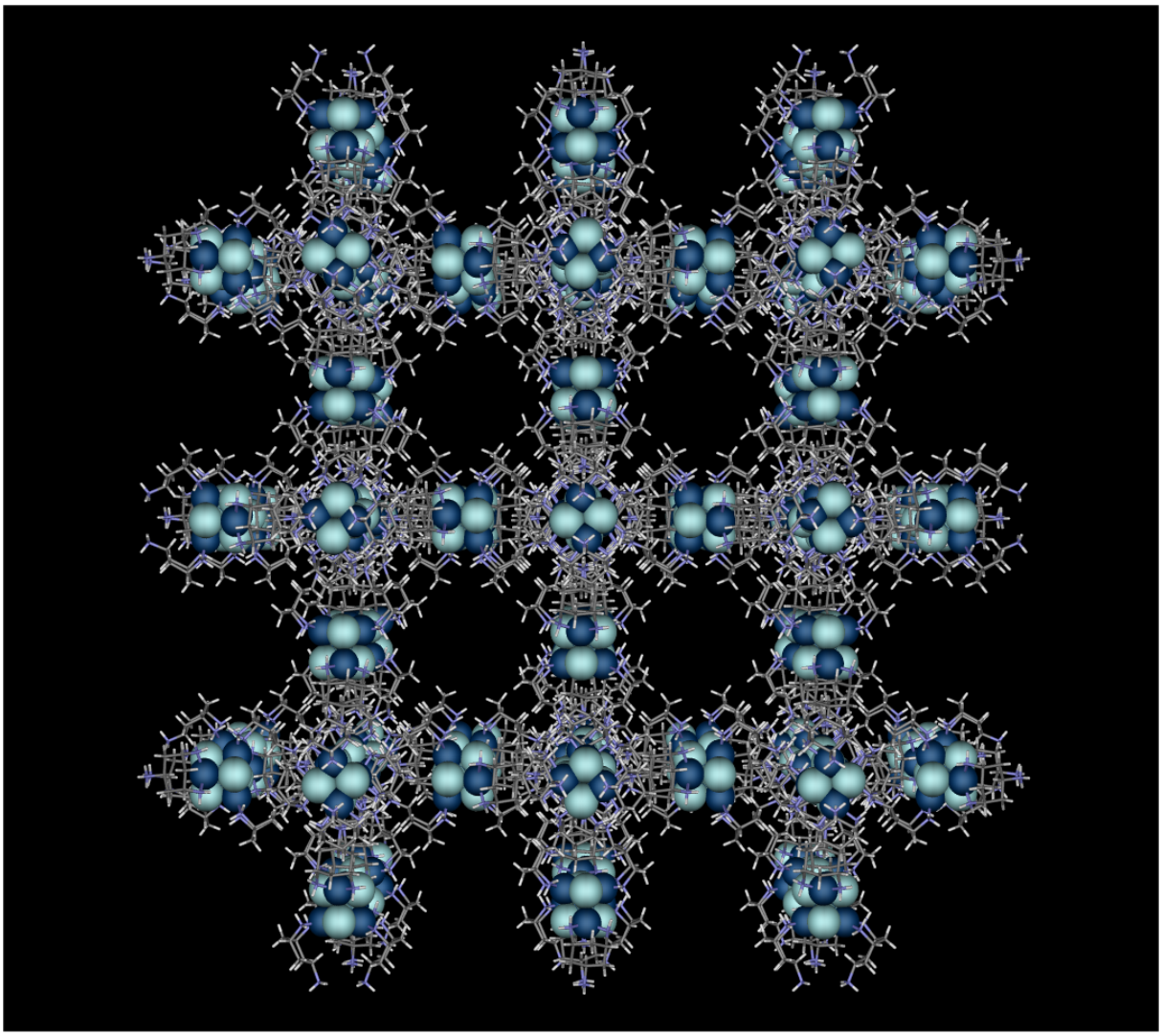

Figure 59 3-D hydrogen-bonded cubic framework composed of copper(II)-fluoro cubane units **45**. Counterions and solvent molecules are omitted. The coordination cube is shown in a space filling and *trans*-tach in a stick representation. Copper(II) is shown in dark blue, fluoride in sky blue, nitrogen in light blue, carbon in grey and hydrogen in white.

The 'bottom up' construction of the three-dimensional hydrogen-bonded network is illustrated in Figure 60. Level **A** represents the truncated octahedron formed upon hydrogen-bonded interactions between protonated pendant amino residues and fluoride counterions. This polyhedron represents an octahedral junction from which the tetranuclear cubes are assembled perpendicular to each other, gradually forming the overall structure. Level **B** shows the linear growth of two cubane units connected to the polyhedron; level **C** represents the growth in all three dimensions around the polyhedron (*LHS*: represented with incomplete cubane fragments around one polyhedron; *RHS*: completed fragments further connecting to additional junctions). Level **D** shows the fully-grown cubic framework of the three-dimensional hydrogen-bonded network.

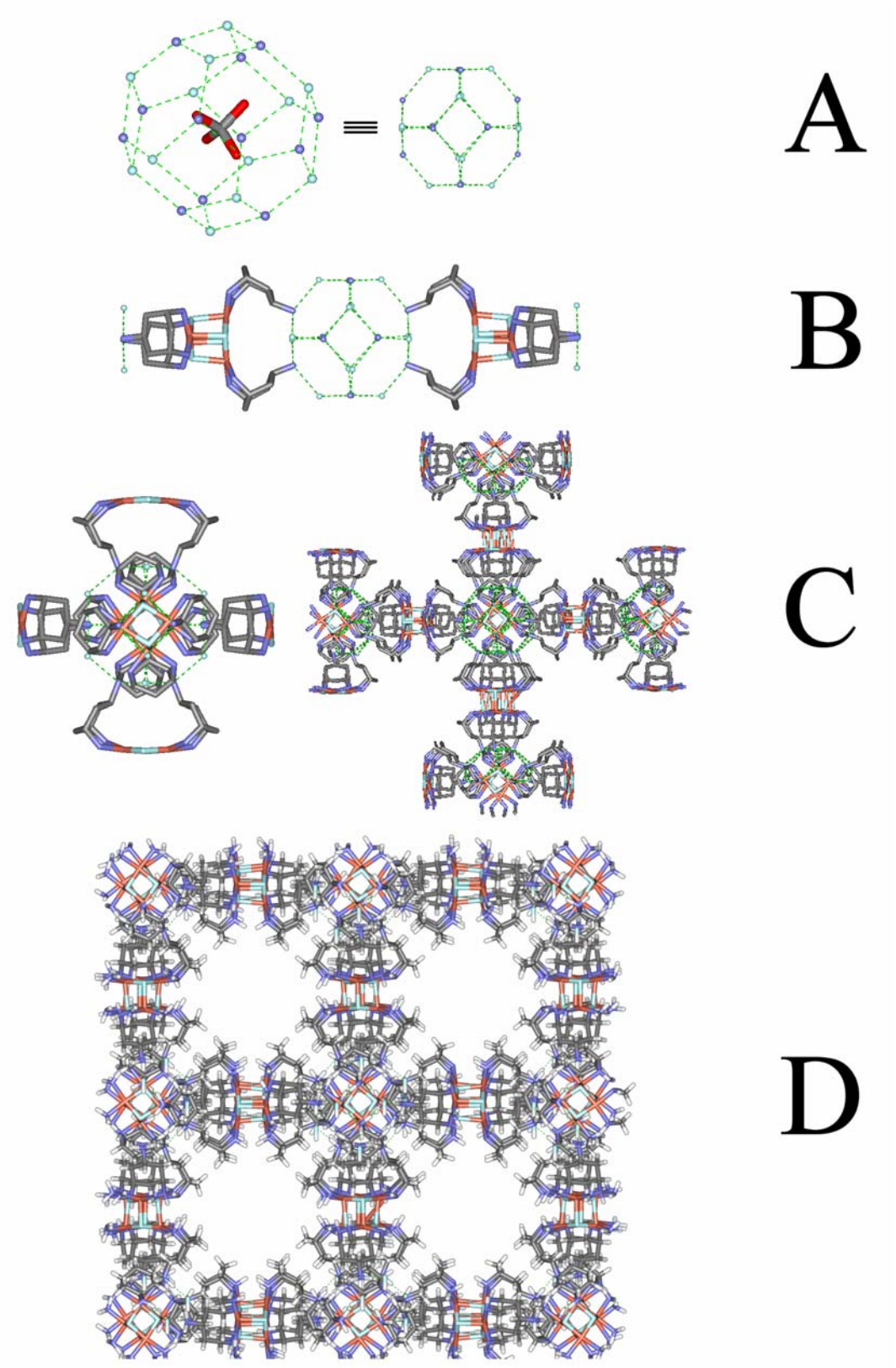

Figure 60 Construction of the 3-D hydrogen-bonded network formed from the cubane complex **45**. The levels **A-D** illustrate the gradual growth starting from the octhahedral junction (level **A**) to the nanoporous three-dimensional architecture (level **D**).

3.4.2.5 Copper(II) sulphate

3.4.2.5.1 $CuSO_4$ at unadjusted pH, complex 46

Reaction of copper(II) sulphate with *trans*-tach at unadjusted pH results in the formation of the diligand complex **46**. The *trans*-tach ligands are orientated *syn* to each other, with a centroidal separation of the cyclohexane rings of 5.51 Å. The tetragonal pyramidal coordination environment (τ = 0.04)[167] around the copper(II) ion is completed by apical coordination of a sulphato oxygen atom ($d_{Cu...O}$ = 2.438 Å).

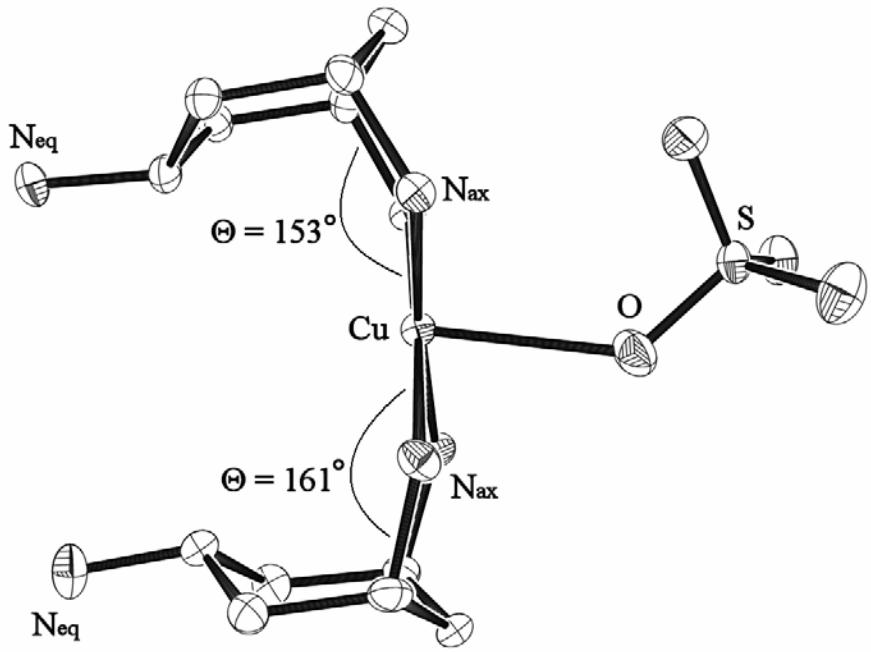

Figure 61 Ortep-3 representation of the diligand complex [Cu(**L**)$_2$(SO_4)] (**46**) at 50% thermal ellipsoids. Solvent molecules are omitted.

It is interesting to note that the two *trans*-tach ligands exhibit different interplanar angles of Θ = 152.8 and 161.3°. This is the first example observed in *trans*-tach coordination where two ligands differ by 8.5° in their coordination to the same metal centre. The pendant amino residues are *not* protonated and **46** does not aggregate *via* hydrogen-bonded interactions to form a nanoporous structure. The isolated units of complex **46** arrange in layers along the crystallographic *c* axis. These layers are held together by weak hydrogen-bonded interactions to methanol solvent molecules. Within each layer, strong hydrogen bonded interactions are

observed between the complexes forming a two-dimensional hydrogen-bonded network (Table 6).

Table 6 2-D-hydrogen-bonded network[166] (Å /°) for

[Cu(*trans*-tach)$_2$(SO$_4$)] (**46**)

D-H ··· A	D-H	H ··· A	D ··· A	D-H ··· A
N(1) - H(1A) ··· N(3)[a]	0.90	2.09	2.965(4)	163
N(1) - H(1B) ··· O(2)[b]	0.90	2.13	2.973(4)	155
N(2) - H(2A) ··· O(3)[c]	0.90	2.09	2.974(3)	168
N(2) - H(2B) ··· O(1)	0.90	2.18	3.012(3)	153
N(3) - H(3A) ··· O(3)[e]	0.89	2.16	2.970(4)	150
N(3) - H(3B) ··· O(5)[e]	0.89	2.60	3.212(4)	127
N(3) - H(3C) ··· N(1)[d]	0.89	2.11	2.965(4)	162
N(4) - H(4A) ··· O(2)[b]	0.90	2.00	2.850(4)	157
N(4) - H(4B) ··· N(6)[a]	0.90	2.13	3.028(5)	172
N(5) - H(5B) ··· O(3)[c]	0.90	2.21	2.966(4)	141
N(6) - H(6C) ··· O(3)[d]	0.89	2.35	3.105(5)	142
N(6) - H(6D) ··· N(4)[d]	0.89	2.18	3.028(5)	159

N(3) and N(6) represent the pendant amino group nitrogen atoms, O(1)-O(4) the coordinating sulphato ligand and O(5) the oxygen atoms of methanol solvent molecules.

Symmetry Code: a) 1-x,1/2+y,z; b) -1+x,y,z; c) 2-x,-1/2+y,z; d) 1-x,-1/2+y,z; e) -x,-y,1/2+z.

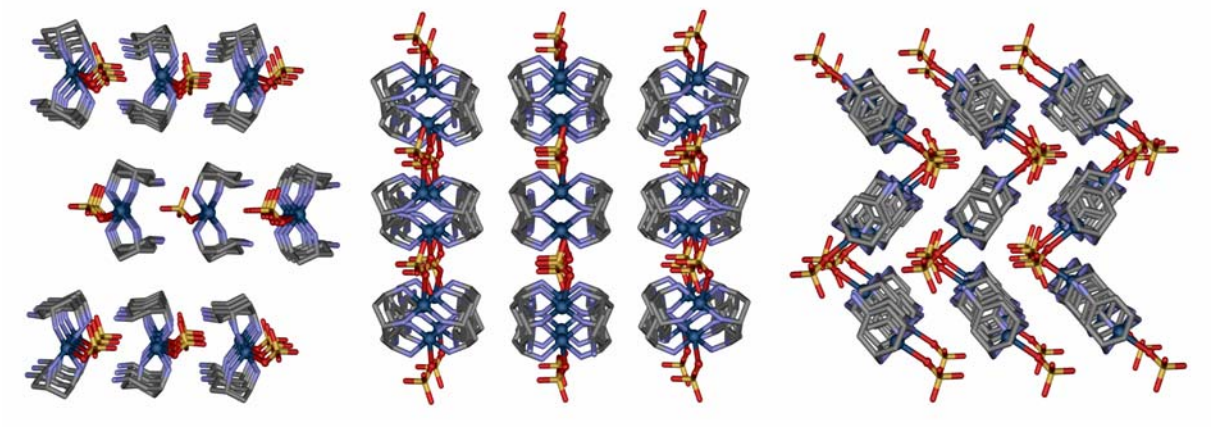

Figure 62 Crystal packing of **46** along the crystallographic *a* (*Left*), *b* (*Centre*) and *c* (*Right*) axes. The layer arrangement of **46** can be seen clearly. Copper(II) is shown as dark blue spheres, nitrogen in light blue, sulphur in yellow, oxygen in red and carbon in grey. Solvent molecules are omitted.

3.4.2.5.2 $CuSO_4$ adjusted to pH 8.8 with sulphuric acid 46 · H_2SO_4

Reaction of copper(II) sulphate and *trans*-tach at a pH adjusted to 8.8 with sulphuric acid, forms the identical diligand complex as observed for reaction at unadjusted pH. However, in

this complex, the pendant amino residues are protonated, resulting in **46** • H_2SO_4 (Figure 63). The tetragonal pyramidal coordination sphere ($\tau = 0.00$)[167] of the copper(II) ion is formed by basal coordination to two bidentate *trans*-tach ligands and apical coordination to one sulphato ligand ($d_{Cu...O}$ = 2.322 Å). The major difference between **46** and its protonated analogue **46** • H_2SO_4 lies in a more pronounced difference in the interplanar angles Θ within the protonated diligand complex (153.3 and 175.5° for **46** • H_2SO_4 and 153 and 161° for **46**). This large difference in angles of 22.2°, observed in one complex, underlines the flexibility of *trans*-tach in adopting strained conformations. This is further illustrated by a larger centroidal separation of the cyclohexane rings of 5.68 Å.

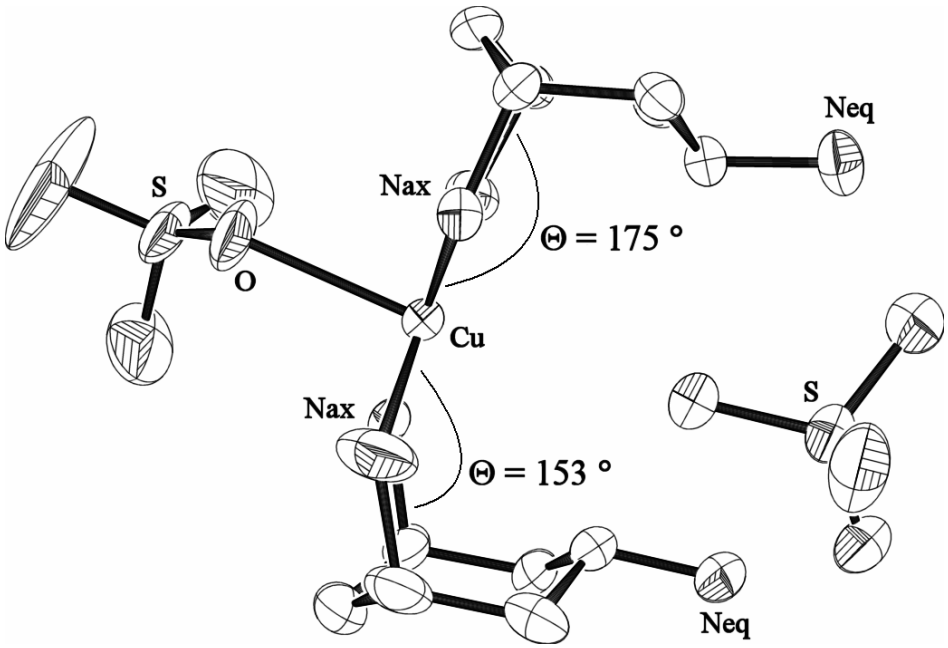

Figure 63 Ortep-3 representation of the diligand complex [Cu(**L**H)$_2$(SO$_4$)](SO$_4$) (**46** • H_2SO_4) at 50% thermal ellipsoids. Solvent molecules are omitted.

The complex units arrange in hexagonal layers along the crystallographic *c* axis. Hydrogen-bonded interactions form a three-dimensional network comprising one-dimensional channels of 15 Å in diameter. The channels are arranged hexagonally and are separated by 28.37 Å (Figure 64). Only solvent molecules are located within the channels as all sulphate counterions are incorporated within the hydrogen-bonded framework. It is noteworthy that, due to protonation of the pendant amino residues, which are separated by 4.86 Å, three complex units arrange in a trigonal fashion (Figure 65, Level **B**, *LHS*). These subunits are held together by hydrogen-bonded interactions between the protonated amino groups, sulphate counterions and methanol solvent molecules (Table 7).

Table 7 3-D-hydrogen-bonded network[166] (Å /°) for

[Cu(*trans*-tachH)$_2$(SO$_4$)](SO$_4$) (**46** · H_2SO_4)

D-H ··· A	D-H	H ··· A	D ··· A	D-H ··· A
N(1) - H(1A) ··· O(12)[a]	0.90	2.24	3.003(13)	163
N(1) - H(1B) ··· O(3)	0.90	2.07	2.920(19)	155
N(2) - H(2A) ··· O(1)[b]	0.90	2.32	3.206(16)	168
N(2) - H(2B) ··· O(8)[b]	0.90	2.40	3.245(12)	153
N(3) - H(3A) ··· O(7)[b]	0.89	1.86	2.728(12)	150
N(3) - H(3B) ··· O(6)[c]	0.89	2.18	3.042(11)	127
N(3) - H(3B) ··· O(7)[c]	0.89	2.57	3.126(15)	162
N(5) - H(5A) ··· O(2)	0.90	2.37	3.213(17)	157
N(5) - H(5B) ··· O(12)[a]	0.90	2.09	2.992(13)	172
N(6) - H(6C) ··· O(6)[b]	0.89	1.90	2.786(13)	141
N(6) - H(6D) ··· O(5)[a]	0.89	2.01	2.833(14)	142
N(6) - H(6D) ··· O(8)[a]	0.89	1.75	3.225(13)	159

N(3) and N(6) represent the pendant amino group nitrogen atoms, O(1)-(O4) the coordinating sulphato ligand and O(5)-O(8) the sulphate counterion.

Symmetry Code: a) y,-x+y,-z; b) y,x,1/2-z; c) 1+x-y,1-y,1/2-z.

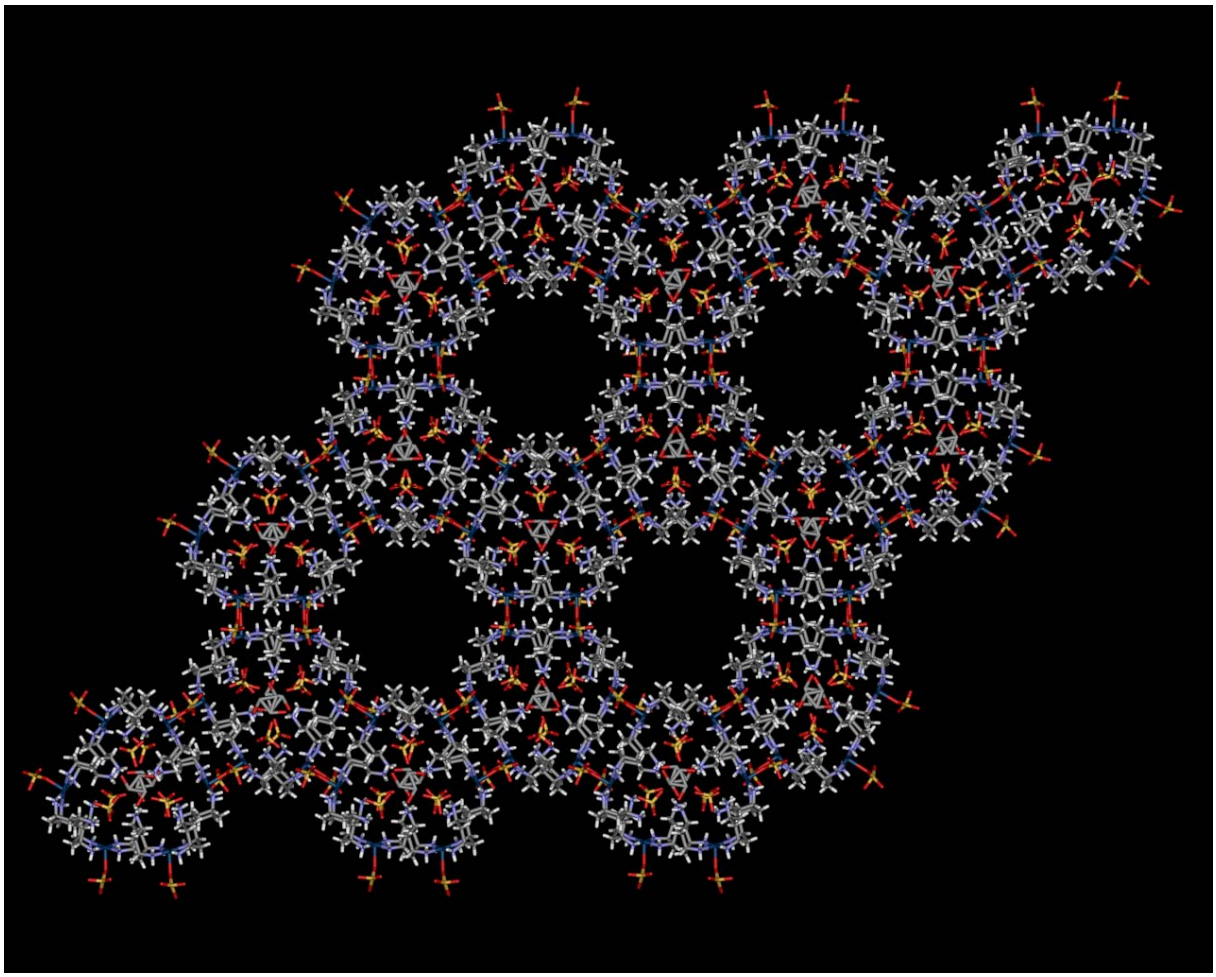

Figure 64 3-D hydrogen-bonded hexagonal framework composed of diligand complexes **46** · H_2SO_4. Solvent molecules are omitted. The channels are 15 Å in diameter and separated by 28.37 Å. Copper(II) is shown as dark blue spheres, nitrogen in light blue, sulphur in yellow, oxygen in red, carbon in grey and hydrogen in white.

Interestingly, the methanol solvent molecule is rotationally disordered over three positions along the C_3 axis located at the centre of the trigonal arrangement (Figure 65, Level **A**). Adjacent layers are rotated by 60° to each other forming trigonal prismatic units throughout the crystal lattice (Figure 65, Level **B**, *RHS*). These prismatic units are connected *via* their edges, forming the one-dimensional nanoporous structure observed within the crystal lattice of **46** • H_2SO_4 (Figure 65, Level **C-D**).

To understand the formation of the nanoporous structure, it is informative to abbreviate the three-dimensional prismatic unit as a two-dimensional triangular unit. Edge sharing of each triangular unit consequently leads to the formation of the hexagonal structure (Figure 65). It is crucial for the formation of the nanoporous structure that this triangular units 'lack' corners, resulting in a structure that exhibits holes. In the three dimensional complex, the prismatic arrangement exhibits 'rounded corners' as well as spaces between the shared edges, which allow the formation of one-dimensional channels throughout the crystal lattice.

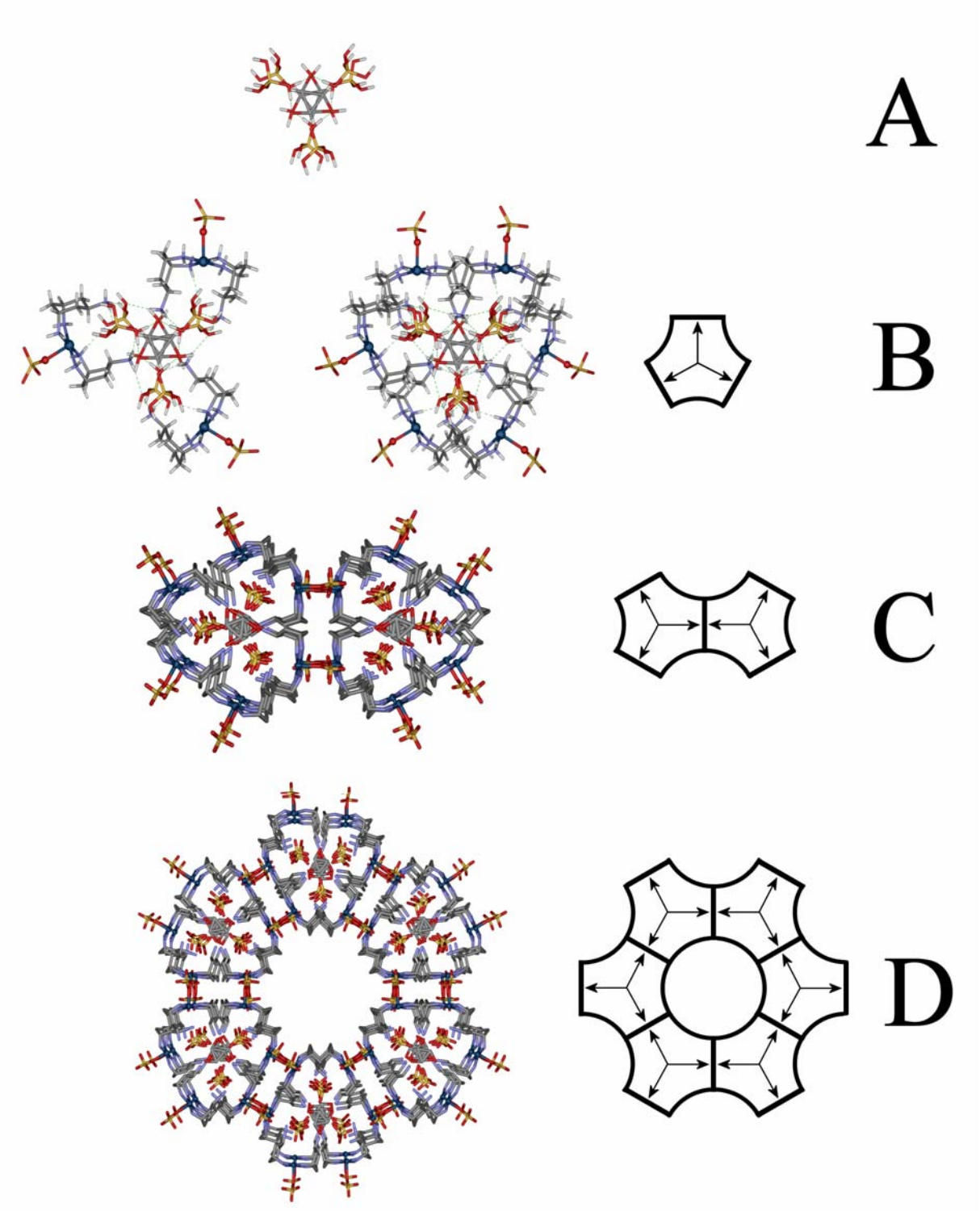

Figure 65 View along the crystallographic *c* axis. Construction of the 3-D hydrogen-bonded network formed from the diligand complex **46** · H_2SO_4. The levels **A-D** illustrate the gradual growth starting from the hydrogen-bonded three-fold disordered methanol molecule (level **A**) to the one-dimensional nanoporous architecture (level **D**).

3.4.3 Palladium(II) coordination

The non-interacting binding sites on *trans*-tach (**L**) provide a number of different coordination modes upon complexation to square planar Pd(II) centres. The monoligand complexes $[Pd(\mathbf{L}H)Cl_2]Cl$ (**47**) and $[Pd(\mathbf{L}H)Br_2]_2[PdBr_4]$ (**48**) (Figure 66, *Top-right*) are obtained with two *cis* sites occupied by the 'Head' chelation of *trans*-tach and the two remaining sites occupied by halide ligands. Coordination of a second *trans*-tach ligand can either occur *via* a second 'Head' chelation ('Head to Head' complexes $[Pd(\mathbf{L}H)_2]X$, X = $(NO_3)_4$ **49**, $(SO_4)_2$ **50**) or *via* 'Tail' coordination of its *trans* amino group ('Head to Tail' complexes $[\{Pd(\mathbf{L})X\}_6]X_6$ (X = Cl **51** and Br **52**). A further coordination mode is observed in the trinuclear complex $[Pd\{Pd(\mathbf{L})Cl_2\}_2Cl_2]$ (**53**), where the centre Pd(II) ion is ligated by a 'Tail to Tail' coordination of two *trans*-tach ligands in addition to their 'Head' amino groups individually chelating other Pd(II) ions.

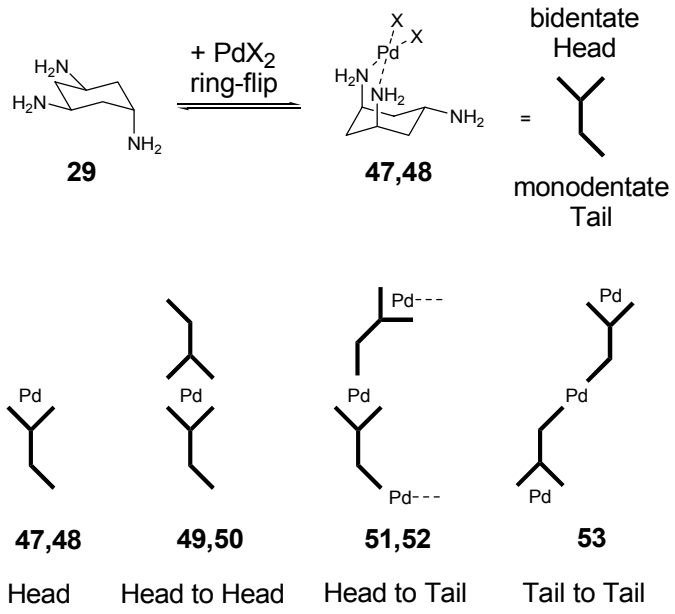

Figure 66: *Top-left*: *tris*-monodentate conformation; *Top-right*: ring-flip to chelating 'Head' and monodentate 'Tail' conformation upon Pd(II) coordination; *Bottom*: Various coordination modes of *trans*-tach with Pd(II); remaining coordination sites are occupied by halide ligands: 'Head' **47**, **48**; 'Head to Head' **49**, **50**; 'Head to Tail' **51**, **52**; 'Tail to Tail' **53**.

Table 8 Selected bond lengths (Å) and angles (°) for **47** - **53**

[Pd(**L**H)Cl_2]Cl (**47**)	[Pd(**L**H)Br_2]$_2$[$PdBr_4$] (**48**)	[Pd(**L**H)$_2$](NO_3)$_4$ (**49**)	[Pd(**L**H)$_2$](SO_4)$_2$ (**50**)	[{Pd(**L**)Cl}$_6$]Cl_6 (**51**)	[{Pd(**L**)Br}$_6$]Br_6 (**52**)	[Pd{Pd(**L**)Cl_2}$_2$$Cl_2$] (**53**)
Pd - N	*Pd - N*	*Pd - N*	*Pd - N*	*Pd - N*	*Pd - N*	*Pd - N*
Head	*Head*	*Head*	*Head*	*Head*	*Head*	*Head*
Pd-N1 2.041(7)	Pd1-N1 2.036(6)	Pd-N1 2.054(6)	Pd-N1 2.063(2)	2.034(6)	2.040(5)	Pd1-N1 2.042(11)
Pd-N2 2.038(7)	Pd1-N2 2.062(6)	Pd-N2 2.053(6)	Pd-N2 2.055(2)	≤Pd-N≤	≤Pd-N≤	Pd1-N2 2.061(10)
				2.063(5)	2.077(5)	
				Tail	*Tail*	*Tail*
				Pd1-N9 2.072(5)	Pd1-N9 2.061(5)	Pd2-N3 2.063(12)
				Pd2-N3^b 2.067(5)	Pd2-N3^b 2.058(5)	
				Pd3-N6 2.063(5)	Pd3-N6 2.066(5)	
Pd - Cl	*Pd -Br*	/	/	*Pd – Cl*	*Pd – Br*	*Pd - Cl*
Pd-Cl1 2.325(2)	Pd1-Br1 2.4319(8)			Pd1-Cl1 2.316(2)	Pd1-Br1 2.4238(8)	Pd1-Cl1 2.325(3)
Pd-Cl2 2.317(2)	Pd1-Br2 2.4404(7)			Pd2-Cl2 2.308(2)	Pd2-Br2 2.4263(8)	Pd1-Cl2 2.318(3)
				Pd3-Cl3 2.292(2)	Pd3-Br3 2.4430(8)	Pd2-Cl3 2.302(3)
cis Cl-Pd-Cl	*cis Br-Pd-Br*	*cis N-Pd-N*	*cis N-Pd-N*	*cis N-Pd-Cl*	*cis N-Pd-Br*	*Cl-Pd-Cl*
Cl1-Pd-Cl2 92.6(1)	Br1-Pd1-Br2 92.1(3)	N1-Pd-N2 89.5(2)	N1-Pd-N2 94.79(6)	86.9(2) – 91.4(2)	88.2(2) – 91.6(2)	Cl1-Pd1-Cl2 93.9(1)
		N1-Pd-N2^a 90.5(2)	N1-Pd-N2^a 85.2(6)			Cl3-Pd2-Cl3^c 177.3(2)
cis N-Pd-Cl	*cis N-Pd-Br*			*cis N-Pd-N*	*cis N-Pd-N*	
N1-Pd-Cl2 88.1(2)	N1-Pd1-Br2 85.73(2)	*trans N-Pd-N*	*trans N-Pd-N*	91.1(2) – 92.9(3)	89.4(2) – 92.1(2)	*cis N-Pd-Cl*
N2-Pd-Cl1 88.2(2)	N2-Pd1-Br1 87.7(2)	N1-Pd-N1^a 180.0(3)	N1-Pd-N1^a 180.0(1)			86.6(3) – 90.5(3)
				trans N-Pd-N	*trans N-Pd-N*	
cis N-Pd-N	*cis N-Pd-N*			175.7(2) – 177.3(2)	174.7(2) – 177.7(2)	*N-Pd-N*
N1-Pd-N2 91.1(2)	N1-Pd1-N2 94.7(2)					N1-Pd1-N2 91.4(4)
						N3-Pd-N3^c 177.8(6)
Θ 146.0°	Θ 170.8°	Θ 142.8°	Θ 165.2°	Θ_1 148.5, χ_1 123.5 Θ_2 147.2, χ_2 116.6 Θ_3 159.7, χ_3 112.1	Θ_1 148.9, χ_1 122.4 Θ_2 149.6, χ_2 127.6 Θ_3 148.0, χ_3 114.7	Θ 150.3°, χ 133.6°

Θ, χ angles defined in Figure **34**. Indices$_{1,2,3}$ correspond to Ring units 1, 2, 3.

Symmetry Codes: a = -x, -y, -z; b = -x+1, -y+2, -z+1, c = -x+3/2, y, -z.

3.4.3.1 'Head' coordination - monoligand complexes 47 and 48

Reactions of *trans*-tach trihydrochloride or -bromide salt with one equivalent of the corresponding palladium(II) halide, in aqueous solution under reflux for two days produces the monoligand complexes [Pd(**L**H)Cl_2]Cl (**47**) or [Pd(**L**H)Br_2]$_2$[$PdBr_4$] (**48**) in good yield, which have been fully characterised. In both complexes, the cyclohexane rings adopt a chair

conformation with the 'Head' amino groups involved in a chelating coordination to the Pd(II) ions. The square planar coordination spheres are completed by two chloro (**47**) or bromo (**48**) ligands, see Figure 67. The remaining 'Tail' amino groups are protonated and complexes **47** and **48** crystallise as chloride (**47**) or tetrabromopalladate (**48**) salts. The Pd-N and Pd-X bonds lie within expected ranges for square planar *cis*-diamino-dichloro, and -dibromo palladium(II) complexes.[201-204]

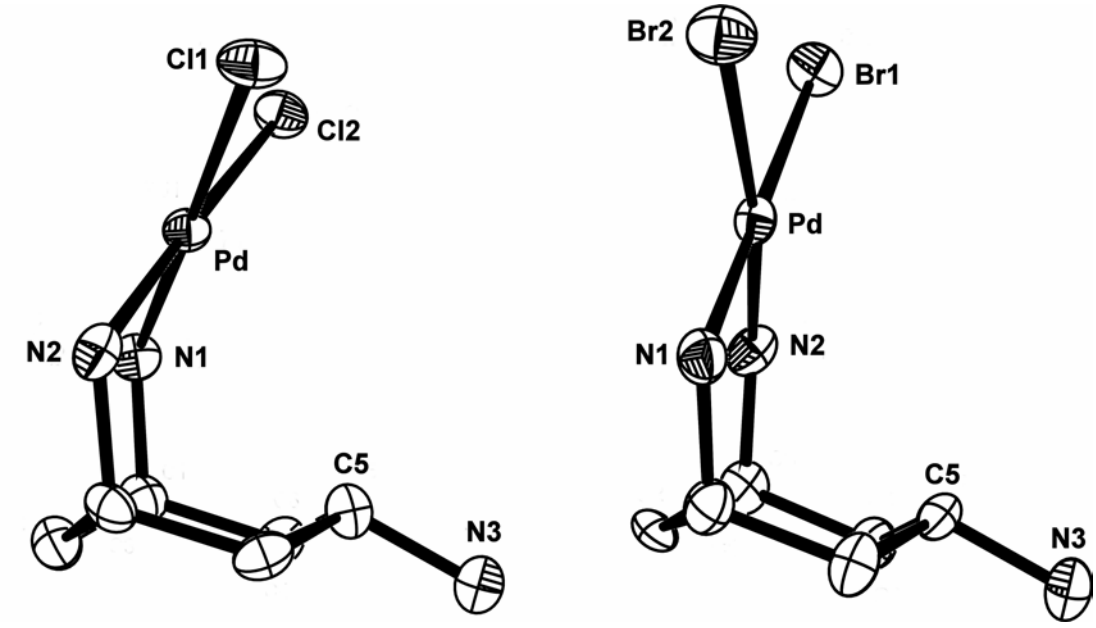

Figure 67 Ortep-3 representation of the monoligand cations of $[Pd(\mathbf{L}H)Cl_2]Cl$ (**47**, *LHS*) and $[Pd(\mathbf{L}H)Br_2]_2[PdBr_4]$ (**48**, *RHS*) at 50% thermal ellipsoids. Counterions and solvent molecules are omitted. The more compressed conformation of **47** can be seen clearly. Selected bond lengths and angles are given in Table 8.

The orientation of the Pd(II) ions towards the cyclohexane ring is greater for **47** (Θ = 146.0°) than for **48** (Θ = 170.8°), resulting in a more compressed structure for **47** with the Pd(II) ion almost centred over the cyclohexane ring. Contrary to this, the Pd(II) coordination plane A in structure **48** is nearly parallel to plane B in Figure **34** with one of the largest interplanar angle Θ observed for *trans*-tach, being close to 180°. This results in a distorted chair conformation for the six membered metallacycle, placing the Pd(II) towards the edge of the cyclohexane ring. The ^{1}H-NMR spectra of **47** and **48** are discussed in Chapter 3.4.3.5.

3.4.3.2 'Head to Head' coordination – anti-diligand complexes 49 and 50

Adsorption of **47** onto a strongly alkaline ion exchange resin, followed by neutralisation with nitric acid, forms the fully characterised complex $[Pd(\mathbf{L}H)_2](NO_3)_4$ (**49**, Figure 68, *LHS*) in good yield, whereby the *trans*-tach ligands are coordinated in a 'Head to Head' fashion. Under the strongly basic conditions it appears that the chloro ligands of **47** are hydrolysed and subsequent reaction results in the formation of the *anti*-diligand complex **49**. An alternative route can be taken by the direct reaction of *trans*-tach with palladium(II) nitrate under reflux in water. In this reaction, the labile nitrato ligands are replaced by two *trans*-tach ligands to form the *anti*-diligand coordination of **49**. However, by using palladium(II) nitrate, the formation of an intermediate *mono*ligand complex is not observed. Both cyclohexane rings adopt chair conformations with each of the 'Head' amino groups involved in a chelating coordination to the Pd(II) centre. The two 'Tail' amino residues in **49** are protonated and the complex crystallises as its *tetrakis*-nitrate salt. The Pd-N bonds lie within expected ranges for square planar tetra-amino palladium(II) complexes.[205] The separation of the *anti*-orientated ligand centroids is 5.87 Å, resulting in an interplanar angle Θ of 142.8°, placing the Pd(II) ion neatly over the centre of the cyclohexane ring (Figure 68, *LHS*).

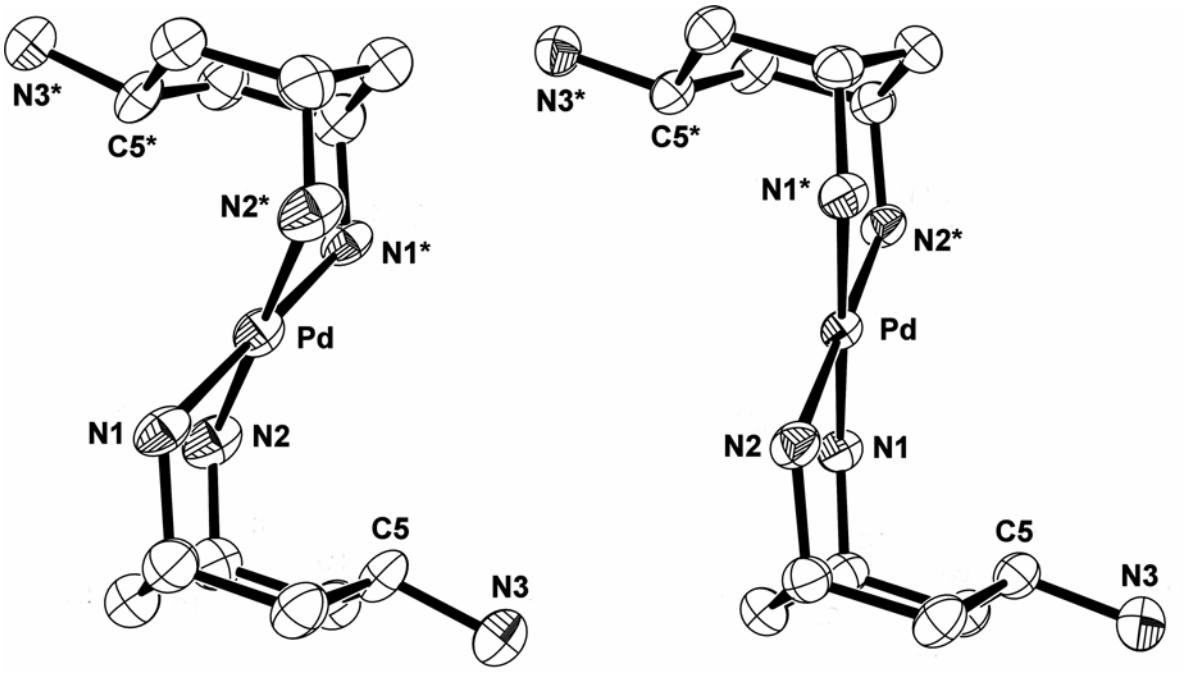

Figure 68 Ortep-3 representation of the *anti*-diligand cations of $[Pd(\mathbf{L}H)_2](NO_3)_4$ (**49**, *LHS*) and $[Pd(\mathbf{L}H)_2](SO_4)_2$ (**50**, *RHS*) at 50% thermal ellipsoids. Counterions and solvent molecules are omitted. The compressed conformation of **49** can be seen clearly. Selected bond lengths and angles are given in Table 8.

An identical *anti*-diligand coordination isomer is obtained by reaction of *trans*-tach with palladium(II) sulphate. This results in the formation of complex $[Pd(\mathbf{L}H)_2](SO_4)_2$ (**50**) that has been fully characterised. Similar to the reaction with palladium(II) nitrate, no intermediate *mono*ligand complex was observed upon reflux in water. Presumably the labile sulphato ligands are replaced by two *trans*-tach ligands to form the thermodynamically favoured *anti*-diligand coordination (**50**, Figure 68, *RHS*). Both 'Tail' amino residues are protonated and the complex crystallises as its *bis*-sulphate salt. The Pd-N bonds lie within expected ranges for square planar tetra-amino palladium(II) complexes.[205] The Pd(II) ion of **50** is oriented towards the edge of the cyclohexane ring with an interplanar angle Θ of 165.2°. This larger angle results in an increased distance of 6.22 Å between the centroids of the *anti*-orintated ligands. Complex **50** therefore adopts a less compressed conformation than **49** with a more distorted chair conformation for the six membered metallacycle. Comparison of the crystal packing of both complexes reveals that the singly negatively charged nitrate counterions in **49** (Figure 69, *LHS*) enable a denser packing of the $[Pd(\mathbf{L}H)_2]^{4+}$ tetra-cations within the crystal lattice than the doubly negative charged sulphate ions in **50** (Figure 69, *RHS*), where additional water molecules are incorporated into the lattice. Structural analysis reveals that both **49** and **50** comprise 3-D (Table 9) hydrogen-bonded networks (Table 10). This demonstrates the ability of *trans*-tach coordination to compress in order to accommodate a variety of geometrically constraining parameters such as optimum packing effects and hydrogen-bonded interactions. The ^{1}H-NMR spectra of **49** and **50** are discussed in Chapter 3.4.3.5.

Table 9 3-D hydrogen-bonded network[166] (Å /°) for $[Pd(\mathbf{L}H)_2](NO_3)_4$ (**49**)

D-H ··· A	D-H	H ··· A	D ··· A	D-H ··· A
N(1) - H(1A) ··· O(4)[a]	0.90	2.03	2.900(8)	162
N(1) - H(1B) ··· O(1)[b]	0.90	2.49	3.255(10)	143
N(1) - H(1B) ··· O(2)[b]	0.90	2.20	3.040(8)	156
N(2) - H(2A) ··· O(3)[c]	0.90	2.25	3.036(10)	145
N(2) - H(2B) ··· O(6)[c]	0.90	2.20	2.912(9)	136
N(3) - H(3A) ··· O(2)[a]	0.89	1.96	3.832(9)	166
N(3) - H(3B) ··· O(1)[d]	0.89	2.59	3.225(10)	129
N(3) - H(3B) ··· O(5)[e]	0.89	2.17	2.915(9)	141
N(3) - H(3C) ··· O(4)	0.89	2.52	3.082(9)	121
N(3) - H(3C) ··· O(5)	0.89	2.16	3.005(9)	159

N(3) represents the pendant amino group nitrogen atom, O(1)–O(6) the oxygen atoms of the nitrate counterions.

Symmetry Code: a) 1-x, -y, 1-z; b) 2-x, -y, 1-z; c) 1+x, y, 1+z; d) x, y, 1+z; e) x, ½-y, ½+z.

Table 10 3-D hydrogen-bonded network[166] (Å /°) for $[Pd(\mathbf{L}H)_2](SO_4)_2$ (**50**)

D-H ··· A	D-H	H ··· A	D ··· A	D-H ··· A
N(1) - H(1A) ··· O(7)[a]	0.90	2.07	2.907(2)	155
N(1) - H(1B) ··· O(4)[b]	0.90	2.19	3.089(2)	176
N(2) - H(2A) ··· O(5)[c]	0.90	2.10	2.997(2)	171
N(2) - H(2B) ··· O(3)[d]	0.90	2.06	2.925(2)	160
N(3) - H(3A) ··· O(1)[c]	0.89	2.07	2.820(2)	141
N(3) - H(3A) ··· O(3)[c]	0.89	2.36	3.181(2)	153
N(3) - H(3B) ··· O(7)	0.89	1.96	2.810(2)	159
N(3) - H(3C) ··· O(6)[e]	0.89	1.86	2.733(3)	166
O(5) - H(51) ··· O(4)[b]	0.84	1.94	2.768(2)	172
O(5) - H(52) ··· O(2)	0.83	1.95	2.780(2)	173
O(6) - H(61) ··· O(5)	0.85	1.88	2.741(2)	172
O(6) - H(62) ··· O(3)[a]	0.83	1.96	2.785(2)	170
O(7) - H(71) ··· O(2)	0.85	1.87	2.709(2)	175
O(7) - H(72) ··· O(1)[b]	0.83	1.91	2.706(2)	160

N(3) represents the pendant amino group nitrogen atom, O(1)–O(4) the sulphate counterion and O(5)-O(7) the oxygen atoms of solvent water molecules.

Symmetry Code: a) -1+x,y,z; b) 1-x,-y,1-z;

c) x,y,1+z; d) -1+x,y,1+z; e) 1/2+x, 1/2 -y,1/2+z.

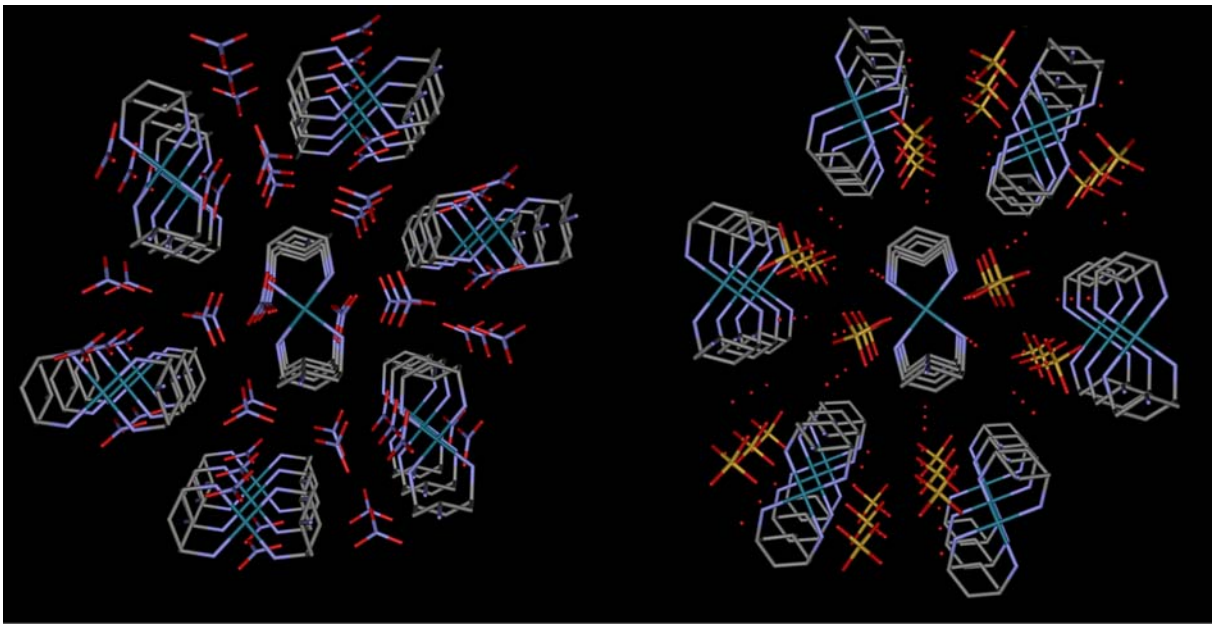

Figure 69 Crystal packing of *anti*-diligand complexes **49** (*LHS*) and **50** (*RHS*) along the crystallographic *a* axis. Pd(II) centres are shown in turquoise, nitrogen in blue, oxygen in red, sulphur in yellow and carbon in grey.

3.4.3.3 'Head to Tail' coordination - hexanuclear ring structures 51 and 52[§§]

Neutralisation of mother liquor solutions of **47** and **48** result in the formation of the cyclic hexanuclear Pd(II) complexes $[\{Pd(\mathbf{L})Cl\}_6]Cl_6$ (**51**) and $[\{Pd(\mathbf{L})Br\}_6]Br_6$ (**52**), respectively. These complexes are isostructural despite the sterically constrained cavity present in both metallamacrocycles. Before neutralisation, the mother liquor solutions were eluted through an ion exchange resin, exchanging the counterions to the corresponding chloride and bromide anions, thus preventing competing nucleophilic reactions with palladate ions to occur. In case of **47**, the ion exchange before neutralisation increased the originally reported[164] yield for **51** from 30% up to 65%. This indicates the presence of interfering palladate counterions in the mother liquor solution of **47** upon formation of **51** by alternative nucleophilic substitution pathways. The proposed mechanism for the formation of the hexanuclear metallamacrocyles **51** and **52** starts with the deprotonation of the protonated 'Tail' amino moieties of **47** and **48**. Thus, the resulting nucleophilic complexes can react with each other by substitution of one chloro (**47**) or bromo (**48**) ligand from a second moiety of **47** and **48**, respectively, leading to the 'Head to Tail' coordination of the resulting cyclic structures **51** and **52** (Figure 70). High dilution and elevated reaction temperatures facilitate the formation of the discrete ring structures rather than the formation of oligo- or polymeric units.[33]

Examination of the structures of **51** and **52** shows that each Pd(II) ion is chelated by a 'Head' amino group of one *trans*-tach ligand and by a monodentate 'Tail' coordination of an adjacent ligand. With this 'Head to Tail' coordination, *trans*-tach acts both as a bridging ligand and as a corner unit, overcoming the need for ancillary ligands to complete the metallamacrocyclic arrangement. The square planar coordination sphere is completed by a chloro (**51**) or bromo (**52**) ligand.

[§§] Complexes **51** and **52** were re-numbered from the original published scheme[164] for systematic comparison between crystallographic and NMR data: The most low field shifted NMR signals Ha, Hb and Hc in the original manuscript correspond to the methine protons on C5, C11 and C17 respectively and are referred to as Ha1, Ha2 and Ha3 in this thesis. Hd corresponds to the *axial* methylene proton on C12 (H12a) and is here referred to as Hb2. A detailed list of the re-numbered scheme is given in the supplementary data, chapter 7.3.

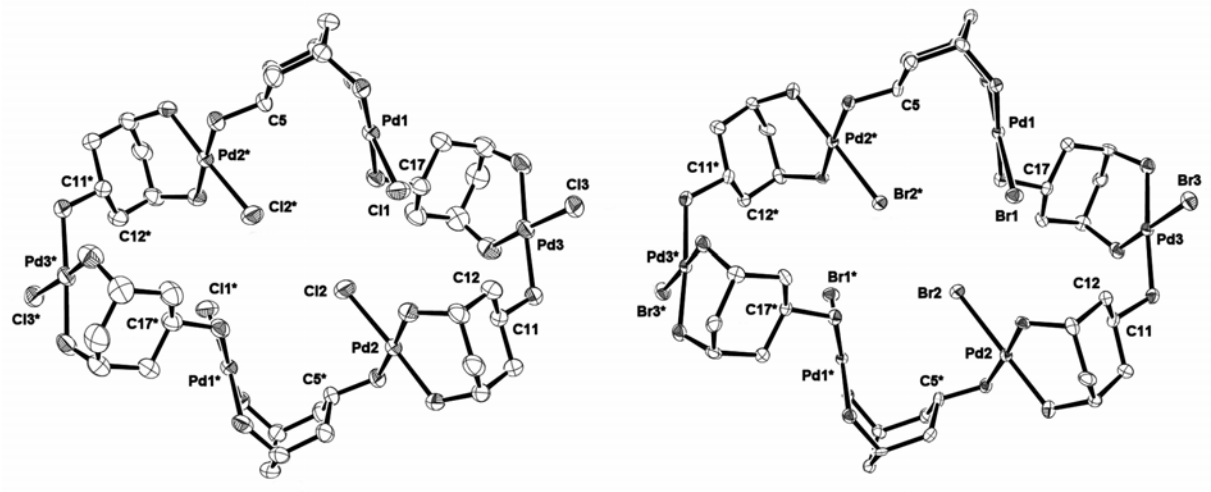

Figure 70 Ortep-3 representation of the cyclic cations of [{Pd(**L**)Cl}$_6$]Cl$_6$ (**51**, *LHS*) and [{Pd(**L**)Br}$_6$]Br$_6$ (**52**, *RHS*) at 50% thermal ellipsoids. Counterions and solvent molecules are omitted. Selected bond lengths and angles are given in Table 8.

Both complexes comprise three crystallographically independent ring units[***] {Pd(**L**)X} (X = Cl (**51**), Br (**52**)). A crystallographic inversion centre lies between the two coordinated halide ligands that point towards the centre of the cavity (X2 and X2*; Cl2…Cl2* = 3.51 Å, Br2…Br2* = 3.50 Å). In both complexes the six Pd(II) ions adopt an elongated pseudo chair conformation with the closest Pd1…Pd2 distances being 5.19 and 5.10 Å and the furthest Pd3…Pd3* distances being 13.72 and 13.76 Å for **51** and **52**, respectively (Figure 71).

[***] Ring unit 1 consists of Pd1, N1-N3 and C1-C6; Ring unit 2 consists of Pd2, N4-N6 and C7-C12; Ring unit 3 consists of Pd3, N7-N9 and C13-C18. The cyclic complexes are formed by connection of each ring through the 'Tail' amino group coordinating to Pd(II) chelated by the 'Head' amino groups of an adjacent ring. Connectivity as follows: Ring1-Ring2, Ring2-Ring3, Ring3-Ring1.

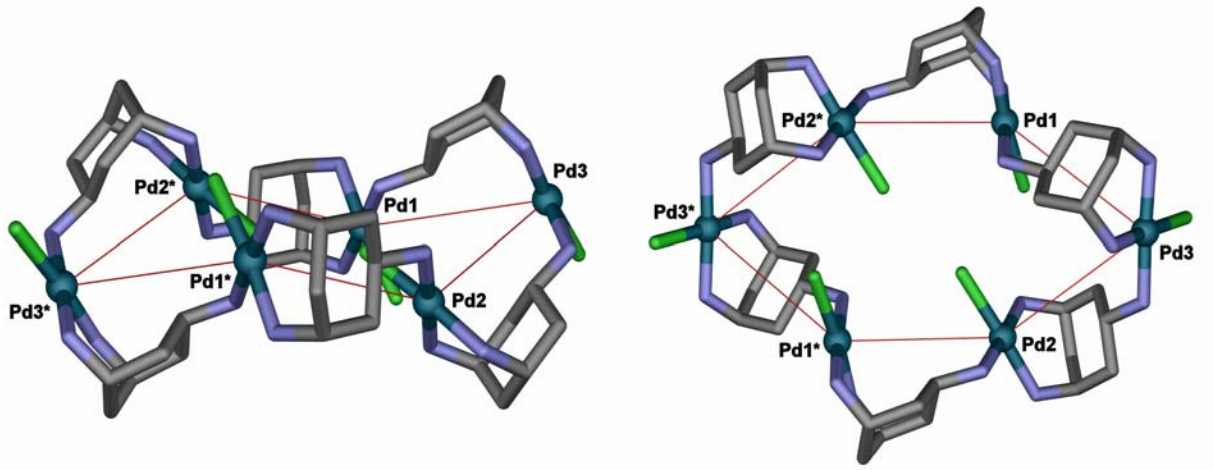

Figure 71 Two views of the elongated pseudo chair conformations of the six Pd(II) ions in the cyclic hexanuclear complexes **51** and **52**, exemplified on complex **51**.

The three crystallographically independent Pd(II) centres are oriented towards the cyclohexane rings by which they are chelated with interplanar angles Θ of 148.5° and 148.9° for Pd1, 147.2° and 149.6° for Pd2 and 159.7° and 148.0° for Pd3 in **51** and **52**, respectively. These variations in angles and thus different orientations of the Pd(II) centres demonstrate the flexibility of *trans*-tach needed to adopt strained conformations, particularly in these cyclic structures. The similarity of the two complexes appears remarkable; a direct comparison by overlaying the weight centres[†††] of the palladium(II) ions in both crystal structures shows only slight deviations from one another (Figure 72). The greatest deviations are 0.39 and 0.64 Å for Pd2 and X3, respectively. These deviations are reflected in the largest differences in Θ and χ being 11.7° for Θ_3 and 11° for χ_2.

[†††] The centroids of the six palladium(II) ions in the clusters were overlayed and the centroid distances of each set of crystallographically independent palladium(II) ions were minimised.

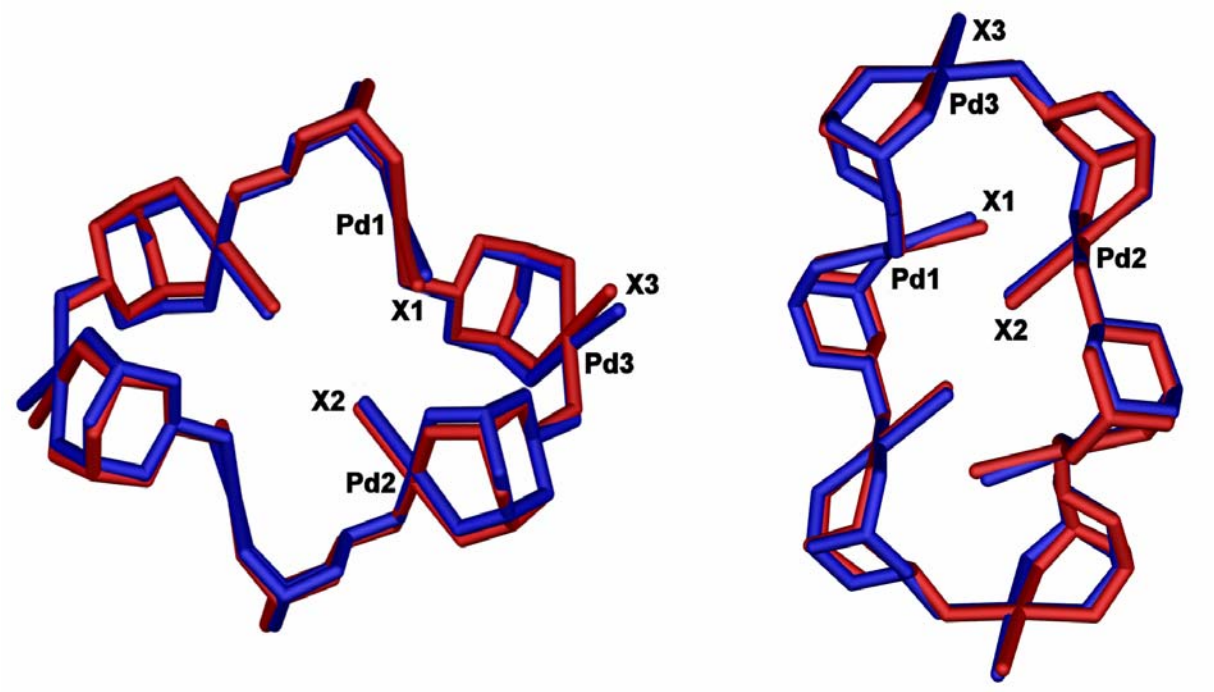

Figure 72 Two views of the overlay of the weight centres of the palladium(II) ions in the cyclic cations **51** (Cl, blue) and **52** (Br, red). The Pd(II) centres deviate in distances 0.15, 0.33 and 0.39 Å for Pd1, Pd3 and Pd2, respectively, and the halide centres deviate in distances 0.25, 0.36 and 0.64 Å for X2, X1 and X3, respectively.

The stability and rigidity of the hexanuclear ring clusters **51** and **52** are illustrated by their consistent NMR spectra in solution, ranging from room temperature up to 65°C without change. Such rigidity is probably attributable to the two '*endo*' halide ligands (X2/X2*) which 'fill' the cavity and the two '*exo*' ligands (X3/X3*) which protrude from the cavity along with the two remaining halides (X1/X1*) which have intermediate positions between the *endo* and *exo* orientation. It therefore appears that these halide ligands 'lock' the geometry of the rings; this can be seen by examination of the CPK model of the structures (Figure 73).

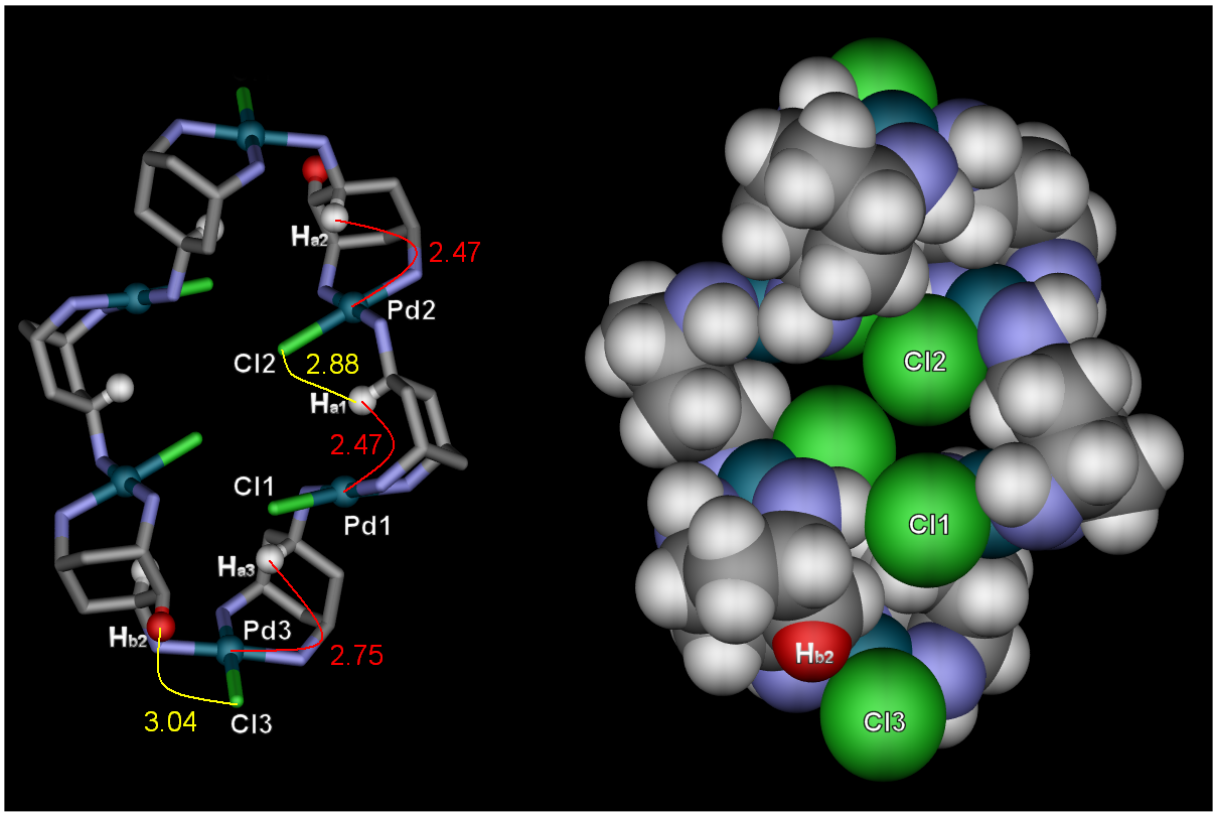

Figure 73 *LHS*: Ball and Stick representation of **51**. Distances (Å) between the *axial* methine protons H_{a1}, H_{a2}, H_{a3} (white) and the *axial* methylene proton H_{b2} (red) to its adjacent Pd(II) and Cl ions, shown in red and yellow, respectively. *RHS*: Space filling representation of **51** showing '*endo*' (Cl2) chloro ligands filling the cavity and '*exo*' (Cl3) ligands protruding from the cavity. The short contact between H_{b2} and Cl3 can be seen clearly.

A comparison between the ^{1}H-NMR spectra of **51** and **52** is shown in Figure 74. It is notable that differences in chemical shifts arise from the exchange of chloro (**51**) to bromo (**52**) ligands, whether due to the nature of the coordinating halides or due to solvent interactions. However, key features due to the structural restrictions of the metallamacrocyles are identical. The inversion centre present in both structures is maintained in solution and therefore three independant *trans*-tach environments are observed. Of particular interest are the most low field shifted signals H_{a1}, H_{a2}, H_{a3}. Each of these *axial* methine protons represent one of the three independent ring units, integrating to one of the total number of 27 CH_n (n = 1, 2) protons in the asymmetric unit. The remaining protons are grouped into three sets of signals. Additionally, one isolated resonance for the *axial* methylene proton H_{b2} is observed, which exhibits a *trans* coupling to H_{a2} (correlated NMR spectra are given in the supplementary data, chapter 7.4).

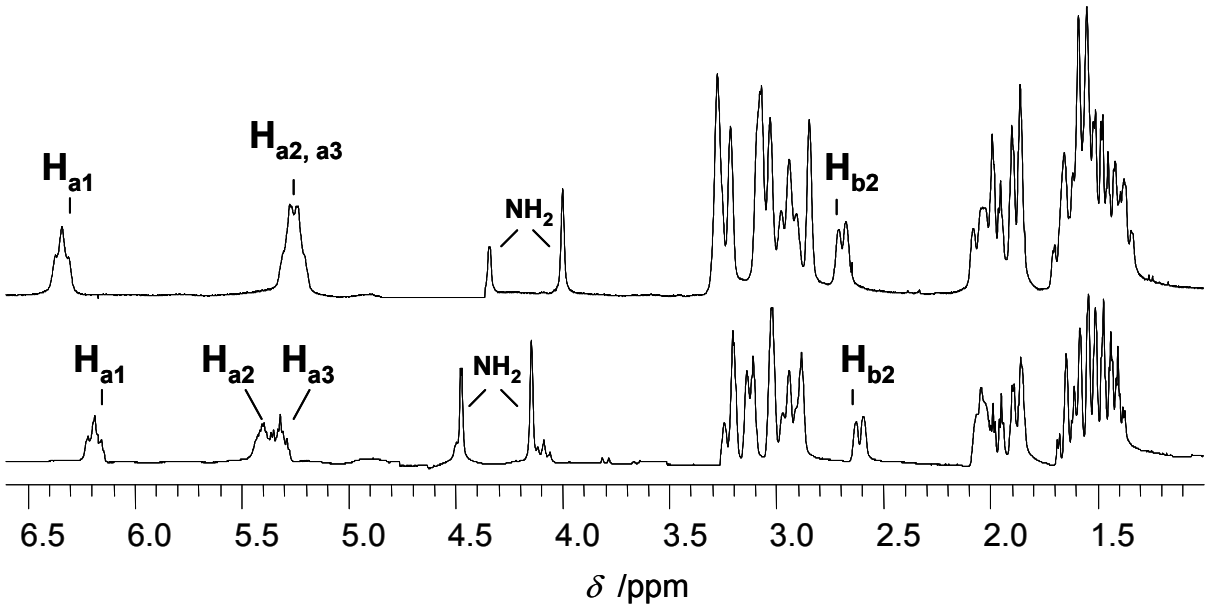

Figure 74 ^{1}H-NMR (400 MHz, D_2O) spectra of chloro- (**51**, *Bottom*) and bromo- (**52**, *Top*) metallamacrocycles. Solvent signals are removed for clarity. **51** (*Bottom*): 6.21, 5.45, 5.35 ($H_{a1,2,3}$), 2.65 (H_{b2}); **52** (*Top*): 6.34, 5.25 ($H_{a1,2,3}$), 2.66 (H_{b2}).

A comparison of the chemical shifts δ between the most deshielded *axial* methine protons in complexes **47** to **52** is given in Table 11. It is evident that the diamino-dihalide complexes **47** and **48** exhibit the most low field shifted signals around 6.2 ppm. The tetra-amine complexes **49** and **50** are up-field shifted around 5.4 ppm. It is therefore interesting that in the hexanuclear complexes **51** and **52**, which represent a triamino-monohalide coordination, the three observed signals are distributed over the range from 6.3 to 5.3 ppm. It appears that the deshielding effects[164,201,206] of the nearby Pd(II) ions exhibit the most influence, however, other factors influence the chemical shifts as well. It is evident that interactions with the coordinated halide ligands play an important role. Both Pd…H and Cl…H interactions can be referred to as hydgrogen bonded[207] interactions. These interactions are difficult to quantify,[208] given the built-in geometrical restrictions of the cyclic complexes. Since the ^{1}H-NMR spectra show features of an inversion centre as observed in the solid state, a possible assignment of the ^{1}H-NMR signals is based on the crystal data for complex **51.** Comparable analysis of the bromo complex **52** has proven to be inconclusive due to less significant differences in the structural data of each ring unit ($\Theta_{1,2,3}$ = 148.9, 149.6, 148.0°) and signal overlap in the ^{1}H-NMR spectrum. The distances between the palladium(II)-*axial* methine proton for **51** are identical for both Pd1…H_{a1} and Pd2…H_{a2} with 2.47 Å, but significantly longer for Pd3…H_{a3} with 2.75 Å (Figure 73, *LHS*). This is reflected in the interplanar angles Θ being closer for

ring units 1 (148.5°) and 2 (147.2°) but showing the greatest deviation for ring unit 3 (159.7°). This suggests that H_{a3} on C17 is the least deshielded of the methine protons. Differentiation between H_{a1} and H_{a2} is possible by analysis of their contacts to coordinating chloro ligands. H_{a1} is influenced by a close contact to Cl2 with a distance of 2.88 Å (Figure 73, *LHS*), whereas H_{a2} does not have any close contact to chloro ligands. This suggests H_{a1} as the most deshielded proton on carbon C5 and H_{a2} on carbon C11. This assignment is also supported by the *trans-axial* coupling observed between H_{a2} and H_{b2} on carbon C12. H_{b2} is deshielded from the bulk methylene protons and analysis of the crystal structure confirms that H_{b2} is the only methylene proton in the asymmetric unit that is in close contact with a chloro ligand (H_{b2}…Cl3 = 3.04 Å, Figure 73, *RHS*).

3.4.3.4 'Tail to Tail' coordination - trinuclear complex 53

The 'Tail to Tail' coordination mode is observed in the trinuclear complex $[Pd\{Pd(\mathbf{L})Cl_2\}_2Cl_2]$ (**53**), which was obtained in moderate yield and characterised by elemental analysis, IR spectroscopy and X-ray crystallography. Analysis by NMR was not possible due to insolubility. High temperature crystallisation of mother liquor of **47** results in the linkage of two complexes of **47** by coordination of their 'Tail' amino groups to a *trans* dichloro-palladium(II) unit (Figure 75). The Pd(II) ions adopt a square planar coordination environment and the complex shows a somewhat twisted geometry around the *trans*-substituted Pd-N bond with a torsion angle of 76.9(8)° (C5-N3-Pd2-Cl3). The Pd-N and Pd-Cl bond lengths lie within expected ranges for square planar *cis*- and *trans*-substituted diamino-dichloro palladium(II) complexes.[201,202,209,210] The interplanar angle Θ of the terminal Pd(II) ions (150.3°) is close to the value observed in the mononuclear dichloro-palladium(II) complex **47**. In complex **53**, the ligand is more twisted than in **51** or **52** with respect to the 'Tail' amino coordination, showing a larger torsion angle χ = 133.6°.

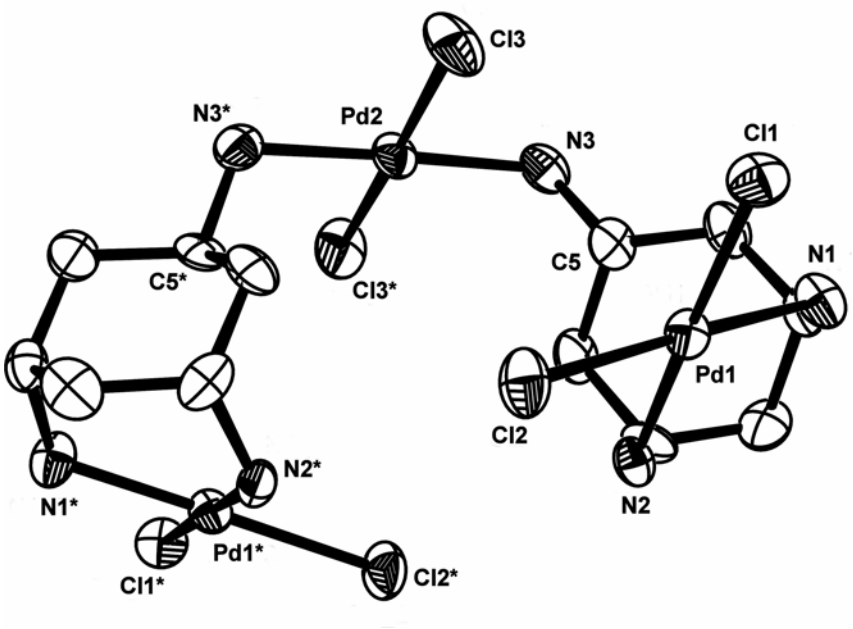

Figure 75 Ortep-3 representation of the trinuclear Pd(II) complex [Pd{Pd(**L**)Cl_2}$_2$$Cl_2$] (**53**) at 50% thermal ellipsoids. The twisted geometry can be seen clearly, torsion angle = 76.9(8)° (C5-N3-Pd2-Cl3). Selected bond lengths and angles are given in Table 8.

The complex forms a 1-D polymeric chain along the crystallographic *c* axis with each terminal Pd(II) unit bridging two adjacent molecules *via* Cl…H hydrogen-bonded interactions. The two pairs of chloro ligands lie *trans* to one another with respect to the Pd-Pd axis (Pd…Pd = 3.406(5) Å,Figure 76). Weak hydrogen-bonded interactions are observed between the *cis*-chloro ligands and the chelating amino group hydrogens (Cl…H = 2.57 and 2.51 Å) positioning the chloro- and amino- ligands in an eclipsed conformation. This is consistent with observations and theoretical studies on similar compounds by Hambley *et al*.[211]

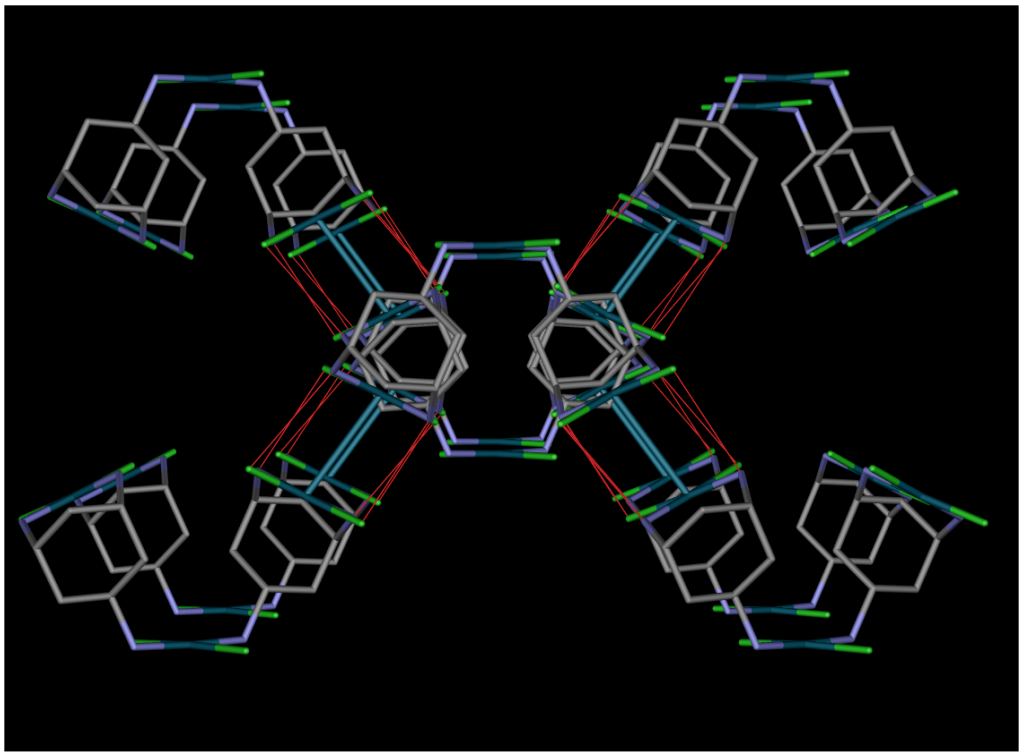

Figure 76 View along the crystallographic *a* axis, 1-D-coordination polymer of **53** along the *c* axis. Each unit is connected through hydrogen-bonded interactions (red lines) between chloro ligands (green) and amino group nitrogens (blue). Pd(II) centres are shown in turquoise and carbon in grey.

The formation of complex **53** suggests the presence of tetrachloropalladate ions in the mother liquor of **47**. This assumption is in accordance with the yield increase of the formation of **51** after ion exchange to chloride anions as described above. In addition, tetrabromopalladate ions are formed upon similar reaction conditions and starting materials by the formation of complex **48**. Interestingly, the two monoligand Pd(II) units are linked *trans* to each other and not *cis* as would be expected due to *trans*-guiding effects of chloro ligands at nucleophilic substitution reactions on tetrachloropalladate ions.[168] This might be due to steric hindrance for substitutions at the *cis* position. In accordance with this, no higher substituted complexes with three or four mononuclear palladium(II) units of **47** around the bridging Pd(II) ion were observed.

3.4.3.5 ^{1}H-NMR data for complexes 47 - 52

As described for the NMR of *trans*-tach (Chapter 3.1.1), the ring-flipped cyclohexane ring also represents an ABB'CC'DD'EF spin system.‡‡‡ This results in a second order spectrum for the protons B, C and D, which do not lie in the mirror plane that includes the protons A, E and F. However, the ^4J coupling constants between pairs of B, C and D protons are small and not resolved. Therefore, the data is interpreted as pseudo first order spectra. Additionlly, not all coupling constants are resolved, resulting in an overlap of signals that is reflected in line broadening of the peaks. Chemical shifts for the ^{1}H-NMR spectra of the complexes **47** to **52** are given in Table 11.

Table 11 ^{1}H-NMR chemical shifts (δ /ppm) and spin multiplicities for **47**-**52**

	$\mathbf{H_a}$	$\mathbf{2^{\bullet}H_d}$	$\mathbf{2^{\bullet}H_c}$	$\mathbf{H_e}$	$\mathbf{2^{\bullet}H_b}$	$\mathbf{H_f}$
[Pd(**L**H)Cl_2]Cl	6.22	2.98	2.22	2.02	1.75	1.60
(**47**)	t	bs	d	d	td	d
[Pd(**L**H)Br_2]$_2$[$PdBr_4$]	6.20	3.06	2.20	2.06	1.76	1.65
(**48**)	t	bs	d	d	td	d
[Pd(**L**H)$_2$]$(NO_3)_4$	5.38	3.16	2.16	1.95	1.82 – 1.60	
(**49**)	tt	bs	bd	dt	m	
[Pd(**L**H)$_2$]$(SO_4)_2$	5.36	3.12	2.12	1.89	1.70 – 1.52	
(**50**)	tt	bs	bd	dt	m	
[{Pd(**L**)Cl}$_6$]Cl_6	6.21, 5.45, 5.35				2.65	
(**51**)	tt				bd	
[{Pd(**L**)Br}$_6$]Br_6	6.34 (tt), 5.25 (m)				2.66	
(**52**)					bd	

‡‡‡ Except for the cyclic structures **51** and **52**, where all 27 protons in the asymmetric unit are diastereotopic due to lack of symmetry. These spin systems are ABCDEFGHI type and are not resolved in their individual coupling constants due to signal overlap.

Comparison of the low field signals for the *axial* methine protons H_a shows that the most deshielded protons are found in the complexes comprising two halide ligands at the palladium(II) centres (**47** and **48**). Contrary to this, the H_a protons for the tetra-amino coordinated palladium(II) centres (**49** and **50**) resonate at higher field around δ = 5.4 ppm. Interestingly, in the intermediate case of tri-amino, mono-halide coordination (**51** and **52**), one of the three sets of ligand signals lies in the region observed for the di-halogen coordination around δ = 6.2 ppm, whereas the remaining two lie within the region of the tetra-amino coordination around δ = 5.4 ppm. This suggests that geometrical orientation of the palladium(II)-halide coordination sphere, which is restricted in the hexanuclear metallamacrocycles, plays an important role in halide-proton interactions and thus the chemical shifts of the *axial* methine protons H_a (see also Chapter 3.4.3.3).

The ^{1}H-NMR spectra of **47** and **48** (Figure 77) show similar chemical shifts δ and coupling constants J (Figure 78) and are discussed together. The conclusive assignment of the signals was achieved by measuring ^{1}H-^{1}H and ^{1}H-^{13}C correlated spectra as well as NOE experiments.

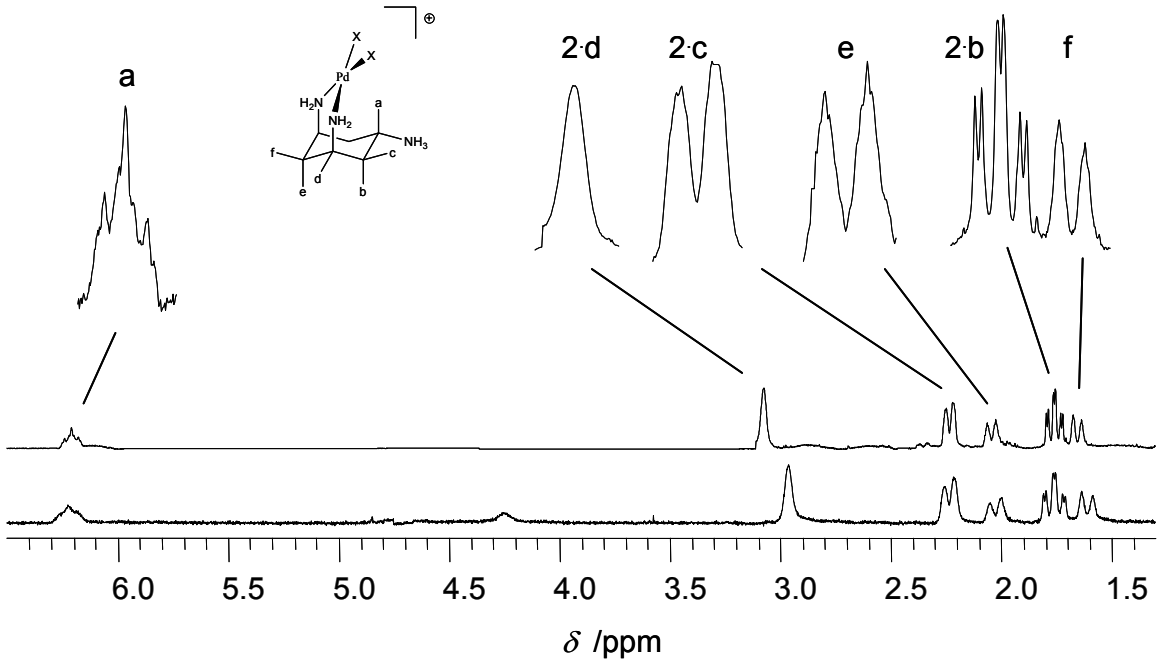

Figure 77 ^{1}H-NMR (400 MHz, D_2O) spectra of chloro- (**47**, *Bottom*) and bromo- (**48**, *Top*) monoligand complexes. δ /ppm 6.22, 6.20 (H_a), 2.98, 3.06 ($2^{\bullet}H_d$), 2.22, 2.20 ($2^{\bullet}H_c$), 2.02, 2.06 (H_e), 1.75, 1.76 ($2^{\bullet}H_b$), 1.60, 1.65 (H_f) for **47** and **48**, respectively. Figure 78 shows the coupling constants J /Hz. Solvent signals are removed for clarity.

It is interesting to note that the resonances for the *axial* methine protons H_a in both complexes give rise to the lowest field shifted signals. This is presumably due to the the two coordinating halide ligands at the palladium(II) centre.[164,201,206] Only the large *trans-axial* coupling towards H_b is resolved, resulting in a triplet splitting for H_a. Due to signal broadening, the *equatorial* methine protons H_d are observed as singlets. Both sets of *equatorial* methylene protons H_c and H_f resonate further upfield and show only *geminal* couplings to their methylene partners H_b and H_e, respectively. The signal for H_b is split into a triplet of doublets due to the large *vicinal* coupling to H_a, an identical *geminal* coupling to H_c and a small ^3J coupling to H_d. The highest field signal H_f is split into a doublet by its *geminal* coupling to H_e.

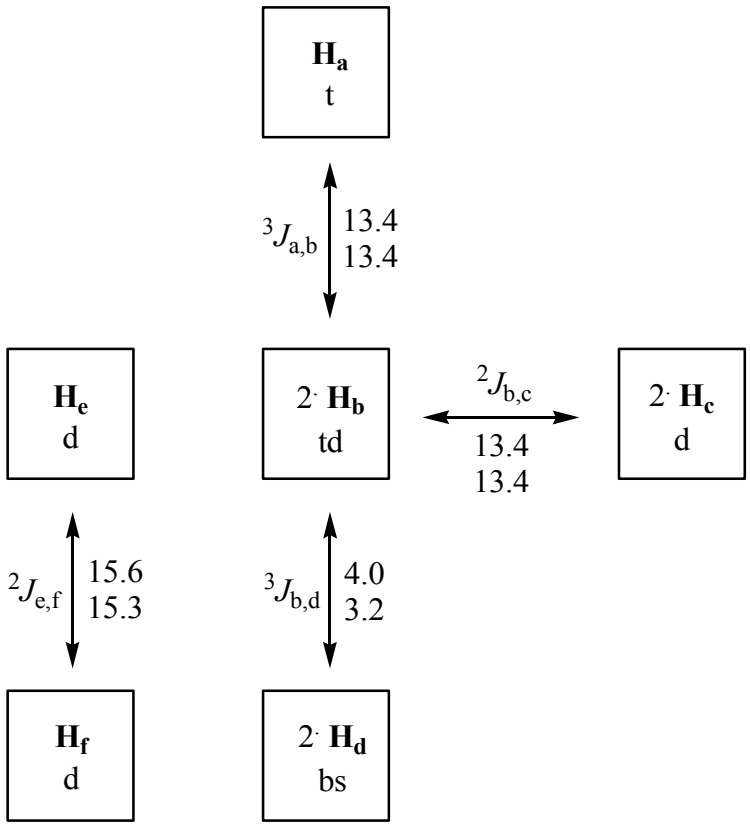

Figure 78 Coupling constants *J* as absolute values (Hz) for the chloro- (**47**, *lower* values) and bromo- (**48**, *upper* values) monoligand complexes.

In solution, both *anti*-diligand complexes **49** and **50** show similar ^{1}H-NMR spectra (Figure 79) with respect to chemical shifts δ and coupling constants J (Figure 80), and are discussed together.

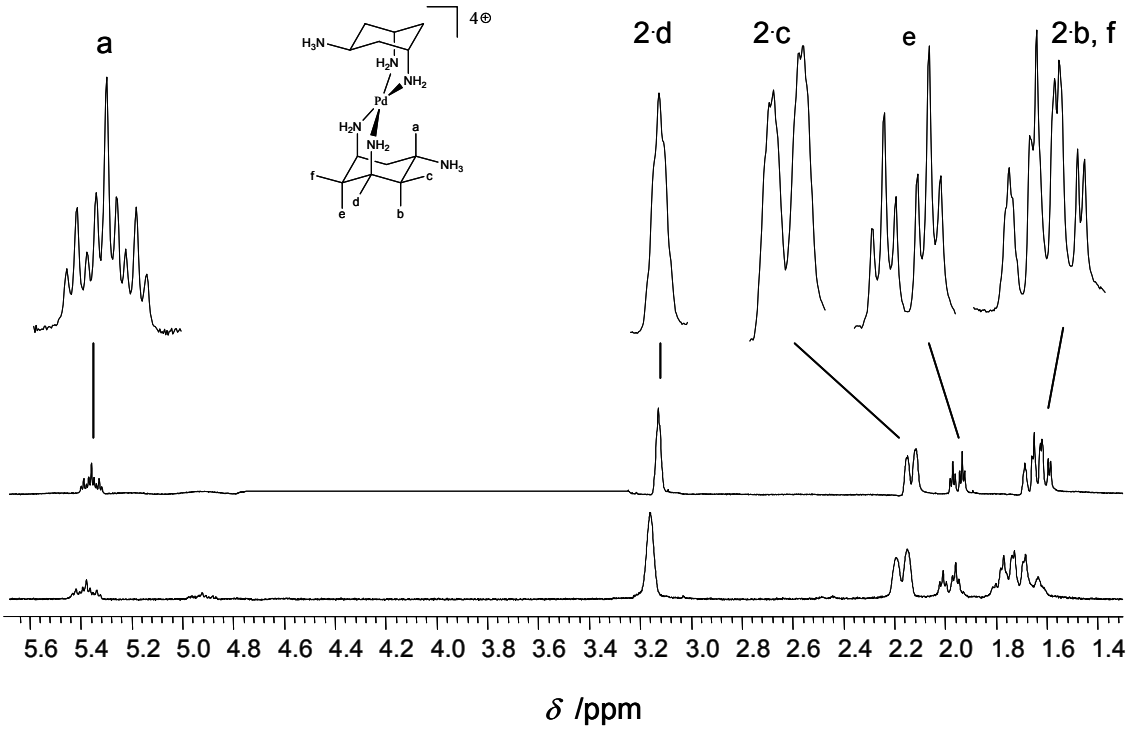

Figure 79 ^{1}H-NMR (400 MHz, D_2O) spectra of *tetrakis*-nitrate- (**49**, *Bottom*) and *bis*-sulphate- (**50**, *Top*) *anti*-diligand complexes. δ /ppm 5.38, 5.36 (H_a), 3.16, 3.12 ($2^{\bullet}H_d$), 2.16, 2.12 ($2^{\bullet}H_c$), 1.95, 1.89 (H_e), 1.82-1.60, 1.70-1.52 ($2^{\bullet}H_{b,}$ H_f) for **49** and **50**, respectively. Figure 80 shows the coupling constants J /Hz. Solvent signals are removed for clarity.

The low field *axial* methine protons H_a are less deshielded compared to those in the monoligand complexes **47** and **48**, presumably due to the lack of halide ligands at the palladium(II) centre. However, the well resolved triplet of triplets signals are due to a large *trans-axial* coupling to two H_b protons and a smaller *cis-equatorial* coupling to two H_c protons. Signal broadening results in a singlet for the *equatorial* methine protons H_d. The broadened signals of the *equatorial* methylene protons H_c exhibit a large *geminal* coupling to H_b. H_e shows a doublet of triplet signal due to a large *geminal* coupling to H_f and a smaller *vicinal* coupling to two H_d protons. The signals of the remaining protons H_b and H_f overlay and are not further resolved. This similarity in values suggests that unlike in the solid state, both cations of **49** and **50** adopt similar compressed structures in solution.

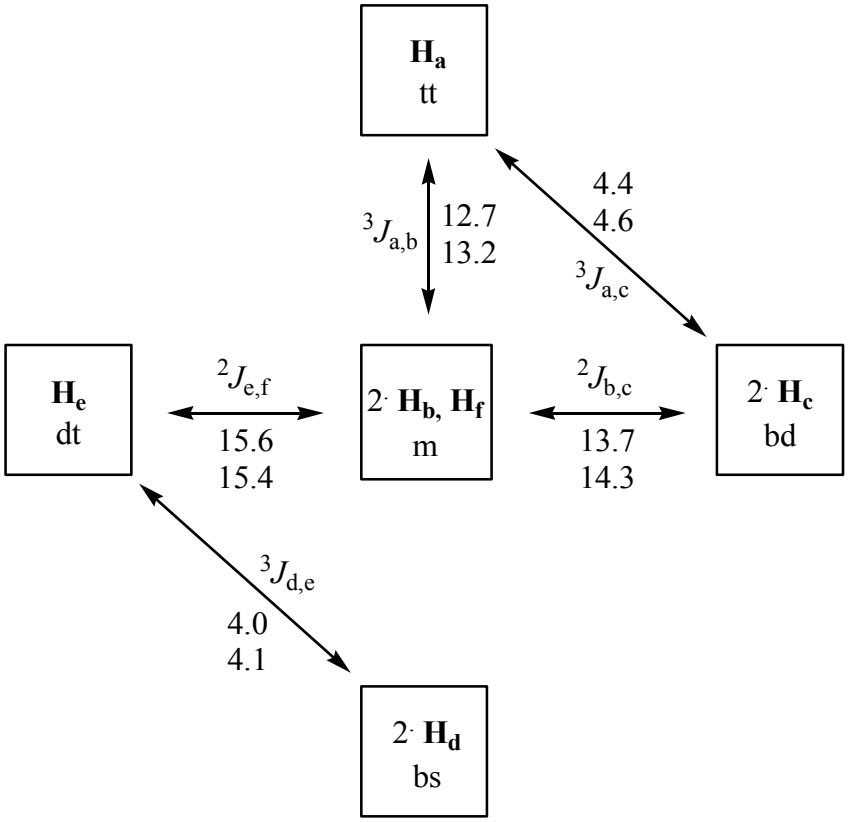

Figure 80 Coupling constants *J* as absolute values (Hz) for the *bis*-sulphate- (**49**, *lower* values) and *tetrakis*-nitrate- (**50**, *upper* values) *anti*-diligand complexes.